DISSERTATION

Longitudinal evaluation of aortic hemodynamics in patients with aortic valve pathology using four-dimensional flow cardiovascular magnetic resonance imaging

Longitudinale Evaluierung der Aortenhämodynamik bei Patienten mit Aortenklappenpathologie mittels vierdimensionaler kardiovaskulärer Magnetresonanztomographie

zur Erlangung des akademischen Grades
Doctor medicinae (Dr. med.)

vorgelegt der Medizinischen Fakultät

Charité – Universitätsmedizin Berlin

von

Ahmed Elagamy Musa

Erstbetreuung: Prof.Dr.med. Jeanette Schulz-Menger

Datum der Promotion: 30.06.2024

Teilergebnisse der vorliegenden Arbeit wurden veröffentlicht in: Front Cardiovasc Med. 2023 Feb 14;10:1071643. DOI: 10.3389/fcvm.2023.1071643

Wiesemann S, Trauzeddel RF, Musa A, Hickstein R, Mayr T, von Knobelsdorff-Brenkenhoff F, Bollache E, Markl M, Schulz-Menger J. Changes of aortic hemodynamics after aortic valve replacement-A four dimensional flow cardiovascular magnetic resonance follow up study. Front Cardiovasc Med. 2023 Feb 14;10:1071643. DOI: 10.3389/fcvm.2023.1071643

Table of Contents

List of Tables and Figures

1. Abbreviations

3D	Three-dimensional	JCS	Japanese Circulation Society
4D	Four-dimensional	**LVEF**	**L**eft **V**entricular **E**jection **F**raction
4D flow MRI	4-dimensional-flow **M**agnetic **R**esonance **I**maging	**LV**	**L**eft **V**entricle
AR	**A**ortic **R**egurgitation	**LVEDV**	**L**eft **V**entricular **E**nd-**D**iastolic **V**olume
AS	**A**ortic **S**tenosis	**LVSV**	**L**eft **V**entricular **S**troke **V**olume
ASI	**A**ortic **S**ize **I**ndex	**LVMI**	**L**eft **V**entricular **M**ass **I**ndex
AVR	**A**ortic **V**alve **R**eplacement	**MR**	**M**itral **R**egurgitation
ACC	**A**merican **C**ollege of **C**ardiology	**MAP kinase**	**M**itogen-**A**ctivated **P**rotein kinase
BAV	**B**icuspid **A**ortic **V**alve	**MSCT**	**M**ulti-**s**lice **C**omputed **T**omography
BMI	**B**ody **M**ass **I**ndex	**NOP**	**N**on-**op**erated group
BSA	**B**ody **S**urface **A**rea	**OP**	**Op**erated group
CMR	**C**ardiac **M**agnetic **R**esonance	**P**	**P**rimary study
CDC	**C**enters for **D**isease **C**ontrol	**PC-MRA**	**P**hase **C**ontrast **M**agnetic **R**esonance **A**ngiogram
CABG	**C**oronary **A**rtery **B**ypass **G**raft	**STJ**	**S**ino**t**ubular **J**unction
CXR	**C**hest **X**-**R**ay	**SBP**	**S**ystolic **B**lood **P**ressure
CT	**C**omputed **T**omography	**TAV**	**T**ricuspid **A**ortic **V**alve
DBP	**D**iastolic **B**lood **P**ressure	**TAA**	**T**horacic **A**ortic **A**neurysm
ESC	**E**uropean **S**ociety of **C**ardiology	**TTE**	**T**rans**t**horacic **e**chocardiography
FU	**F**ollow **U**p study	**TEE**	**T**rans**e**sophageal **e**chocardiography
HR	**H**eart **R**ate	**VENC**	**Ve**locity **En**coding
IRAD	**I**nternational **R**egistry of **A**ortic **D**issection	**WSS**	**W**all **S**hear **S**tress

2. Abstract

Background

Four-Dimensional Flow Magnetic Resonance Imaging (4D flow MRI) provides a non-invasive assessment of aortic hemodynamics and insight into blood flow patterns and wall shear stress (WSS). Aortic valve stenosis (AS) and bicuspid aortic valves (BAV) cause substantial changes in blood flow patterns and elevated and asymmetrically distributed WSS in the ascending aorta (1,2,3,4). The AS and BAV patients exhibited more helical, vortical, and eccentric flow (1,2). This study aimed to understand better the evolution of aortic hemodynamics in aortic valve pathologies.

Methods

After receiving ethical approval and informed consent, 20 patients from the primary studies (1,3) were reevaluated using cardiovascular MRI. There were 14 patients with BAV and 6 with stenotic tricuspid aortic valves (TAV). Between primary (P) and follow-up (FU) examination, 1 TAV and 6 BAV underwent aortic valve replacement (AVR). The patients were divided into 2 groups: non-operated (NOP) (n=13) and operated (OP) (n=7). The average duration from P to FU was 4 years. The mean age at FU was 73.3±4.4 years for OP and 57.5±15.9 for NOP. MRI studies were performed on 1.5 T (n=4) and 3.0 T (n=16) systems. Aortic valve morphology, LV function, and mass were assessed using ECG-gated breath-hold SSFP cine imaging. Aortic dimensions were measured using non-contrast magnetic resonance angiography in FU and axial SSFP imaging of the thorax in P. Standard cardiac MRI analysis was performed using cvi42. Thoracic aorta 4D flow MRI using ECG gating and respiratory navigators was acquired. Hemodynamic parameters were evaluated, including net flow, peak systolic velocity, WSS, and helical and vortical flow patterns.

Results

NOP and OP groups significantly differed in age and BMI. After surgery, LV mass and WSS magnitude were significantly decreased in OP in FU. WSS was significantly correlated with peak systolic velocity, helical flow, and LV mass. Peak velocity in the ascending aorta and aortic arch of OP declined significantly in FU but remained constant in NOP. There was a significant increase in net flow in certain aortic planes in OP in FU. In some cases, the helical and vortical flow patterns changed.

Conclusion

Aortic valve pathologies can affect the left ventricle and aortic hemodynamics, resulting in ventricular remodeling, altered blood flow patterns, and elevated WSS. AVR, however, improves the parameters. Hemodynamic changes may contribute to aortic dilatation and dissection. Our study found that aortic WSS was higher in areas with the highest dissection frequency.

The aortic disease management field strives for new parameters beyond aortic size to improve surgical decisions and predict dissection. We propose developing non-size criteria, such as WSS, as a potential parameter for individualizing aortic disease management. Ultimately, we have provided hypotheses for further, more extensive research to validate our results.

Abstrakt

Hintergrund

Die vierdimensionale Fluss-Magnetresonanztomographie (4D-Flow-MRT) ermöglicht eine nicht-invasive Beurteilung der Aortenhämodynamik und bietet Einblick in die Blutflussmuster und die Wandschubspannung (WSS). Aortenklappenstenose (AS) und bikuspide Aortenklappen (BAV) verursachen erhebliche Veränderungen der Blutflussmuster und erhöhte und asymmetrisch verteilte WSS in der Aorta ascendens (1,2,3,4). Ziel der Studie war es, die Entwicklung der Aortenhämodynamik bei Aortenklappenpathologien besser zu verstehen.

Methodik

Nach Erhalt der ethischen Genehmigung und informierten Zustimmung wurden 20 Patienten aus den Primärstudien (1,3) mittels CMR erneut untersucht. Es handelte sich um 14 Patienten mit BAV und 6 mit stenotischen trikuspidalen Aortenklappen (TAV). Zwischen der Erst- (P) und Nachuntersuchung (FU) unterzogen sich 7 Patienten einem Aortenklappenersatz (AVR). Die Patienten wurden in 2 Gruppen eingeteilt: nicht operiert (NOP) und operiert (OP). Die Dauer von P bis FU betrug circa 4 Jahre. Die MRT-Untersuchungen wurden mit 1,5 T und 3,0 T Systemen durchgeführt. Die Aortenklappenmorphologie, LV-Funktion und Masse wurden mittels SSFP-Cine-Bildgebung beurteilt. Die

Aortenabmessungen wurden mittels kontrastfreier Magnetresonanzangiographie bei FU und axialer SSFP-Bildgebung des Thorax bei P gemessen. Die Standardanalyse der kardialen MRT wurde mit cvi42 durchgeführt. Die 4D-Flow-MRT der Aorta wurde mit EKG-Gating und Atemnavigator durchgeführt. Es wurden hämodynamische Parameter ausgewertet, darunter Nettofluss, systolische Spitzengeschwindigkeit, WSS sowie helikale und vortikale Flussmuster.

Ergebnisse

Die NOP- und OP unterschieden sich signifikant in Alter und BMI. Nach der AVR waren die LV-Masse und die WSS-Größe bei OP in FU signifikant verringert. Die WSS korrelierte signifikant mit der systolischen Spitzengeschwindigkeit, dem helikalen Fluss und der LV-Masse. Die Spitzengeschwindigkeit in der Aorta ascendens und im Aortenbogen der OP nahm in FU signifikant ab. Der Nettofluss in bestimmten Aortenebenen war bei OP in FU signifikant erhöht. In einigen Fällen veränderten sich die helikalen und vortikalen Flussmuster.

Fazit

Aortenklappenpathologien können die Hämodynamik des linken Ventrikels und der Aorta beeinträchtigen. Die AVR verbessert die Parameter. Die hämodynamischen Veränderungen können zur Aortendilatation und Dissektion beitragen. In dieser Studie wurde festgestellt, dass das WSS der Aorta in Gebieten mit der höchsten Dissektionshäufigkeit höher war.

Das Management von Aortenerkrankungen sucht nach neuen Parametern, die über die Aortengröße hinausgehen, um chirurgische Entscheidungen zu verbessern und Dissektionen vorherzusagen. Wir schlagen vor, Kriterien, die nicht die Größe betreffen, wie das WSS, als potenziellen Parameter für die individuelle Behandlung von Aortenerkrankungen zu entwickeln. Letztlich haben wir Hypothesen für weitere, umfassendere Studien aufgestellt, um unsere Ergebnisse zu validieren.

3. Introduction

Aortic valve stenosis is the most common primary valvular heart disease requiring surgical or catheter-related intervention in Europe and North America (5). The aging population is contributing to the increasing prevalence of aortic stenosis. Bicuspid aortic valve is the most common congenital heart defect, affecting up to two percent of the population (9).

3.1. Aortic valve diseases

Aortic valves are typically tricuspid. Aortic valve abnormalities include stenosis or regurgitation, or both.

3.1.1. Aortic valve stenosis (AS)

The most common primary valvular heart disease requiring surgical or catheter-related intervention in North America and Europe is aortic stenosis (AS) (5). Aortic stenosis can be congenital (bicuspid or unicuspid aortic valves) or acquired (degenerative or rheumatic). Degenerative stenosis is Europe's most common acquired cause of aortic stenosis due to calcium deposition on valve leaflets that occurs as we age. Calcific AS affects about 2% of people aged 65 and older. Years of valvular mechanical stress have been thought to cause calcific aortic stenosis; however, recent studies suggest that the disease process results from proliferative and inflammatory changes, lipid accumulation, increased angiotensin-converting enzyme activity, oxidative stress, and infiltration of macrophages and T lymphocytes (6,7,8). Most patients are initially asymptomatic; however, symptoms such as exertional dyspnea, chest pain, dizziness, syncope, or even sudden death may emerge as stenosis progresses. As a compensation mechanism to overcome stress induced by aortic valve narrowing, concentric left ventricular hypertrophy occurs. As a result, the ventricles become stiffer, which causes more blood to return to the lungs, resulting in more breathlessness and chest pain.

3.1.2. Quantification of aortic valve stenosis

Echocardiography is a crucial diagnostic tool for confirming aortic stenosis, LV function, and mass. It also helps in discovering other associated valvular or aortic pathologies. Despite being the ideal measurement for assessing the degree of valvular stenosis from a theoretical perspective, aortic valve area (AVA) has numerous technical limitations in clinical practice. Measuring the mean pressure gradient (MPG) across the aortic valve remains the most reliable way to quantify the stenosis severity. In the setting of low-gradient aortic stenosis, non-invasive imaging modalities such as multi-slice computed tomography (MSCT) and

cardiac magnetic resonance (CMR) can provide additional geometrical and dimensional information on the aortic root and ascending aorta, as well as detecting the degree of valvular calcification facilitating the quantification of stenosis severity. Detecting and quantifying myocardial fibrosis is another CMR application that provides further prognostic information. If the non-invasive evaluation is inconclusive, an invasive method (heart catheterization) is considered.

According to the latest 2021 European Society of Cardiology (ESC) guidelines for the treatment of valvular heart disease, aortic valve stenosis can be classified into four types as listed below in Table and Figure 1 (5).

	HG-AS$_a$	LFLG-AS$_b$	LFLG-AS$_c$	NFLG-AS$_d$
AVA (cm^2)	<1.0	<1.0	<1.0	<1.0
MPG (mmHg)	>40	<40	<40	<40
LVEF (%)	-	<50	≥50	≥50
SVi (ml/m^2)	-	≤35	≤35	>35

Table 1. Types of severe aortic stenosis based on the latest 2021 ESC guidelines for the management of valvular heart disease. AVA = aortic valve area, LVEF = left ventricular ejection fraction, MPG = mean pressure gradient, SVi = stroke volume index. a) HG-AS = high-gradient aortic stenosis. b) LFLG-AS = Low-flow, low-gradient aortic stenosis with impaired ejection fraction. c) LFLG-AS = Low-flow, low-gradient aortic stenosis with preserved ejection fraction. d) NFLG-AS = Normal-flow, low-gradient aortic stenosis with preserved ejection fraction. Note: table based on the 2021 ESC guidelines (5).

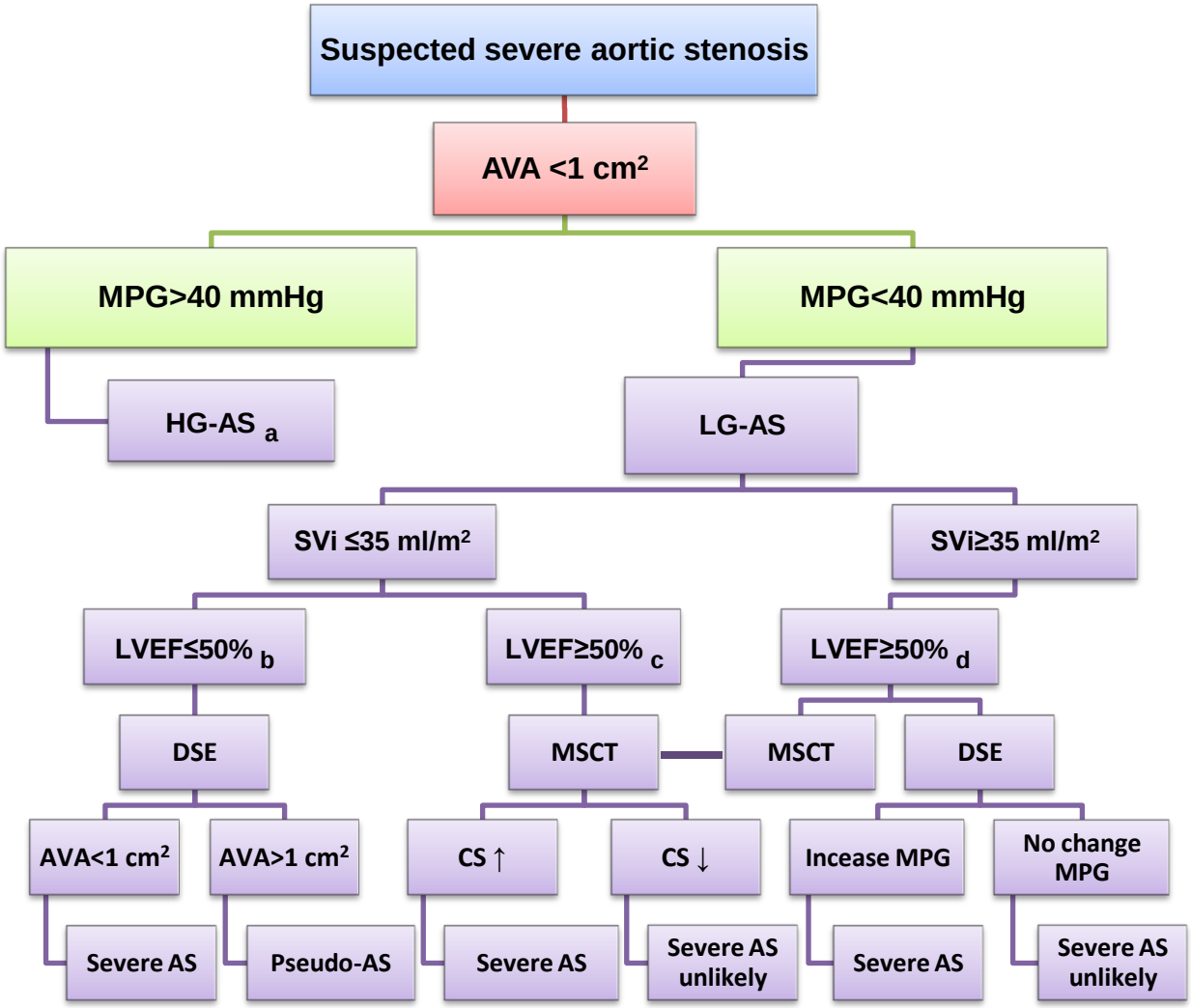

Figure 1. AVA = aortic valve area, LVEF = left ventricular ejection fraction, MPG = mean pressure gradient, SVi = stroke volume index, DSE = dobutamine stress echocardiography, MSCT = multi-slice computed tomography, CS = calcium scoring. a) HG-AS = high-gradient aortic stenosis; regardless of LVEF and flow, severe aortic stenosis can be diagnosed. b) LFLG-AS = Low-flow, low-gradient aortic stenosis with impaired ejection fraction. In this situation, low dose dobutamine stress echocardiography is recommended to distinguish between true severe aortic stenosis and pseudo-severe aortic stenosis. AVA >1.0 cm2 with flow normalization indicates pseudo-severe stenosis. c) LFLG-AS = Low-flow, low-gradient aortic stenosis with preserved ejection fraction. Typically, this occurs in elderly patients with severe LV hypertrophy and small ventricular size or may also result from conditions associated with low stroke volume (e.g., moderate/severe mitral regurgitation, severe tricuspid regurgitation, severe mitral stenosis, large ventricular septal defect, and severe RV dysfunction). The assessment of valve calcification by MSCT is important to confirm the diagnosis. Calcium scoring thresholds (Agatston units) for severe aortic stenosis: men

>3000, women >1600 = highly likely; men >2000, women >1200 = likely; men <1600, women <800 = unlikely. d) NFLG-AS = Normal-flow, low-gradient aortic stenosis with preserved ejection fraction. This group of patients is most likely to have moderate aortic stenosis. Stress echocardiography is usually recommended to confirm or rule out the diagnosis. A rise in mean pressure gradient during exercise indicates significant aortic valve stenosis. Note: figure based on the 2021 ESC guidelines (5).

● The indications for intervention in symptomatic and asymptomatic aortic stenosis according to the 2021 ESC guidelines for the management of valvular heart disease (5)

A) Patients with symptomatic aortic stenosis should undergo intervention if:	**Class [a]**
Severe high-gradient aortic stenosis [peak velocity ≥4.0 m/s, mean gradient ≥40 mmHg, and valve area ≤1.0 cm^2 (or valve area index ≤0.6 cm^2/m^2)].	I
Severe low-flow (SVi ≤35 ml/m^2), low-gradient (<40 mmHg) aortic stenosis with reduced ejection fraction (<50%), and evidence of contractile reserve.	I
Low-flow, low-gradient (<40 mmHg) aortic stenosis with normal ejection fraction after confirmation that the aortic stenosis is severe.	IIa
Low-flow, low-gradient severe aortic stenosis and reduced ejection fraction without contractile reserve.	IIa
Intervention is not recommended in patients with severe comorbidities when the intervention is unlikely to improve quality of life or prolong survival >1 year.	III
B) Patients with asymptomatic severe aortic stenosis should undergo intervention if:	
Impaired LV systolic function (LVEF<50%) without another cause.	I
Symptoms on exercise testing.	I
Impaired LV systolic function (LVEF<55%) without another cause.	IIa
LVEF >55% and a normal exercise test if there is a low procedural risk and one of the following parameters: • Very severe aortic stenosis (mean gradient ≥60 mmHg or Vmax >5 m/s). • Severe valve calcification (determined by CCT) and Vmax progression ≥0.3 m/s/year. • Significantly elevated BNP levels without another explanation.	IIa

[a]Class = class of recommendation, CCT = cardiac computed tomography, BNP = brain natriuretic peptide. Note: table based on the 2021 ESC guidelines (5).

3.1.3. Aortic valve regurgitation

Aortic regurgitation is recurrent blood flow from the aorta into the left ventricle during diastole. The most common etiology of aortic regurgitation in Western countries is degenerative (10). Infective and rheumatic endocarditis are other possible causes. Aortic regurgitation can either be acute or chronic. Aortic dissection and infective endocarditis can both lead to acute aortic regurgitation. Chronic aortic regurgitation usually remains asymptomatic for years thanks to the left ventricular compensatory mechanisms (dilating its cavity and increasing its myocardial thickness). As soon as the ventricle fails, heart failure symptoms such as shortness of breath or chest tightness manifest. Untreated severe chronic aortic regurgitation may result in irreversible left ventricular myocardial damage, even without symptoms. When it comes to diagnosing and quantifying aortic regurgitation and understanding the underlying mechanisms, echocardiography is unsurpassed. Whenever echocardiography is inconclusive, CMR can quantify the regurgitant fraction. Asymptomatic patients who do not meet surgical criteria could benefit from frequent follow-up and exercise testing to identify borderline symptoms as early as possible. In addition, it is essential to perform regular echocardiographic assessments to determine the best time for intervention. Finally, if LV dilatation or systolic dysfunction develops, early intervention is recommended to prevent irreversible myocardial damage from volume overload.

● The indications for intervention in severe aortic regurgitation according to the 2021 ESC guidelines for the management of valvular heart disease (5)

Patients with severe aortic regurgitation should undergo intervention if:	Class [a]
Symptomatic regardless of LV function.	I
Asymptomatic patients with LVESD >50 mm or LVESD >25 mm/m^2 BSA or resting LVEF ≤50%.	I
Asymptomatic patients with LVESD >20 mm/m^2 BSA or resting LVEF ≤55%, if surgery is at low risk.	IIb
Symptomatic and asymptomatic patients with severe aortic regurgitation undergoing CABG or surgery of the ascending aorta or of another valve.	I
Aortic valve repair may be considered in selected patients at experienced centres when durable results are expected.	IIb

[a]Class = class of recommendation, BSA = body surface area, CABG = coronary artery bypass graft surgery. Note: table based on the 2021 ESC guidelines (5).

3.1.4. Bicuspid aortic valve

Bicuspid aortic valve is the most common congenital heart disease (9). In patients younger than 70, it accounts for more than 50% of aortic stenosis cases (10). The bicuspid aortic valve has unequal-sized cusps that create turbulence in blood flow. Turbulent blood flow increases the likelihood of calcium deposition on the valve, which can result in stenosis or regurgitation. Patients with normally functioning bicuspid aortic valves usually remain asymptomatic for years. However, once they develop significant valvular dysfunction, the cardiac compensatory mechanisms fail with time, and the symptoms manifest. Moreover, bicuspid aortic valve patients are more likely to develop infective endocarditis and ascending aortic aneurysms. An ascending aortic aneurysm can lead to two life-threatening complications: aortic rupture and dissection.

The cornerstone of diagnosing bicuspid aortic valves is transesophageal echocardiography (TEE). In addition, MSCT and CMR are valuable investigations, especially if an aortic aneurysm or dissection is suspected.

● The indications for intervention in bicuspid aortic valve according to the 2021 ESC guidelines for the management of valvular heart disease (5)

Indications for surgery in patients with bicuspid aortic valve	Class [a]
AVR is recommended for patients with bicuspid aortic valves if they have symptomatic severe valvular dysfunction, either stenosis or regurgitation.	I
Ascending aortic surgery should be considered in patients with bicuspid aortic valve with maximal aortic diameter ≥55 mm or ≥50 mm with additional risk factors [b] or coarctation.	IIa

[a]Class = class of recommendation, AVR = aortic valve replacement.
[b]Risk factors= family history of aortic dissection, severe aortic or mitral regurgitation, desire for pregnancy, uncontrolled systemic arterial hypertension, and aortic size increase >3 mm/year. Note: table based on the 2021 ESC guidelines (5).

3.2. LV remodeling in aortic valve stenosis

Left ventricle hemodynamics are severely affected by aortic stenosis. Typically, aortic valve stenosis has an indolent course due to the left ventricular compensatory mechanisms. However, symptoms develop once the left ventricle decompensates. The initial response of the left ventricle to aortic stenosis is adaptive remodeling, which may start as a compensation mechanism. However, it evolves into a maladaptive process that causes inappropriate hypertrophy, interstitial fibrosis, and reduced contractility (11). Myocardial fibrosis occurs as the remodeling process proceeds, with potentially irreversible effects on diastolic and systolic function, clinical manifestations, and outcome. According to recent studies, fibrosis plays a crucial role in the development of symptoms in patients with severe aortic stenosis (11,12,14). Unfortunately, fibrosis usually appears before symptoms are evident and, when severe, can persist for years following an aortic valve replacement, significantly reducing its clinical benefit (13).

Maladaptive remodeling is relatively irreversible and appears to correlate to clinical outcomes. Non-invasive measures that can assess the extent of maladaptive left ventricular remodeling and predict its reversal are urgently needed. Such measures would be very helpful in selecting the optimal timing of valve replacement for patients with severe aortic stenosis. The benefits of early valve replacement for asymptomatic patients with maladaptive left ventricular remodeling must be assessed through further research.

According to long-term follow-up studies of patients who underwent aortic valve replacement due to symptomatic aortic valve stenosis, changes within the myocardial extracellular matrix are not entirely resolved following surgery. In contrast, residual changes in the myocardial extracellular matrix often lead to diastolic dysfunction, contributing to persistent symptoms and increased mortality after surgery (13).

As an early marker of left ventricular decompensation, myocardial fibrosis is becoming increasingly important in asymptomatic patients with aortic stenosis. Myocardial fibrosis is divided into two types: irreversible, which is called replacement fibrosis and can be detected using late gadolinium enhancement on CMR; and the second type is diffuse fibrosis, which occurs earlier and is potentially reversible and can be detected with CMR T1 mapping techniques (12).

CMR-based myocardial imaging in aortic stenosis shows promising results, but more clinical trials are needed to improve patient care.

3.3. Thoracic Aortic Aneurysms (TAA)

Thoracic aortic aneurysms (TAAs) are among the leading causes of death in adults (16). TAA is a multifactorial condition incorporating genetic and environmental factors (15). TAAs have become more common over time, but it is unclear whether this is due to increased detection or incidence (16). A TAA is life-threatening due to the risk of potential complications, such as aortic dissection and rupture (acute vascular complications) and aortic regurgitation (chronic valvular complication). In general, TAAs grow at a slow rate - around one millimeter a year. Unless an imaging study is conducted, a TAA usually progresses silently. Therefore, it is vital to extirpate pathologically dilated thoracic aortas before ruptures or dissections occur.

3.3.1. Background

The ascending aorta is home to over half of all TAAs (17). Aortic aneurysms occur when the aorta exceeds 50% of its predicted size (18). A woman's ascending aorta diameter at 75 is 3.6–3.7 cm, and a man's is 4.1–4.2 cm (27). There is still no definite cutoff diameter for defining an aortic aneurysm. It is, therefore, crucial to correlate the ascending aortic size with the patient's size and gender (19).

3.3.2. Pathophysiology and etiology

The aorta comprises three layers: the intima, media, and adventitia. An internal elastic lamina lies between the intima and media. Throughout the cardiac cycle, blood is continuously propelled forward by the elastic medial layer. During systole, elastic fibers store the kinetic energy that the left ventricular contractions produce as potential energy. During diastole, potential energy is converted into kinetic energy, which causes blood to travel distally. Age causes aortic wall elastic fibers to break down and smooth muscles thin out. Amorphous materials replace them in a process called cystic medial degeneration. This results in stiffer and weaker aortic walls that can lead to aortic dilation. Laplace's law states that aortic dilatation increases wall tension, leading the vascular wall to remodel and dilate even further (21).

TAAs are either caused by structural changes in the aorta or changes in intracellular signaling cascades that maintain vascular wall integrity. Transforming growth factor-beta is believed to be primarily responsible for causing this disease since it activates matrix degradation by releasing plasminogen activators and matrix metalloproteinases (21). Cystic medial degeneration can either be inherited or acquired. There is a high incidence of ascending TAAs in connective tissue disorders, such as Marfan syndrome (22),

and congenital diseases, such as bicuspid aortic valves (23). Smoking and hypertension may speed up the process by increasing elastase enzymes in the aortic medial layer (22). Atheromatous plaques have traditionally been thought to be another cause of aortic aneurysms, damaging elastin fibers and destroying smooth muscle cells, leading to aortic wall weakening. Recent research has questioned the validity of this theory, however. According to recent research, atherosclerosis develops concurrently within the diseased aortic medial layer rather than being the primary cause (22).

3.3.3. Diagnosis

Transthoracic echocardiography is a simple, non-invasive method for assessing the morphology and function of the aortic valve, aortic root, ascending aorta, and left ventricle. The aortic dimensions are measured using a leading-to-leading edge approach (24). Even though transesophageal echocardiography (TEE) can visualize nearly the entire thoracic aorta, it is not routinely used for follow-up and screening due to its semi-invasive nature.

CT scanning can be used to define the anatomy of the aorta as it is readily accessible and provides rapid results (25). There are, however, several disadvantages associated with CT scanning, including radiation exposure, contrast-induced nephropathy, teratogenicity, and carcinogenicity. Nonetheless, it is the preferred method of diagnosing complications associated with TAAs.

MR angiography can measure and define aortic anatomy precisely. Cardiovascular MRI can assess ventricular and aortic valve function and aortic root anatomy. Compared to CT, MRI is radiation-free and can be performed without contrast agent administration in patients with severe renal impairment. Native 3D MRA was found to be an appropriate alternative to contrast-enhanced MRA for evaluating the thoracic aorta (26). In contrast to CT, cardiovascular MRI is less accessible and time-consuming. Furthermore, although MRI is not absolutely contraindicated in patients with metallic parts, evaluating and interpreting acquired images can be challenging because of metal-induced artifacts.

3.3.4. Conditions associated with thoracic aortic aneurysms

Genetic and environmental factors contribute to the pathogenesis of thoracic aortic aneurysms. The following conditions are commonly associated with a thoracic aortic aneurysm:

3.3.4.1. Hypertension related thoracic ascending aortic aneurysms

Hypertension predisposes to dilatation of the ascending aorta in pre-existing TAAs and the development of new TAAs. Aortas grow increasingly rapidly once they become aneurysmal (28). Aneurysmal growth rate varies by aneurysm location, with ascending aortic aneurysms growing slower than descending thoracic aneurysms (18). The likelihood of complications with hypertension-related TAAs increases dramatically with progressively larger diameters (>6.0 cm) (22).

3.3.4.2. Bicuspid aortic valve (BAV) associated aortopathy

There is a strong association between bicuspid aortic valves and ascending aortic dilatation (29). It has been estimated that up to eighty percent of BAV patients will develop dilatation of the ascending aorta (30). Furthermore, aortic dilatation was also observed in more than fifty percent of patients with BAV who had normally functioning valves (31). There is evidence that BAV patients with normally functioning valves experienced greater aortic dilatation progression than those with tricuspid aortic valves (TAVs) (32). Another study comparing BAV and TAV patients with similar valvular function found that BAV patients had aortic dilatation earlier and at a younger age than TAV patients (33). It might seem evident that the abnormal shape of the BAV accounts for hemodynamic changes, which are attributed to aortic dilatation.

3.3.4.3. Marfan syndrome

Marfan syndrome is a genetic disorder that arises due to a mutation in the FBN-1 gene. It affects the body's connective tissues and is commonly linked to the dilation and dissection of the ascending aorta in approximately 80% of cases (34). Unfortunately, aortic dissection is the leading cause of mortality among individuals with Marfan syndrome (35). In addition, the growth rate of the ascending aorta can vary significantly among patients with this condition, and complications are more likely to occur in older patients with larger aortas and higher blood pressure (36).

3.3.4.4. Familial thoracic aortic aneurysms and dissections (FTAAD)

In some cases, a person's genetics can increase their likelihood of developing an ascending thoracic aortic aneurysm (TAA) (37). For example, those with a family history of aortic aneurysms, dissections, or sudden deaths are at a higher risk of developing TAA, accounting for around 20% of cases (38).

3.3.4.5. Loeys–Dietz syndrome

Loeys-Dietz syndrome is a genetic disorder resulting from gene mutations that encode the transforming growth factor β receptors 1 and 2. It is identified by several physical features, including hypertelorism, a bifid uvula, and a cleft palate, in addition to vascular aneurysms and dissections (39). The most common complication of this condition is an aortic root aneurysm, which can occur early in life.

3.3.4.6. Ehlers–Danlos syndrome (EDS)

This refers to a set of connective tissue disorders that exhibit joint and skin looseness, with approximately one-third of patients having ascending aortic dilation (40).

4. Guidelines for the management of thoracic aortic aneurysms

Thoracic aortic aneurysms are silent yet debilitating diseases. It is rare for patients to exhibit symptoms before experiencing an acute aortic event, with only about 5% of cases presenting with symptoms beforehand (41). In 95% of cases, aortic dissection or rupture results in death as the first symptom. Therefore, it is crucial to intervene before developing aortic dissection since mortality rates are exceptionally high once the condition has progressed. The observation of the natural history of enlarged aortas has enabled the establishment of specific criteria to predict potential ruptures or dissections. Aortic size has specific "hinging points" where such occurrences may take place. Typically, when the ascending aorta reaches a diameter of 6 cm, about 34% of thoracic aneurysms will either rupture or dissect (41). Therefore, the best course of treatment for an aneurysmal thoracic aorta is to undergo prophylactic surgery before it reaches a diameter of 6 cm to prevent ruptures, dissections, and potentially fatal outcomes associated with aneurysms.

Individuals with genetic causes of aortopathy may require surgery at an earlier point. Tables 2, 3, and 4 compare international guidelines for managing thoracic aortic aneurysms in diverse circumstances (5,42,43,44). Although these criteria apply to asymptomatic aneurysms, symptomatic aneurysms should be resected regardless of size.

Although aortic diameters may be small, aortic dissection can still happen. The International Registry of Aortic Dissection has shown that 60% of aortic dissections occur in aortas less than 5.5 cm in diameter and 40% in those less

than 5.0 cm. These findings highlight the importance of having more stringent criteria for elective repair (20). Due to these findings, some experts developed other measures to predict complications more accurately, especially for small or large BMIs, such as the aortic size index (ASI). The maximal aortic diameter should be divided by the body's surface area to calculate the ASI (19).

JCS 2020	ACC 2013	ESC 2021
Surgical intervention is warranted in the following situations:		
Aortic root or ascending aortic diameter ≥55 mm.		
Aortic root or ascending aortic diameter <55 mm with aneurysmal annual growth rate >5 mm.	Aortic root or ascending aortic diameter <55 mm with aneurysmal annual growth rate >5 mm.	Aortic root or ascending aortic diameter ≥45 mm for patients who have an indication for aortic valve replacement/repair.
Aortic root or ascending aortic diameter ≥50 mm for patients who have an indication for aortic valve replacement/repair.	Aortic root or ascending aortic diameter ≥45 mm for patients who have an indication for aortic valve replacement/repair.	

Table 2. International guidelines for the management of TAA in patients without a genetic predisposition. JCS = Japanese Circulation Society, ACC = American College of Cardiology, ESC = European Society of Cardiology.

JCS 2020	ACC 2020	ESC 2021
The following situations warrant surgical intervention:		
Aortic root or ascending aortic diameter ≥55 mm.		
Aortic root or ascending aortic diameter ≥50 mm with one of the following risk factors:		
1. Family history of dissection. 2. Aortic coarctation. 3. Annual growth rate >3 mm. 4. Arterial hypertension. 5. Severe MR or AR. 6. Desire for pregnancy.	1. Family history of dissection. 2. Aortic coarctation. 3. Annual growth rate >5 mm.	1. Family history of dissection. 2. Aortic coarctation. 3. Annual growth rate >3 mm. 4. Arterial hypertension. 5. Severe MR or AR. 6. Desire for pregnancy.
Aortic root or ascending aortic diameter ≥45 mm when AVR is planned.		

Table 3. International guidelines for the management of TAA in patients with BAV. JCS = Japanese Circulation Society, ACC = American College of Cardiology, ESC = European Society of Cardiology. MR = Mitral Regurgitation, AR = Aortic Regurgitation.

JCS 2020	ACC 2013	ESC 2021
The following situations warrant surgical intervention:		
Aortic root or ascending aortic diameter ≥50 mm.		
Aortic root or ascending aortic diameter ≥45 mm with one of the following risk factors: 1. Family history of dissection. 2. Arterial hypertension. 3. Annual growth rate >3 mm. 4. Severe AR or MR.	Aortic root or ascending aortic diameter <50 mm with one of the following risk factors: 1. Family history of dissection. 2. Annual growth rate >5 mm. 3. Severe AR.	Aortic root or ascending aortic diameter ≥45 mm with one of the following risk factors: 1. Family history of dissection. 2. Arterial hypertension. 2. Annual growth rate >3 mm. 3. Severe AR or MR.
Women contemplating pregnancy with aortic diameter:		
≥45 mm	≥40 mm	≥45 mm

Table 4. International guidelines for the management of TAA in patients with Marfan syndrome. JCS = Japanese Circulation Society, ACC = American College of Cardiology, ESC = European Society of Cardiology. MR = Mitral Regurgitation, AR = Aortic Regurgitation.

5. Basic physics of hemodynamics

5.1. Introduction

The study of vascular hemodynamics investigates the factors that impact blood flow in the circulatory system. This flow can potentially harm the walls of blood vessels because of the force the blood exerts (45,46). The force is called wall shear stress (WSS).

5.2. Vessel wall shear stress

Shear stress is the force required per unit area to change the shape of blood. It is calculated by multiplying viscosity and shear rate. Shear rate is the rate of change of shear deformation over time, which is determined by the gradient of blood flow velocity perpendicular to the wall of a vessel. When blood velocity at the vessel's wall is zero, a phenomenon called wall shear stress (WSS) occurs (50). When blood flows through a vessel, its speed changes. The velocity profile across the vessel's diameter takes on a parabolic shape. To find the shearing stress on the vessel walls caused by the flowing blood, multiply this velocity gradient by the blood's viscosity (46).

5.3. Laminar and turbulent blood flow

5.3.1. Laminar flow

Blood flow in the body is mostly laminar, which means that blood travels down a blood vessel in parallel layers while maintaining a constant distance from the vessel's wall. This flow type creates a parabolic velocity profile, with the highest velocity in the middle and the lowest at the vessel wall. While laminar blood flow is usually non-turbulent, it can sometimes become slightly disturbed, resulting in energy loss and turbulent flow (51,52).

5.3.2. Turbulent flow and the Reynolds number

Turbulent flow differs from laminar flow because it has swirling eddy currents that cause higher flow resistance. Turbulent flow occurs when a laminar flow becomes faster, such as after stenotic lesions or sudden changes in vessel diameter. The turbulence in the flow is directly related to vessel diameter, flow velocity, and blood density, but inversely related to blood viscosity. The Reynolds number is a parameter used to express this relationship. A laminar flow becomes

turbulent when the Reynolds number exceeds a specific value. This value is typically between 2000 and 2200 for smooth-walled vessels. Flows with a Reynolds number above 4000 are usually turbulent, while those below 2300 are typically laminar. Flows with a Reynolds number ranging from 2300 to 4000 are known as transitions (51,52).

5.4. Helical and vortical blood flow

When fluids have helical flow, they rotate around an axis parallel to the main flow direction. A vortex is created when the flow of a fluid revolves around a curved or straight axis. Vortices are an essential element of turbulent flows. Typically, the flow velocity is highest near the vortex's axis, while it decreases away from it. Vortices can move, stretch, twist, and interact in complex ways and carry momentum, energy, and mass (53,54).

6. The effect of hemodynamics on aortic wall and cardiac remodeling

Blood vessels experience cyclical mechanical strain due to shear stress and pulsatile blood flow. Any stretch or shear stress alteration impacts the vessel wall, which then adjusts to new conditions and eventually returns to its original tensile and shear stress levels. Vascular cells contain numerous receptors that detect and respond to mechanical pressure and shear stress. The cytoskeleton and other structural components translate and modulate tension in a cell through focal adhesion sites, integrins, cell junctions, and extracellular matrix. Mechanical forces can also initiate signal transduction cascades that affect cellular function and initiate structural changes. Flow or stretch can activate many intracellular pathways, including the MAP kinase cascade, which triggers transcription factor activation and gene expression through sequential phosphorylations (55,56).

6.1. The role of blood flow turbulence in atherosclerosis

It is crucial to understand how cells like endothelial, smooth muscle, and fibroblasts sense and respond to hemodynamic forces like shear stress. This knowledge can help prevent the development and progression of vascular diseases. Endothelial cells control vessel function by sending signals to smooth muscle cells and fibroblasts in response to changes in blood flow. When endothelial cells are damaged, smooth muscle cells are directly exposed to shear stress from blood flow. To prevent atherosclerosis, it is essential to better understand how smooth muscle cells and fibroblasts react to stress caused by blood flow (57).

6.2. The role of blood flow turbulence in the formation of aortic aneurysms

An aortic aneurysm is caused by weak aortic walls that cause dilatation of the aorta accompanied by atherosclerosis, chronic inflammation, and hemodynamic changes. Aortic aneurysms are caused by an imbalance between matrix metalloproteinases (MMPs) and their tissue inhibitors (TIMPs). The mechanisms are not yet completely understood. Inflammatory cells and turbulent blood flow are thought to be responsible for aneurysms of the aorta. In a study published in 2013, a model was developed where turbulent blood flow and inflammation were combined to induce aneurysms. A cascade of events was found to cause the aortic wall to dilate. Endothelial dysfunction caused by turbulent flow likely promotes MMP activity. MMPs destroy elastin fibers, resulting in significant arterial wall remodeling and aneurysmal formation (58,65).

7. Cardiovascular magnetic resonance imaging

Cardiovascular Magnetic Resonance imaging (CMR) is a group of methods that provide information about the heart's structure, function, blood flow, and tissue properties. However, the movement of the heart and lungs during CMR can cause problems. Therefore, methods such as breath-holding or cardiorespiratory gating are implemented to avoid motion artifacts.

7.1. Basic principles of magnetic resonance imaging (MRI)

7.1.1. Pulse sequence

A pulse sequence is a set of radiofrequency (RF) pulses that generate an MR signal. Different sequences can produce a variety of signals based on imaging parameters and the tissue's natural T1 and T2 values. Each pulse sequence gives a unique image contrast (59).

7.1.2. Gradient-echo (GRE) sequence

The GRE technique involves using a weak RF pulse to move the magnetization away from the +z direction. The resulting echo signal is called a gradient echo. Compared to spin-echo sequences, GRE sequences require less scan time. RF pulses with small flip angles are used instead of 90-degree angles to decrease the longitudinal relaxation time. Furthermore, bipolar refocusing gradients remove the need for 180 RF pulses. Fast GRE sequences can capture images in mere milliseconds, making them valuable for dynamic imaging of the left ventricle and flow estimation (59).

7.1.3. Cine MRI

Cine MRI employs a balanced steady-state free precession (bSSFP) technique that involves retrospective ECG gating. This fast gradient-echo (GRE) sequence uses the T1/T2 contrast to create high tissue contrast in the blood and myocardium. Cine MRI is the preferred method for evaluating left ventricular systolic function due to its exceptional accuracy and reproducibility. It is widely considered the gold standard in this field (59).

7.1.4. Flow imaging

7.1.4.1. Physical basics of Phase-Contrast cine

Phase-contrast cine is a technique that captures images of the heart during its cycle by using cardiac gating. To display flow velocity, both magnitude and phase images are required. This method measures the phase shift caused by blood flow by using bipolar velocity-encoding gradients and cardiac-gated GRE sequences. The phase shift is proportional to flow velocity. In phase-contrast cine, flowing blood appears either white or black, depending on its direction, while stationary tissues appear gray. To avoid artifacts, the magnitude of the velocity-encoding gradient must be adjusted based on the estimated maximum velocity of the target vessel. The through-plane flow velocity can be measured by applying gradients perpendicular to the imaging plane, and flow velocity can be measured in three dimensions with phase-contrast techniques. In addition, virtual flow lines generated from acquired data can represent blood flow. The primary purpose of phase-contrast cine is to quantify vessel flow by calculating the lumen area's average velocity (59).

7.1.4.2. Basics of 4D flow cardiovascular MRI

Traditionally, phase-contrast flow MRI has been used to assess one-way flow in each slice of two spatial dimensions. However, 4D flow MRI has gained popularity as it can evaluate complex blood flow patterns in a 3D volume with full 3D cine coverage in a reasonable amount of time. The only downside is that volumetric data acquisition is slower than traditional 2D-cine PC, taking up to 20 minutes, which makes breath-holding during exams impossible. To reduce artifacts, respiratory gating is typically used during free breathing, with bellows reading and navigator gating being the most commonly used methods (61,62). In each case, a set of diaphragm positions can be predefined as acceptable. One way to indirectly track diaphragm position and breathing during a bellows reading is by monitoring the movement of the upper abdominal circumference. Another

method involves regularly monitoring the diaphragm position using navigator gating. This technique only accepts data collected within a predetermined end-expiratory or end-inspiratory window, with any data outside of this range being rejected and the acquisition repeated. However, this can result in a longer examination time than non-respiratory-gated acquisitions, as approximately half of the data may be rejected. Phase encoding can reduce the amount of data rejection by about one-third (63,64). Different tools are available to analyze flow data and visualize complex three-dimensional blood flow patterns. A thorough analysis of heart and blood vessel hemodynamics can be conducted through retrospective quantification. Flow volumes and velocities, wall shear stress, energy loss, and blood flow patterns can be measured and analyzed. (60)

8. Aim of the study

The non-invasive visualization of aortic hemodynamics in 4D flow has provided insights into blood flow patterns and wall shear stress. Evidence showed that aortic valve stenosis and BAV are associated with altered flow patterns and elevated WSS in the ascending aorta. Patients with AS or BAV have more helical and vortical flow formation than healthy subjects. Additionally, there is a strong association between the aortic valve orifice area and left ventricular (LV) remodeling.

This study aimed to examine how aortic hemodynamics change over time in patients with aortic valve stenosis or BAV and how this affects the left ventricle and aorta. LV parameters were assessed over time, including left ventricular ejection fraction and mass. LV mass was anticipated to regress after surgery as an indicator of reverse cardiac remodeling after AVR. Furthermore, this study assessed the evolution of hemodynamic parameters, such as WSS magnitude and pattern, peak systolic velocity, and net flow throughout the thoracic aorta. The change in blood flow patterns, including helical and vortical flow, was also evaluated using a semi-quantitative approach.

9. Methods

9.1. Patient recruitment

Patient recruitment was begun following approval from the Ethics Committee of Charité University Berlin. A total of 20 patients were recruited (about 41% of the baseline target). The baseline target number was 48 patients from the previous two primary studies.

28 of the target 48 patients could not be enrolled in our follow-up study due to one of the following factors:

Cause of exclusion	N
No interest in the follow-up study	5
Inability to contact them after moving to a new address	5
Severe comorbidity that requires immediate attention	3
Contraindications to MRI (mostly after pacemaker implantation)	6
Mechanical aortic valve replacement due to associated artifacts	6
Death	3

Table 5. n = number of patients. N.B. Aortic dissection was not the primary cause of death for any of the patients who died.

9.2. Patient characteristics

An overall total of 20 patients from our primary two studies (1,3) were reevaluated as part of a follow-up study (FU) following ethical approval and written informed consent. From the aortic stenosis study (1), 16 of 37 patients (43%) were enrolled and from the BAV study (3), 4 out of 11 patients (36%). The 20 patients consisted of 14 with BAV and 6 with stenotic TAV. The 20 patients were categorized into non-operated (NOP) and operated (OP). Thirteen patients were included in the non-operated group (NOP), including 8 BAV patients and 5 TAV patients (8 males and 5 females). In the NOP group, 7 patients had dilated ascending aortas (1 TAV/6 BAV). An ascending aorta with a diameter indexed by body surface area >2.1 cm/m^2 was considered dilated. The aortic dimensions were measured at the level of the main pulmonary bifurcation. Meanwhile, there were seven patients in the operated group: 1 patient with TAV and 6 patients with BAV (6 males and 1 female). Between the primary examination (P) and the follow-up examination (FU), the operated group underwent aortic valve replacement ± ascending aorta reconstruction. Detailed characteristics of NOP and OP patients are presented in Table 6 and Figure 2.

For the non-operated group (NOP) and the operated group (OP), the mean duration from P to FU was 4.4±1.5 years and 4.3±1.4 years, respectively. The mean age at FU was 57.5±15.9 years for NOP and 73.3±4.4 years for OP.

FU study (n) = 20 patients											
NOP = 13 (8m/5f)									OP = 7 (6m/1f)		
8 BAV							5 TAV		6 BAV		1 TAV
RL						RN			RL	RN	
6						2			5	1	
N	AS III	AI II	AS II +AI II	AS I +AI II	AS I +AI I	AI II	AS I	AS II			AS III
1	1	1	1	1	1	2	4	1	5	1	1

Table 6. Patient characteristics regarding aortic valve morphology, pathology and lesion severity. FU = follow-up, n = number of patients, NOP = non-operated group, OP = operated group, BAV = bicuspid aortic valve, TAV = tricuspid aortic valve, RL = right-left coronary cusps fusion, RN = right-non-coronary cusps fusion, N = normal, AS = aortic stenosis, AI = aortic insufficiency, I = mild, II = moderate, III = severe.

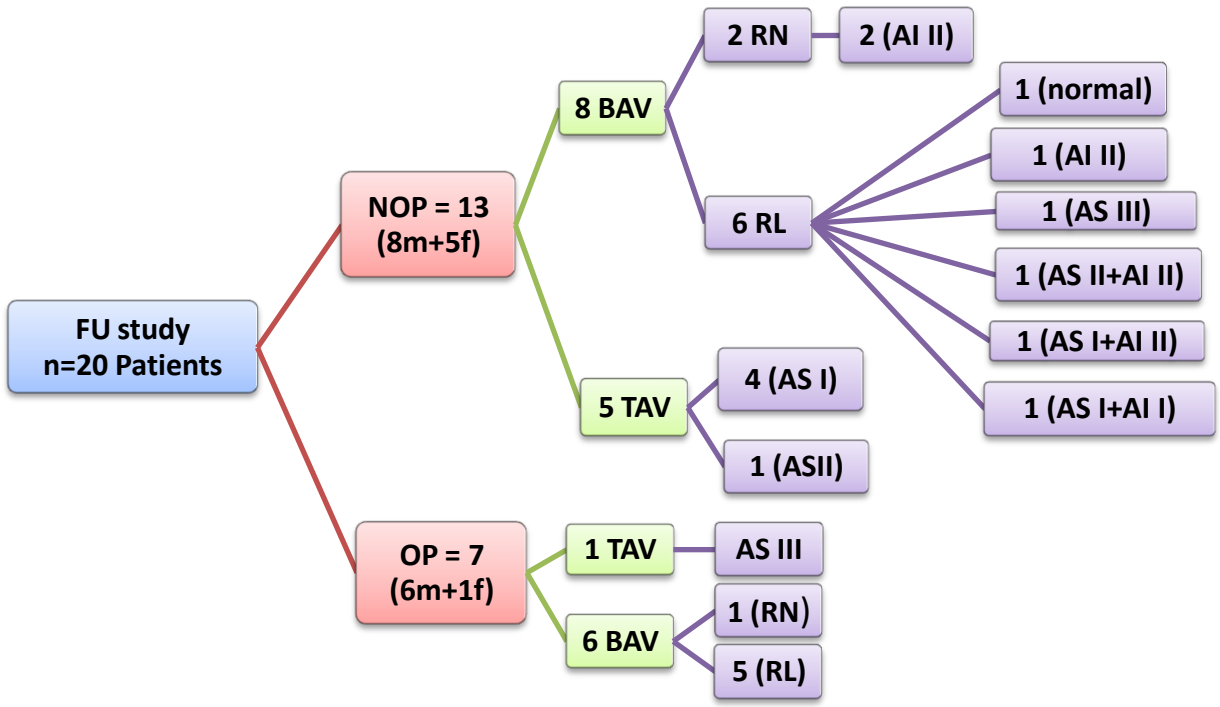

Figure 2. Patient characteristics regarding aortic valve morphology, pathology and lesion severity. FU = follow-up, n = number, NOP = non-operated group, OP = operated group, m = male, f = female, BAV = bicuspid aortic valve, TAV = tricuspid aortic valve, RL = right-left coronary cusps fusion, RN = right-non-coronary cusps fusion, AS = aortic stenosis, AI = aortic insufficiency, I = mild, II = moderate, III = severe.

9.3. Collection and analysis of MR data

9.3.1. Data acquisition

MRI studies were performed on systems of both 1.5 T at the Helios Klinikum Berlin Buch (MAGNETOM Avanto, Siemens Healthcare, Erlangen, Germany) (n=4) and 3 T at the Berlin ultrahigh field facility (B.U.F.F) (MAGNETOM Verio, Siemens Healthcare, Erlangen, Germany) (n=16). A 12 channel receive surface RF Coil was used. For imaging, patients were placed in the standard head-first supine position. ECG-gated, breath-hold SSFP cine imaging and echocardiography were performed to assess aortic valve morphology, lesion severity, and LV systolic function and mass. Aortic dimensions were measured using non-contrast magnetic resonance angiography (NC-MRA). At P, aortic size measurements were obtained from the thorax axial SSFP imaging. In addition, a research 4D flow MRI of the thoracic aorta was acquired using a sagittal oblique 3D volume with prospective ECG-gated imaging and a respiratory navigator placed on the lung-liver interface. Velocity encoding (VENC) was adjusted to minimize velocity aliasing; a typical VENC value for non-stenotic subjects was 1.5 m/s and 2.0-3.0 m/s for stenotic subjects.

9.3.2. MRI Protocol for LV function, aortic valve area and thoracic aorta diameter

A series of SSFP cine images acquired in standard long-axis planes were used to evaluate left ventricular function and mass (Figure 3: taken from reference 122). Representative 1.5T scan parameters were: slice thickness = 6 mm; Echo Time (TE) = 2.3-3.4 ms; Repetition Time (TR) = 4.8-6.6 ms; bandwidth = 440-490 Hz/pixel; Flip Angle (FA) $\alpha = 7°$, resulting in temporal resolutions of 38.4-52.5 ms; Field of View (FOV) = 340-400x200-300 mm with a voxel size of 1.8-2.1 x 1.8-2.1 x 2.0-2.8 mm^3; and 30 phases per R-R interval. Representative 3.0T scans used a slice thickness = 6 mm; TE = 1.3 ms; TR = 3.1 ms; bandwidth = 704 Hz/pixel; Flip Angle (FA) $\alpha = 45°$, resulting in temporal resolutions of 40.8 ms; FOV = 276×340 mm with a voxel size of 2.7×2.3×2.6 mm^3; and 30 phases per R-R interval. Short axes covering the entire left ventricle were acquired (slice thickness = 7 mm, gap = 3 mm) (66).

ECG gating and parallel imaging were used to assess the aortic valve area, with cine images recorded at steady-state free-precession during expiratory breath-holds. Slice thickness = 5 mm without a gap. The 3-chamber view was used to obtain a stack of slices perpendicular to the transvalvular jet by positioning two subsequent planes in the direction of the jet. In one frame, planimetry of the largest systolic orifice area was performed using cvi42 (circle cardiovascular imaging, Calgary, Canada) (Figure 4) (66).

In our primary studies, we used a transverse 2D-CMR to assess the ascending aortic diameter. The entire thorax was imaged by fast, non-contrast-enhanced, non-breathing-hold, steady-state free precession (SSFP) sequences (slice thickness 7 mm, gap 1.8 mm, scan time 10-15 seconds). The aortic diameter was measured in the transverse plane at the level of the pulmonary artery bifurcation (67) (Figure 5). In the follow-up study, non-contrast magnetic resonance angiography (NC-MRA) was used in place of transverse 2D-CMR (SSFP) sequences for measuring aortic dimensions. Similarly, the ascending aortic diameter was measured transversely at the level of pulmonary artery bifurcation.

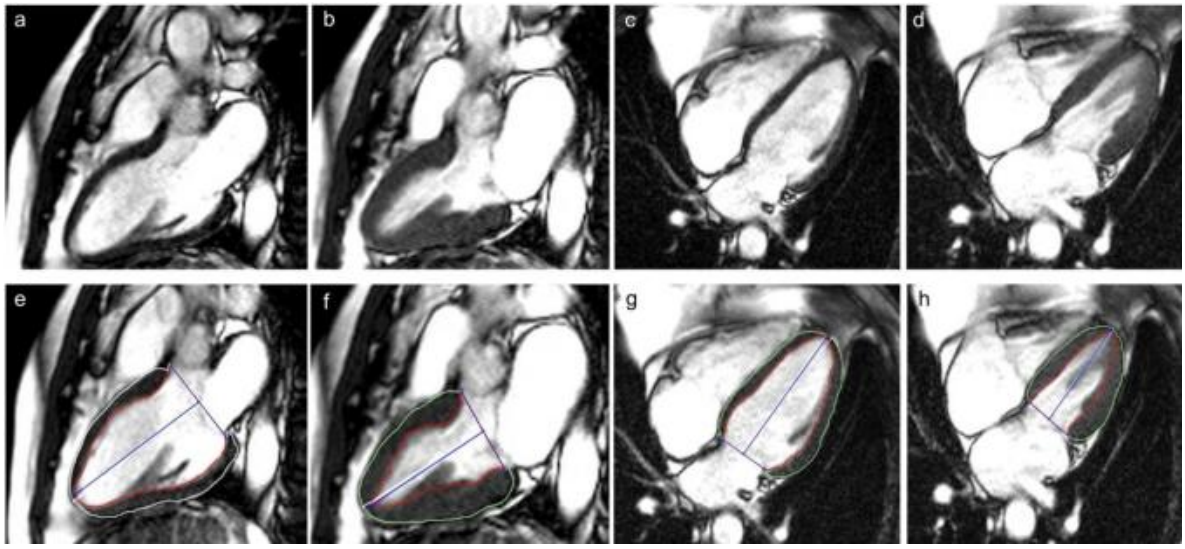

Figure 3. a) Left ventricular 2 chambered view in diastole. b) Left ventricular 2 chambered view in systole. c) Left ventricular 4 chambered view in diastole. d) Left ventricular 4 chambered view in systole. (e and f) Definition of endocardial and epicardial contours in diastole and systole in 2 chambered view. (g and h) Definition of endocardial and epicardial contours in diastole and systole in 4 chambered view. The LV mass is calculated by subtracting the epicardial volume from the EDV and multiplying it by the density of the myocardium. Figure taken from reference 122.

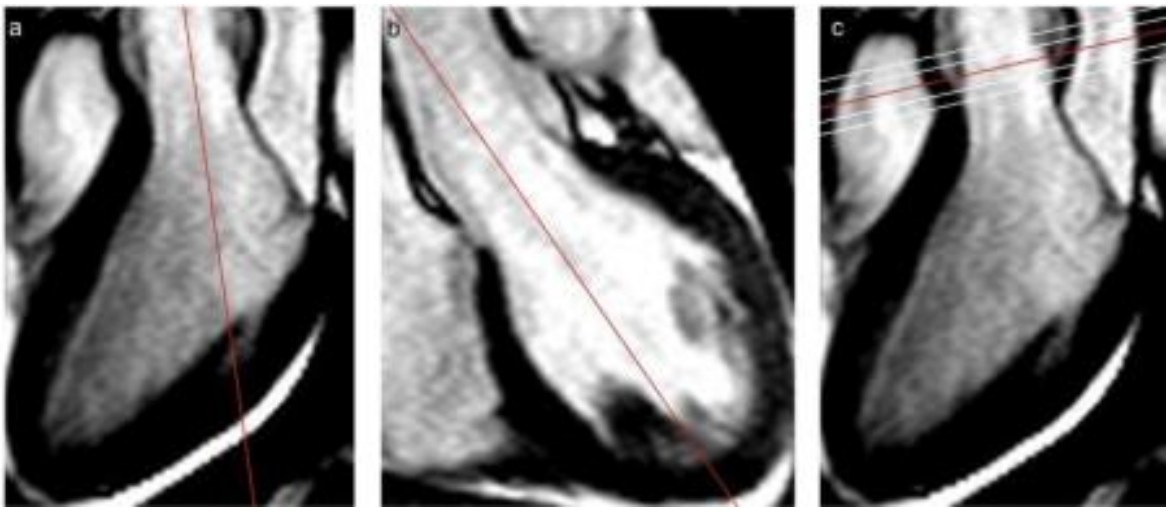

Figure 4. The method to position slices for the purpose of CMR planimetry of the aortic valve orifice. a) Left ventricular outflow tract (LVOT) view shows the placement of the plane centrally through the transvalvular jet. b) Long-axis view of the LVOT and the proximal aorta with positioning of the next plane centrally through the transvalvular jet. (c) The LVOT view shows slices perpendicular to the jet from inferior to the aortic valve up to the sinotubular level to cover the aortic valve during cardiac motion. The optimal slice is selected with cusp closure in diastole. Figure taken from reference 66.

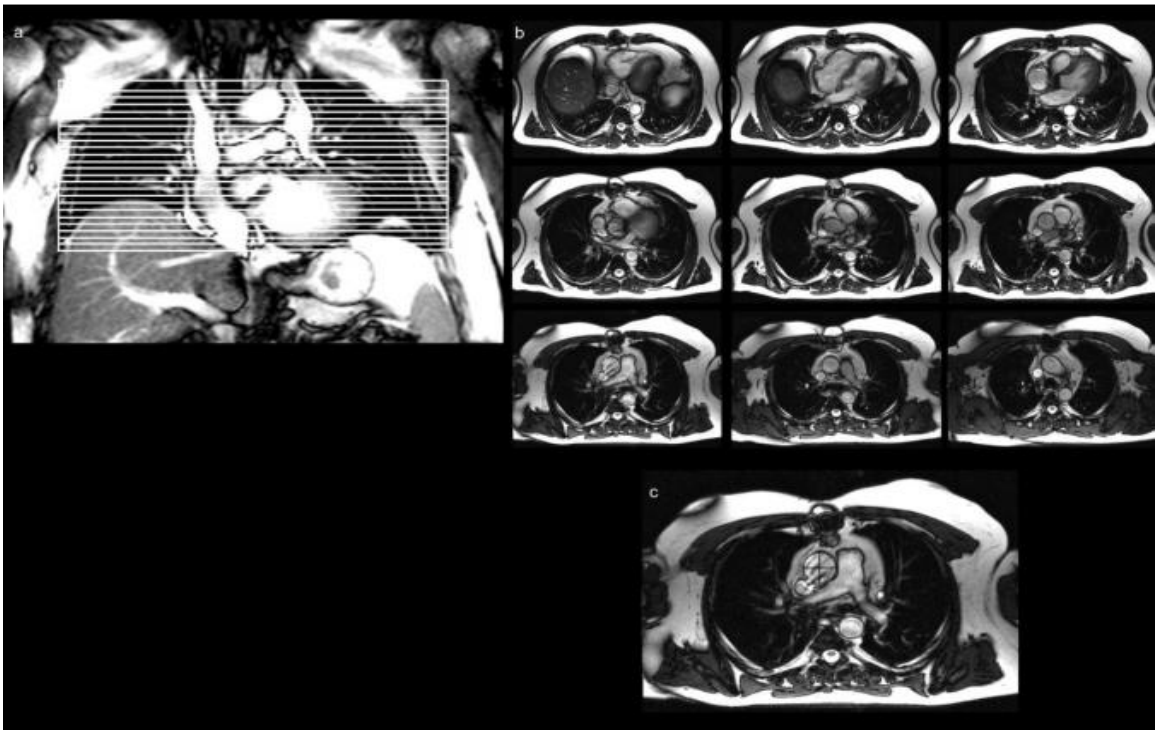

Figure 5. Transverse 2D CMR of the entire thorax, measuring the diameter of the ascending aorta at the level of pulmonary artery bifurcation. Figure taken from reference 67.

9.3.3. Quantification of LV function, aortic valve area and thoracic aorta diameter

A standard CMR analysis to assess left ventricular ejection fraction, end-systolic and diastolic diameter (LVESD, LVEDD) and index (LVESDI, LVEDDI), left ventricular mass (LVM) and mass index (LVMI), ascending aortic dimensions, as well as aortic valve area (AVA), was performed using cvi42 (circle cardiovascular imaging, Calgary, Canada) (Figures 3,4,5).

Using to the latest European Society of Cardiology guidelines, the severity of the valvular lesion was categorized as mild, moderate, and severe. Based on the data from transthoracic echocardiography (mean pressure gradient across the aortic valve; area of the aortic valve using planimetry and continuity equation) or from CMR (planimetry of the orifice area), or both, the lesion severity was assigned. Severe AS was defined as AVA <1 cm^2 or AVA indexed by body surface area <0.6 cm^2/m^2, with moderate AS being 1 to 1.5 cm^2, and mild AS being >1.5 cm^2. A non-contrast magnetic resonance angiography (NC-MRA) was used to measure the ascending aortic diameter. The ascending aortic diameter was measured in axial images at the level of the main pulmonary artery bifurcation. A dilated ascending aorta is defined as having a diameter of >2.1 cm/m^2 indexed by body surface area.

9.3.4. Protocol of 4D flow sequence

In this study, a four-dimensional flow MRI was acquired in a sagittal oblique 3D volume covering the thoracic aorta with prospective ECG-gated imaging and a respiratory navigator placed on the lung-liver interface in late diastole. The late diastolic navigator signal of the lung–liver interface was used for prospective respiration estimation, enabling measurements to be performed during free breathing (68). Velocity encoding (VENC) was adjusted to minimize velocity aliasing; typical VENC values were 1.5 m/s for non-stenotic subjects and 2.0-3.0 m/s for stenotic subjects.

The scan parameters were as follows: TE = 2.4 – 2.5 ms, TR = 4.9 – 5.1 ms, Flip Angle = 7°/10°/15°, temporal resolution = 39.2– 40.8 ms, spatial resolution = 2.0 – 2.6 × 1.7 – 2.1 × 2.0 – 3.0 mm^3, Bandwidth = 480 Hz/pixel, and rectangular FOV= 360 x 270 mm. 4D flow MRI data acquisition time ranged from 20 to 25 min (69).

9.4. Post-processing of flow data

9.4.1. Data preparation

9.4.1.1. Data preprocessing using Matlab tool

All 4D phase-contrast flow MRI data were corrected for eddy currents, Maxwell terms, gradient field inhomogeneities, and velocity aliasing using the experimental software tool Velomap (© Jelena Bock, Universitätsklinik Freiburg) based on Matlab (Mathworks, Natick, MA, USA). The data after correction is converted to the EnSight (Apex, NC) flow velocity data format using the same Velomap software (70). Commercial software (Mimics, Materialise, Leuven, Belgium) was used to manually segment the thoracic aorta based on preprocessed data, which was also utilized to calculate a 3D phase-contrast MR angiogram (PC-MRA). Based on the 4D flow scan's time-averaged velocity magnitude data, the PC-MRA was calculated (71).

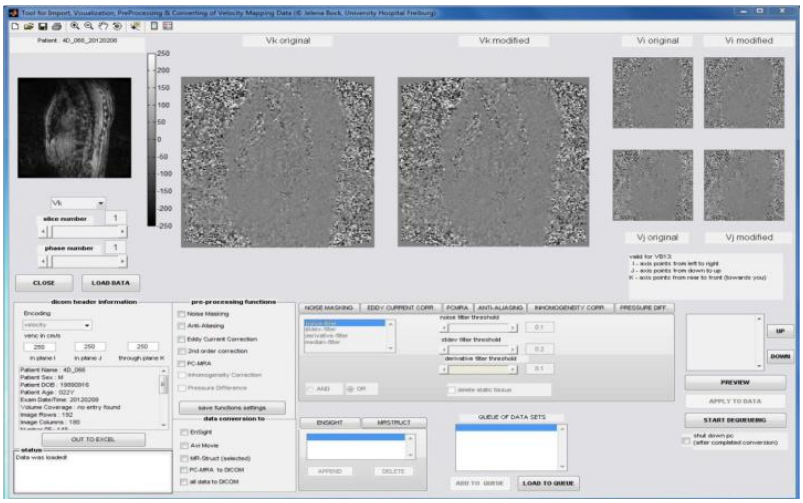

Figure 6. Velomap tool (© Jelena Bock, Universitätsklinik Freiburg).

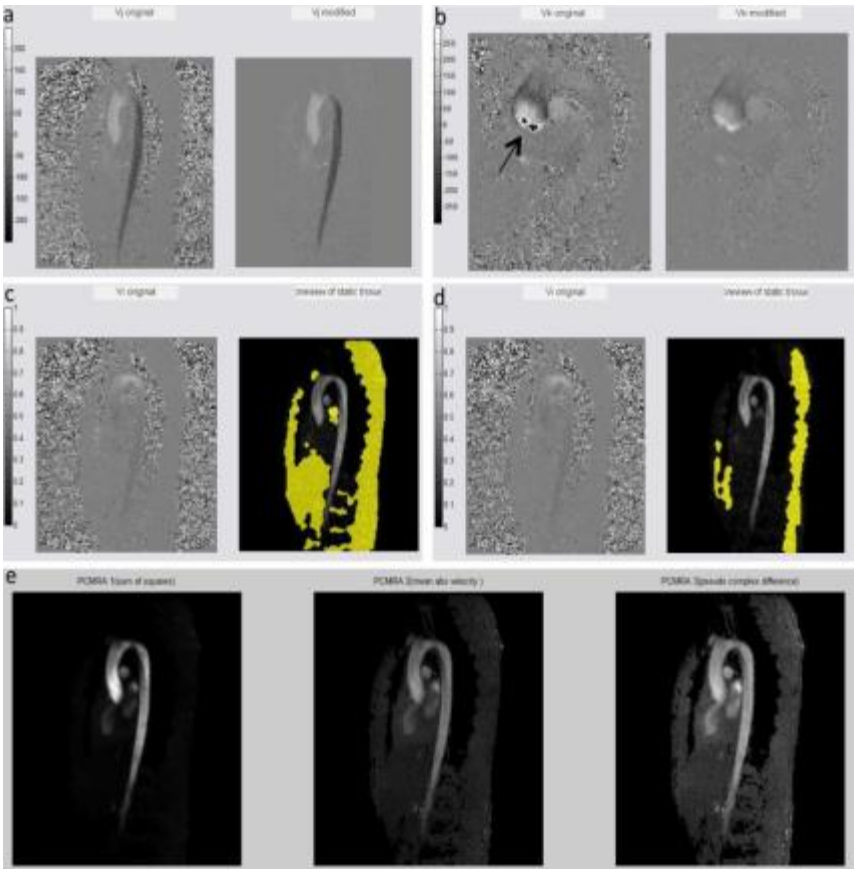

Figure 7. a) image before and after noise masking. b) before and after aliasing correction. c) before and after Eddy current correction. The yellow color represents static tissue. e) simulation of the 3D phase contrast angiogram.

9.4.1.2. Segmentation of the aorta using Mimics

The 3D PC-MRA data were used to segment the aortic lumen in 3D manually (Mimics, Materialise, Leuven, Belgium). Segmentation of the aorta is relatively time-consuming (up to 40 minutes) depending on the 3D PC-MRA image quality.

9.4.2. Processing the 4 D flow data using EnSight 10

Following the preprocessing of 3D PC-MRA with Mimics, the 4D flow CMR data were imported into 3D visualization software (EnSight 10, CEI, Apex, North Carolina). To start with, a centerline was defined and adjusted precisely in the middle along the course of the thoracic aorta, then eight planes (P) were manually placed perpendicular to and along the centreline as follows (Figures 8,9):

P1	at the sinus of Valsalva.
P2	at the proximal ascending aorta just distal to the sinotubular junction.
P3	at the mid ascending aorta.
P4	at the distal ascending aorta just proximal to the brachiocephalic trunk.
P5	at the mid aortic arch just distal to the common carotid artery.
P6	just distal to left subclavian artery.
P7	at the proximal descending aorta.
P8	at the distal descending aorta.

Figure 8. The level of the 8 planes of analysis throughout the thoracic aorta.

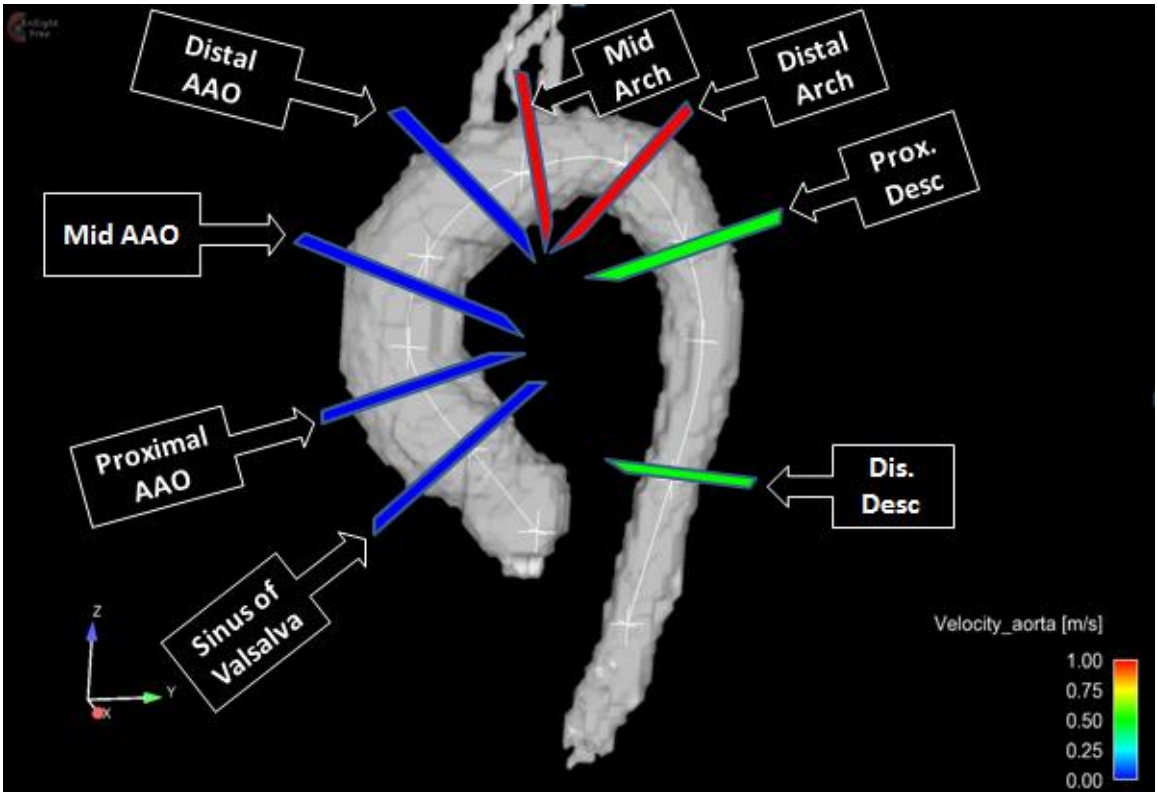

Figure 9. The position of the 8 analysis planes along the centerline of the thoracic aorta. P1: Sinus of Valsalva, P2: proximal ascending aorta, P3: mid ascending aorta, P4: distal ascending aorta, P5: mid aortic arch, P6: distal aortic arch, P7: proximal descending aorta, P8: distal descending aorta.

The most common techniques for visualizing 4D flow are streamlines and pathlines (72). Velocity magnitude is indicated by color-coding. The streamlines are instantaneous traces tangent to the local velocity vectors showing the blood flow directions at a given point in time (73). A time-resolved pathline is a path taken by a virtual massless particle over time, which allows for the flow

visualization over time (74). Multiple flow parameters such as helicity and vorticity can be visualized using streams or pathlines.

4D flow CMR quantifies flow volume and retrograde flow in the same way as conventional cine PC-CMR. In contrast, the volumetric coverage of 4D flow CMR allows flow volume measurements to be acquired retrospectively at any location within the acquired data volume (75).

9.5. Analysis of blood flow patterns and parameters throughout the thoracic aorta

9.5.1. Blood flow visualisation using pathlines or streamlines

After the placement of planes, the blood flow was visualized by creating pathline movies or static streamlines to evaluate helical and vortical blood flow formations in the thoracic aorta.

9.5.2. Semi-quantitative analysis of blood flow pattern in thoracic aorta

Helical flow occurs when a fluid moves parallel to the vessel's longitudinal axis in a corkscrew-like motion. Helical flow formations were semiquantitatively graded as (76):

- 0 (no helical flow)

- 1 mild helical flow (<360°)

- 2 moderate helical flow (>360°)

- 3 severe helical flow (>360° with flow acceleration within the helix)

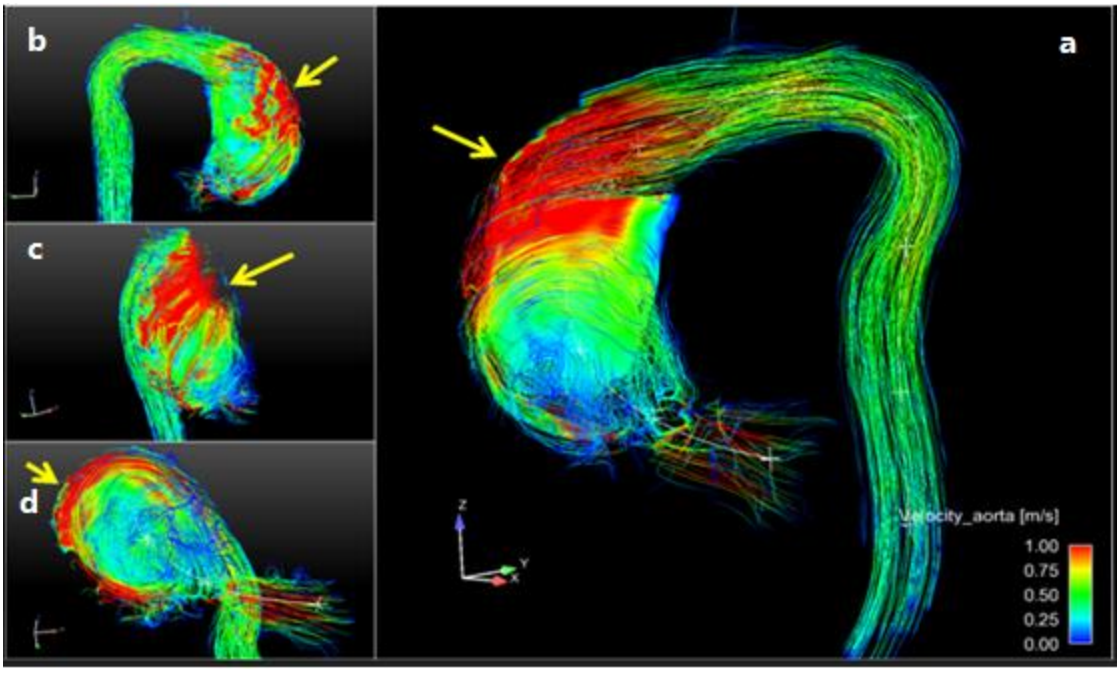

Figure 10. The visualization of helical flow formation in the thoracic aorta of a patient with stenotic BAV using streamlines from different angles of view. a) anterolateral view. b) anteromedial view. c) anterior view. d) axial view.

When particles rotate around a point inside the vessel in a direction that is more than 90° away from the physiological flow direction, a vortex flow formation occurs. Vortical flow was semiquantitatively graded as:

- 0 (no vortical flow)

- 1 (vortical flow is present)

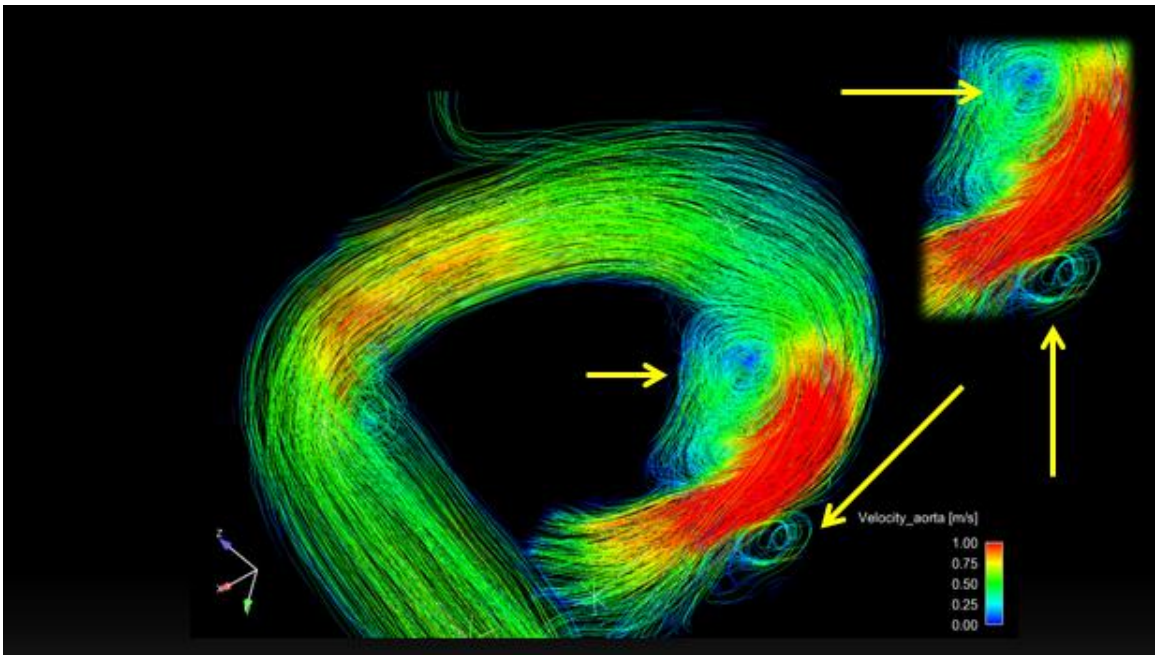

Figure 11. Vortical flow formation visualization in the thoracic aorta using streamlines.

9.6. Quantitative analysis of blood flow parameters in different planes in the thoracic aorta

Two hemodynamic parameters were quantified in each of the eight planes of analysis throughout the thoracic aorta using EnSight 10. At each plane, both net flow and peak systolic velocity were evaluated. In addition, using the velocity mapping tool from Matlab (vel mip gui), systolic peak velocities (PVs) were also calculated in 3 regions of interest: ascending aorta, aortic arch, and descending aorta.

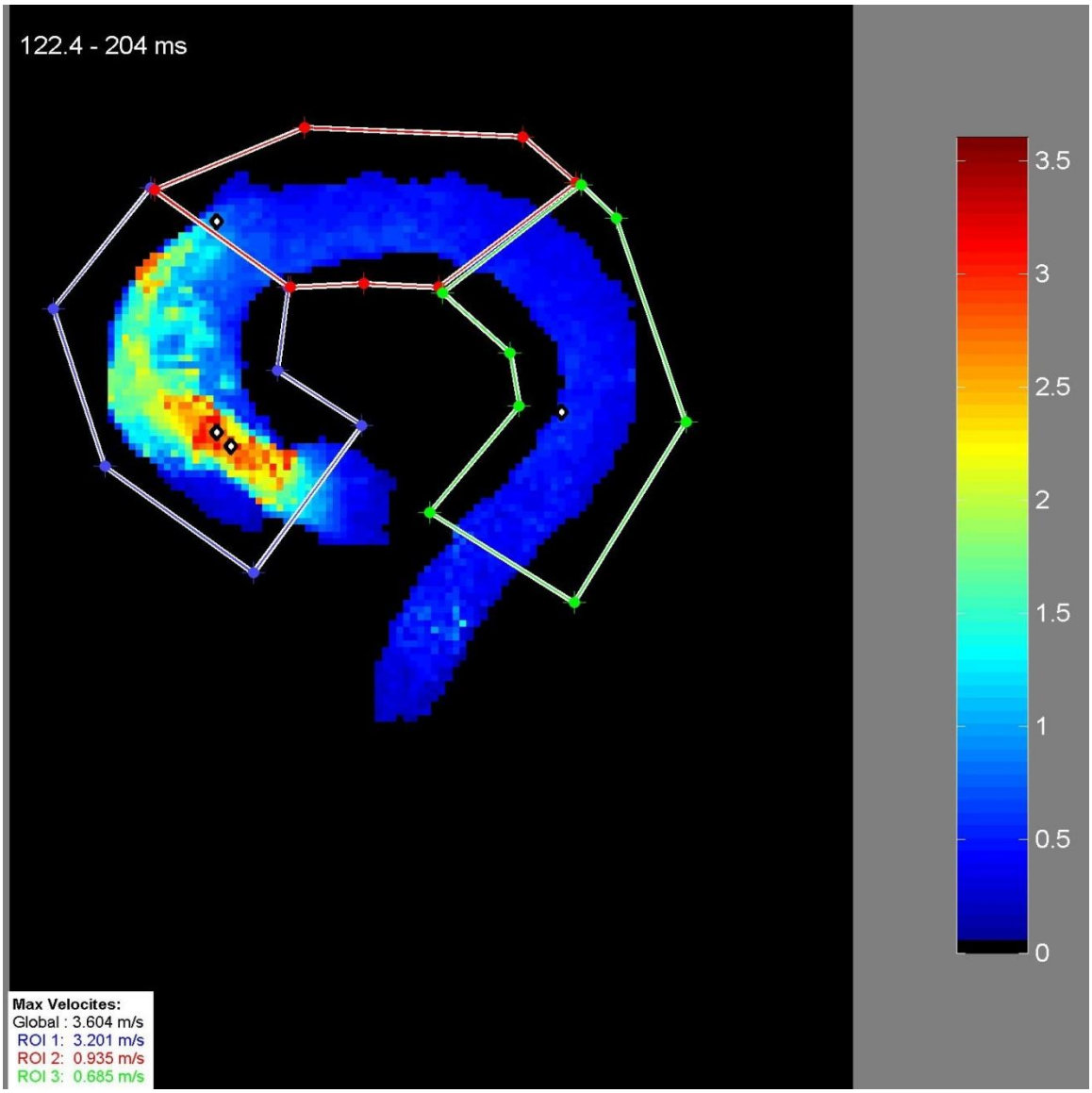

Figure 12. Calculation of the peak systolic velocity in 3 regions of interest (ascending aorta, aortic arch, and descending aorta) using Matlab-based tool (vel mip gui).

9.6.1. Wall shear stress

9.6.1.1. Three-dimensional wall shear stress calculation

Peak systolic 3D wall shear stress (WSSpeak in N/m^2) was calculated along the entire thoracic aorta in an 18-segment model using a Matlab-based tool (The Mathworks Inc., USA). The thoracic aorta was divided into 18 segments, ascending aorta: 6 segments, aortic arch: 6 segments, and descending aorta: 6 segments. Nine segments represented the outer thoracic aortic curvature, and nine represented the inner curvature. Segments with odd numbers (1,3,5,7,9,11,13,15 and 17) represented the outer curvature. Segments with even

numbers (2,4,6,8,10,12,14,16 and 18) represented the inner curvature. Peak WSS was calculated in each of the 18 segments, ascending aorta, aortic arch, descending aorta, and along the outer and inner aortic curvatures.

Segment 1	outer proximal ascending aorta.
Segment 2	inner proximal ascending aorta.
Segment 3	outer mid ascending aorta.
Segment 4	inner mid ascending aorta.
Segment 5	outer distal ascending aorta.
Segment 6	inner distal ascending aorta.
Segment 7	outer proximal aortic arch.
Segment 8	inner proximal aortic arch.
Segment 9	outer mid aortic arch.
Segment 10	inner mid aortic arch.
Segment 11	outer distal aortic arch.
Segment 12	inner distal aortic arch.
Segment 13	outer proximal descending aorta.
Segment 14	inner proximal descending aorta.
Segment 15	outer mid descending aorta.
Segment 16	inner mid descending aorta.
Segment 17	outer distal descending aorta.
Segment 18	inner distal descending aorta.

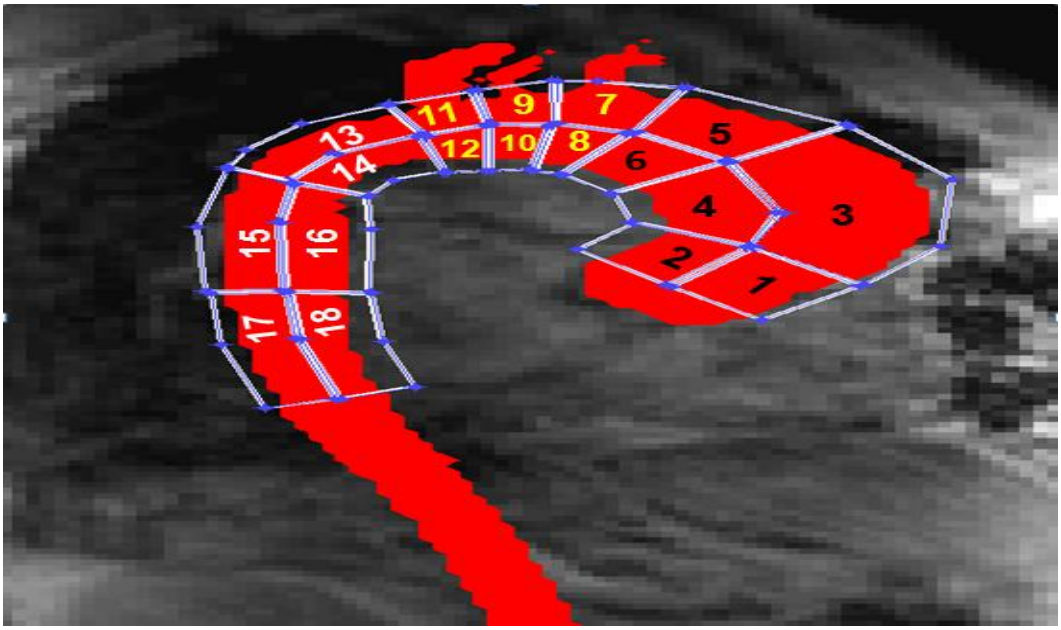

Figure 13. Peak systolic 3D wall shear stress calculated along the entire thoracic aorta in 18-segment model using a Matlab-based tool.

10. Statistical analysis

Statistical data analysis was conducted using SPSS statistics 25 (IBM, Armonk, NY) and Microsoft Excel (Microsoft Office 2010). The graphs were created using Microsoft Excel 2010 and Microsoft Paint (Microsoft Windows 2010). The data were expressed as a mean value ± standard deviation. Normal data distribution was tested with SPSS Statistics 25. An independent t-test was performed to compare the NOP and OP results, and a paired t-test was used to compare the primary and follow-up data. A p value < 0.05 was considered significant. This is a hypothesis-generating study; therefore, an adjustment of the alpha error (e.g., according to Bonferroni) has been omitted, and the results found should be replicated in subsequent larger studies. Linear regression analysis was conducted to assess significant correlations.

11. Results

11.1. Baseline characteristics of the patients

Our follow-up (FU) study comprised 20 patients divided into two groups. The non-operated group (NOP) included 13 patients: 8 males (62%) and 5 females (38%). The operated group (OP) included 7 patients: 6 males (86%) and 1 female (14%) (Figure 14).

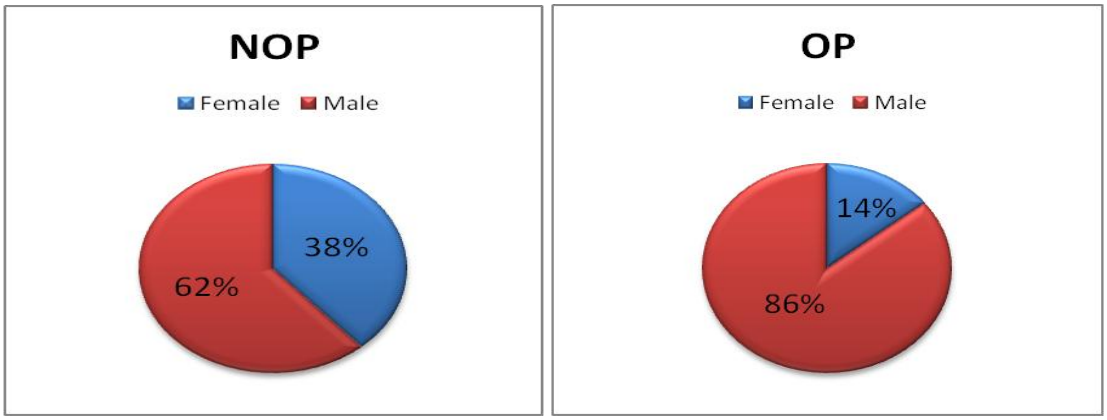

Figure 14. The difference between NOP and OP regarding gender.

The OP and NOP differed significantly in age (NOP: 57.5±15.9 years, OP: 73.2±4.4 years, p value: 0.004) and BMI (NOP: 27.8±3.1 kg/m^2, OP: 24.9±2.05 kg/m^2, p value: 0.026), with OP being older with a lower BMI (Figures 15,16).

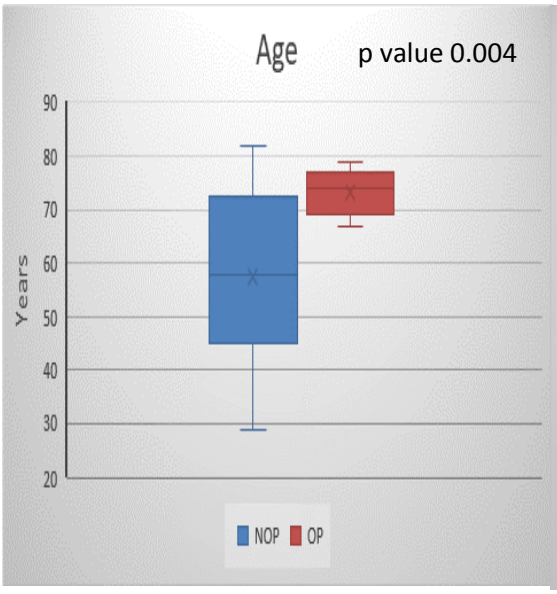

Figure 15. The difference between NOP and OP regarding age.

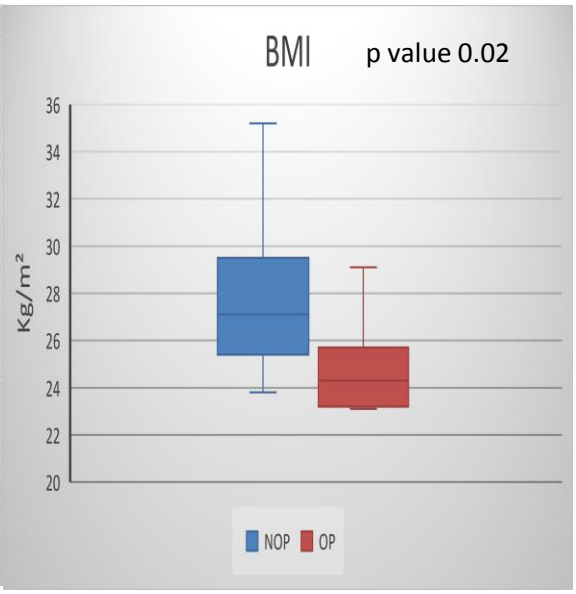

Figure 16. The difference between NOP and OP regarding BMI.

There was no statistical difference between NOP and OP regarding systolic blood pressure, diastolic blood pressure, and heart rate at follow-up (p value for systolic blood pressure (SBP): 0.2, diastolic blood pressure (DBP): 0.4, heart rate: 0.3) (Table 7).

	Unit	NOP	OP	p value
Age	year	57.5±15.9	73.2±4.4	0.004
Height	cm	172.6±9.5	170.7±7.7	0.637
Weight	kg	83.2±13.6	72.8±8.5	0.052
BMI	kg/m^2	27.8±3.1	24.9±2.05	0.026
BSA	m^2	1.9±0.2	1.85±0.14	0.053
SBP	mm Hg	125.7±17.5	136±17.9	0.239
DBP	mm Hg	75.7±13.5	72.2±7.06	0.469
Heart rate	bpm	68.7±13.04	64±10.04	0.385

Table 7. Baseline characteristics of the patients at follow-up study.

Regarding the non-operated group (NOP), there was no statistical difference between primary (P) and follow-up (FU) regarding LVEDV (P: 153±32.9 ml, FU: 151.5±31.6 ml, p value: 0.756), LVSV (P: 91.9±16.9 ml, FU: 92.5±18.1 ml, p value: 0.824), LVEF (P: 60.8±5.7%, FU: 61.7±5.6%, p value: 0.341) and LV mass (P: 151.5±41.2 g, FU: 148.8±39.5 g, p value: 0.578). However, we observed a

statistically significant increase in the maximal aortic diameter over time (P: 39.8±6.8 mm, FU: 40.3±6.1 mm, p value: 0.045) (Table 8).

On the other hand, regarding the operated group (OP), there was a significant statistical difference (significant decrease) between primary (P) and follow-up (FU) regarding LVSV (P: 91.9±6.2 ml, FU: 83.3±6.2 ml, p value: 0.047), LVEF (P: 69±5.7%, FU: 63.7±4.9%, p value: 0.034) and LV mass (P:203.3±90.1 g, FU: 153.4±46.7 g, p value: 0.023). The maximal aortic diameter did not differ statistically significantly after surgery. However, in one case with BAV, we observed an increase in the maximal aortic diameter even after aortic valve replacement (aortic diameter P: 37 mm and FU: 40 mm) (Table 9).

NOP	Unit	P	FU	p value
Aortic diameter	mm	39.8±6.8	40.3±6.1	0.045
LVEDV	ml	153±32.9	151.5±31.6	0.756
LVEDV index	ml/cm	0.88±0.16	0.87±0.16	0.932
LVSV	ml	91.9±16.9	92.5±18.1	0.824
LVEF	%	60.8±5.7	61.7±5.6	0.341
LV mass	g	151.5±41.2	148.8±39.5	0.578
LV mass index	g/cm	0.87±0.21	0.86±0.22	0.903

Table 8. Baseline characteristics of the non-operated group.

OP	Unit	P	FU	p value
Aortic diameter	mm	38.6±4.8	37±4	0.196
LVEDV	ml	133.1±13.6	131.1±13.5	0.331
LVEDV index	ml/cm	0.78±0.07	0.77±0.06	0.310
LVSV	ml	91.9±6.2	83.3±6.2	0.047
LVEF	%	69±5.7	63.7±4.9	0.034
LV mass	g	203.3±90.1	153.4±46.7	0.023
LV mass index	g/cm	1.18±0.48	0.89±0.25	0.022

Table 9. Baseline characteristics of the operated group.

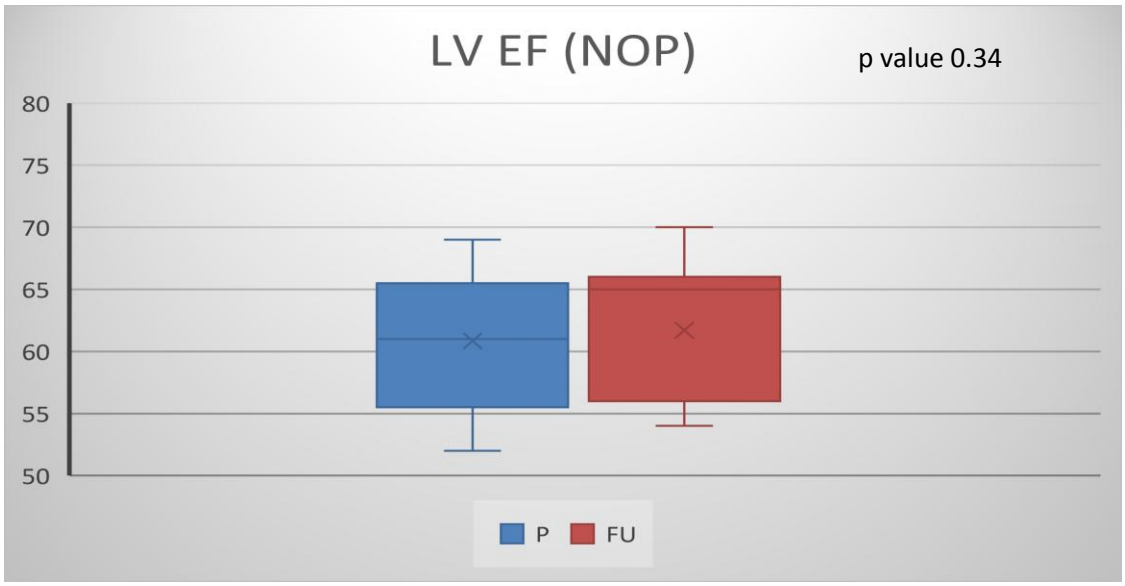

Figure 17. The difference between the LVEF in P and FU studies in NOP.

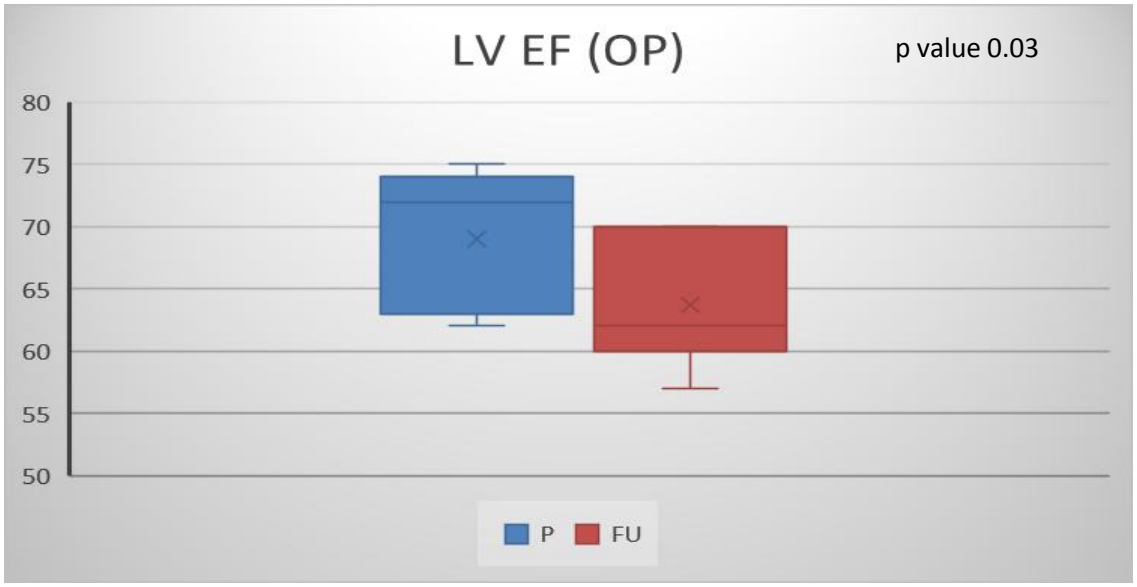

Figure 18. The difference between the LV EF in P and FU studies in OP.

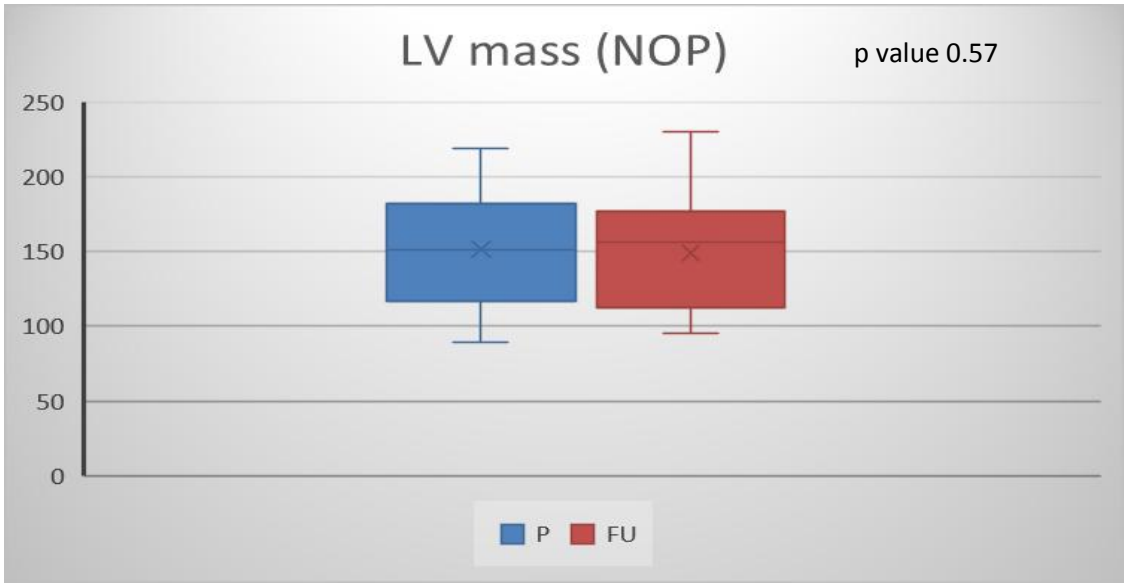

Figure 19. The difference between the LV mass in P and FU studies in NOP.

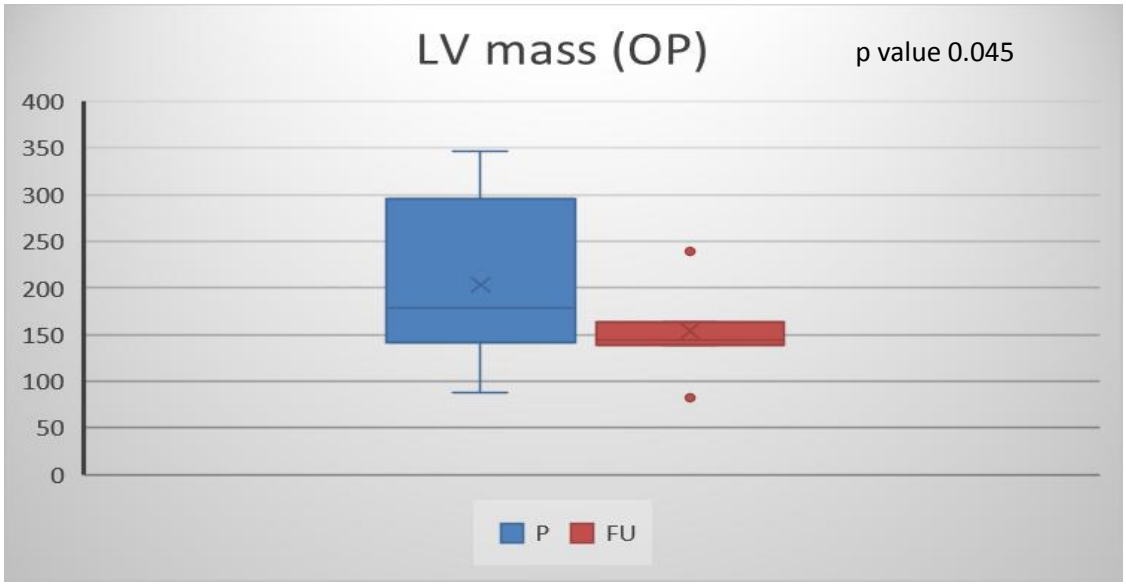

Figure 20. The difference between the LV mass in P and FU studies in OP.

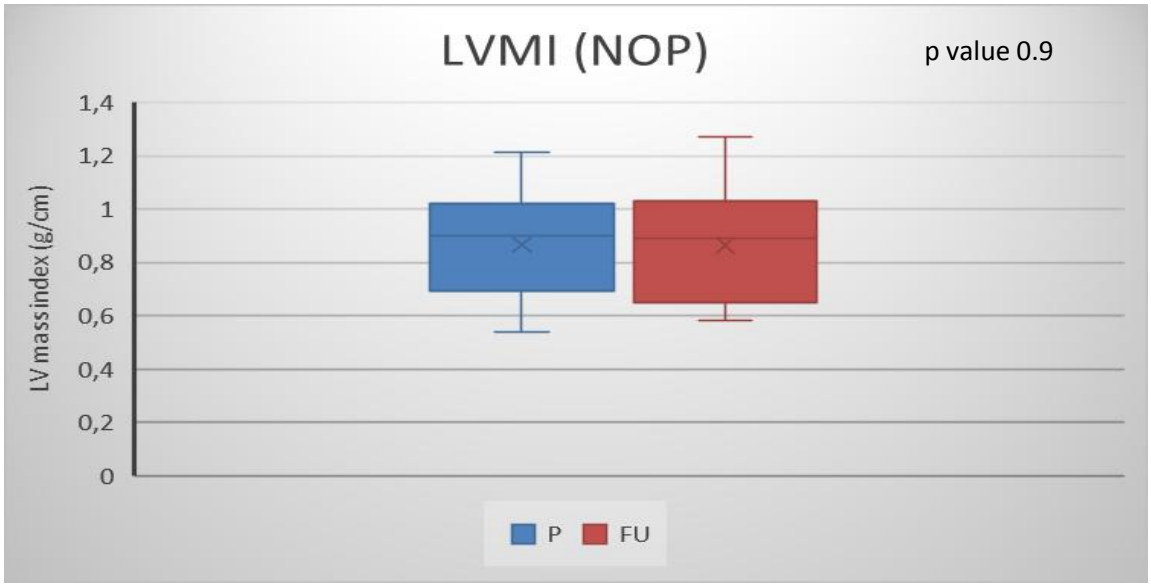

Figure 21. The difference between the LV mass index in P and FU studies in NOP.

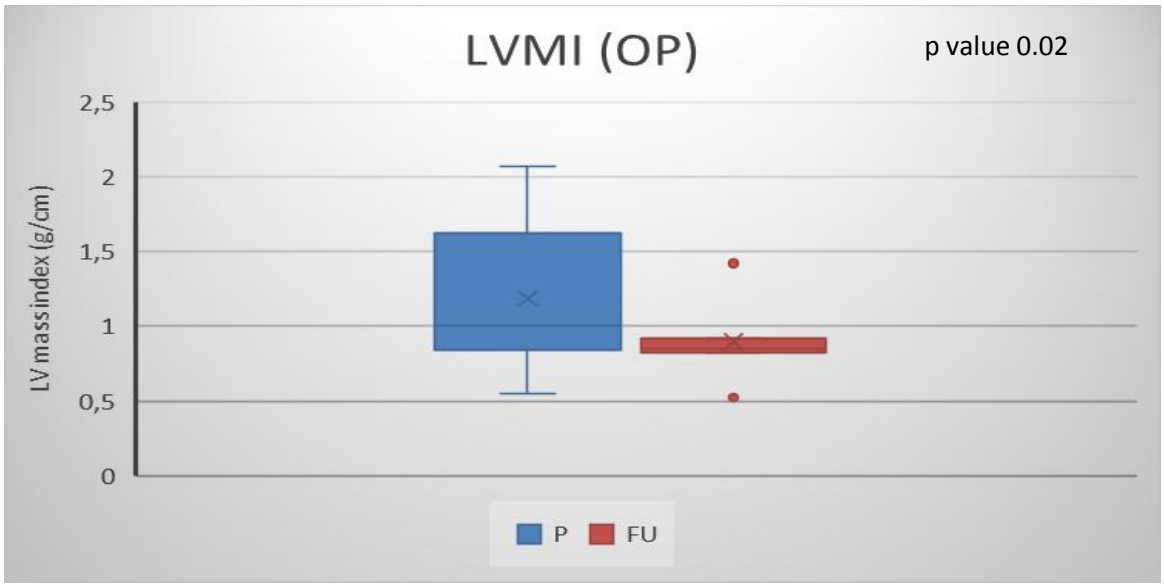

Figure 22. The difference between the LV mass index in P and FU studies in OP.

LV mass and WSS exhibited a statistically significant positive correlation.

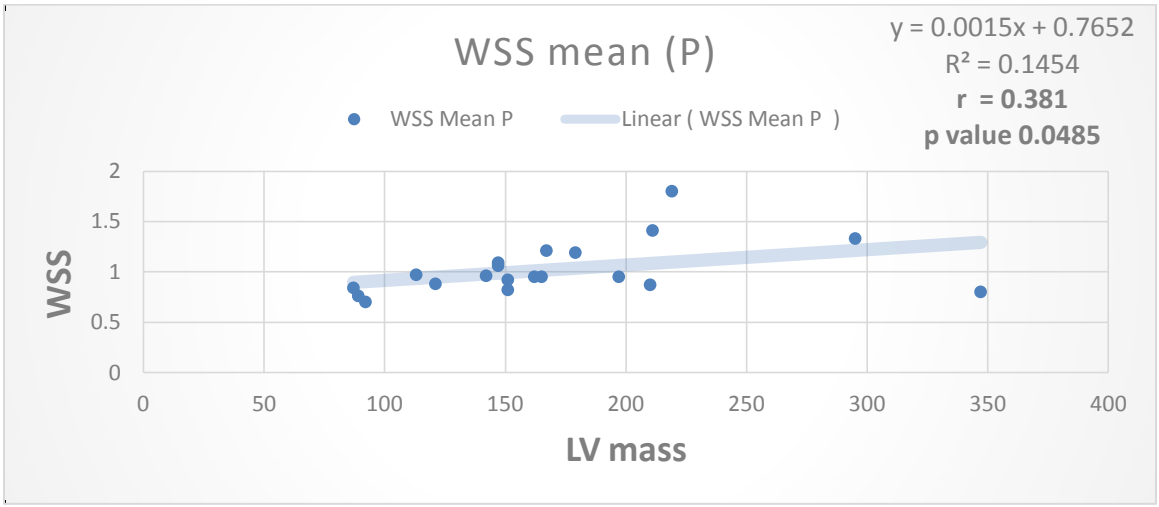

Figure 23. The positive correlation between the LV mass and the mean WSS in the thoracic aorta in P. WSS = wall shear stress, LV = left ventricle, P = primary.

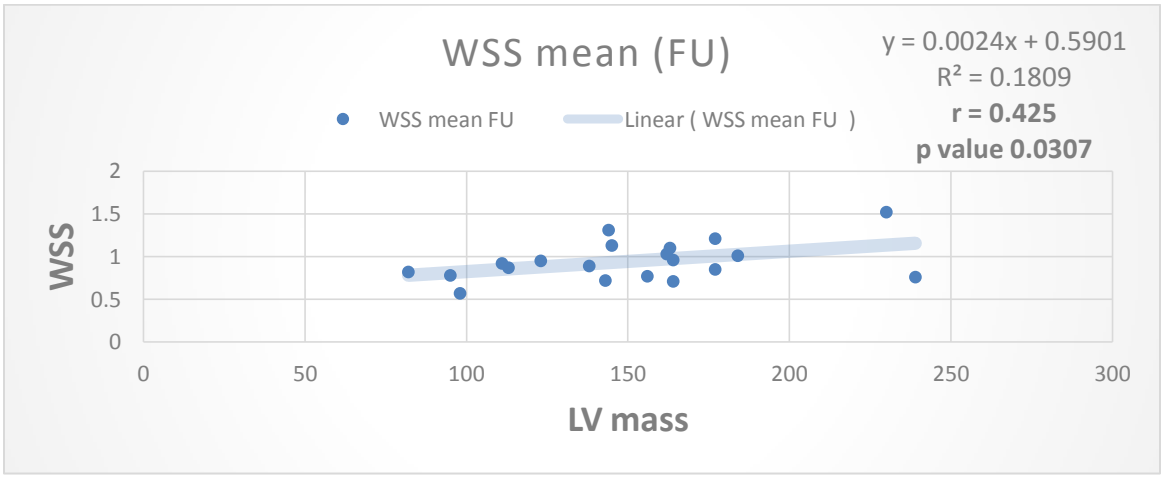

Figure 24. The positive correlation between the LV mass and the mean WSS in the thoracic aorta in FU. WSS = wall shear stress, LV = left ventricle, FU = follow-up.

Furthermore, there was no significant correlation between LVEF and WSS in both P (r = 0.25, p value: 0.29), and FU (r = 0.012, p value: 0.96). Neither P (r = 0.09, p value: 0.69) nor FU (r = 0.30, p value: 0.19) showed a significant correlation between the aortic diameter and WSS. The correlations between WSS and gender (P: r = 0.26, p value: 0.27; FU: r = 0.15, p value: 0.51), blood pressure (SBP: r = 0.24, p value: 0.29; DBP: r = 0.08, p value: 0.74) and heart rate (r = 0.24, p value: 0.31) did not reach significance. WSS tended to negatively

correlate with age (P: r = 0.31, p value: 0.092; FU: r = 0.41, p value: 0.038). The correlation between BMI and WSS, however, was not significant (r = 0.07, p value: 0.77).

11.2. Net flow in thoracic aorta

We used the EnSight program to calculate the net flow along the thoracic aorta in 8 planes. The analysis was conducted at three levels. **Level 1:** a mean flow of the entire thoracic aorta was obtained by summating the results from all eight planes. **At level 2,** the thoracic aorta was divided into three regions: ascending aorta, aortic arch, and descending aorta. In order to calculate the mean net flow in the ascending aorta, we added the results of P1 to 4. Plane 4 is situated in the transitional zone or border between the ascending aorta and aortic arch. By adding P5 and 6, we can obtain a mean flow in the aortic arch. A mean flow in the descending aorta is calculated by adding P7 and 8. **At Level 3,** we analyzed the net flow at each plane separately. Across all levels of analysis, we did not observe any significant changes in the net flow over time in the NOP. In contrast, we noticed a significant increase in the mean net flow of the thoracic aorta after surgery in the OP group. We observed increased mean net flow in the ascending aorta at the second analytical level, but no change in the mean net flow in the aortic arch and descending aorta. At the third level of analysis, net flow significantly increased in planes 1, 2 and 6 in OP (**plane 1**: P: 18.5±29.38 ml, FU: 55.36±12.7 ml, p value: 0.02; **plane 2**: P: 12.99±38.69 ml, FU: 63.67±21.61 ml, p value: 0.007; **plane 6**: P: 39.81±5.01 ml, FU: 42.64±4.6 ml, p value: 0.049).

Level 1 of Analysis:

The net flow from all eight analysis planes was added together to obtain a mean net flow for the entire thoracic aorta. There was no significant change in the net flow in the NOP (P: 56.66±17.87 ml, FU: 56.05±17.93 ml, p value: 0.81). In contrast, there was a significant increase in the mean net flow in the whole thoracic aorta in OP (P: 39.82±23.38 ml, FU: 51.23±15.62 ml, p value: 0.007).

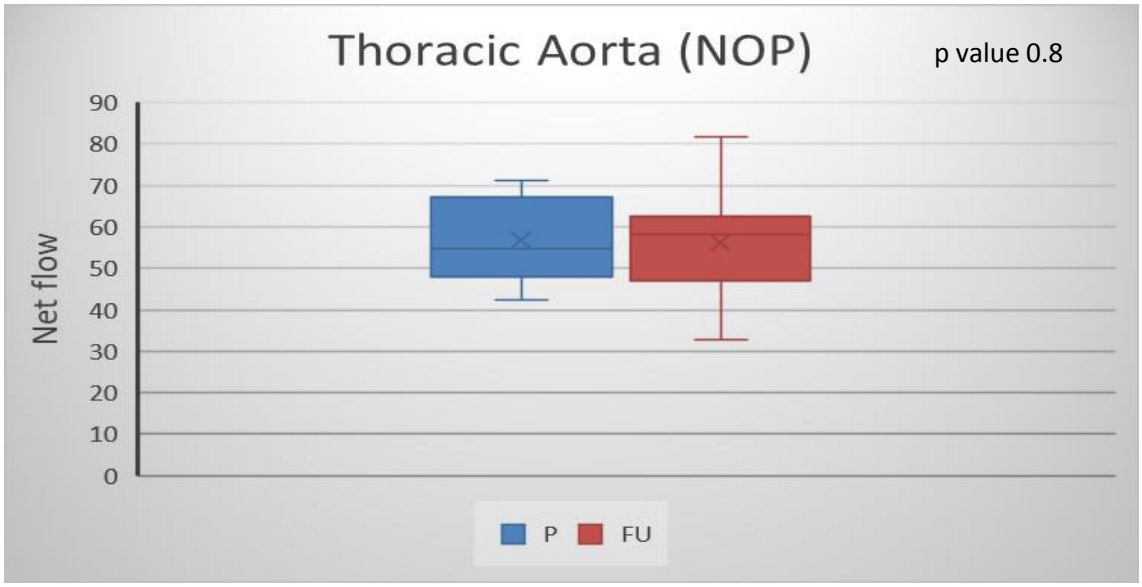

Figure 25. The difference between P and FU regarding the mean net flow in the entire thoracic aorta in NOP.

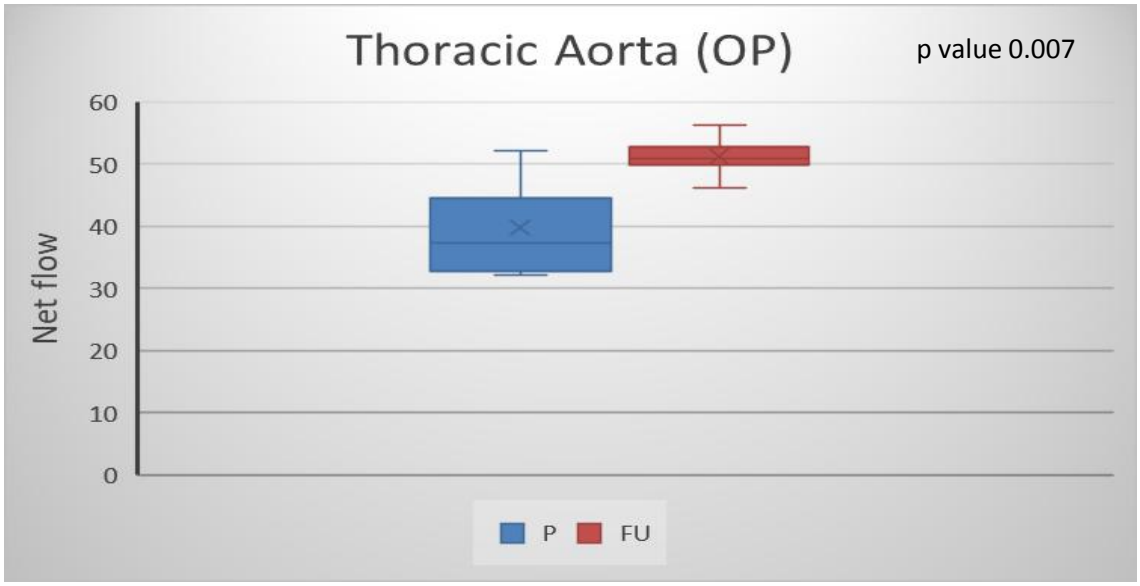

Figure 26. The difference between P and FU regarding the mean net flow in the entire thoracic aorta in OP.

Level 2 of analysis:

The NOP ascending aorta's net flow did not change significantly over time (P: 68.34±12.1 ml, FU: 64.35±13.41 ml, p value: 0.31). In contrast, OP showed a significant increase in ascending aortic mean net flow after surgery (P: 35.22±29.92 ml, FU: 60.81±11.09 ml, p value: 0.01).

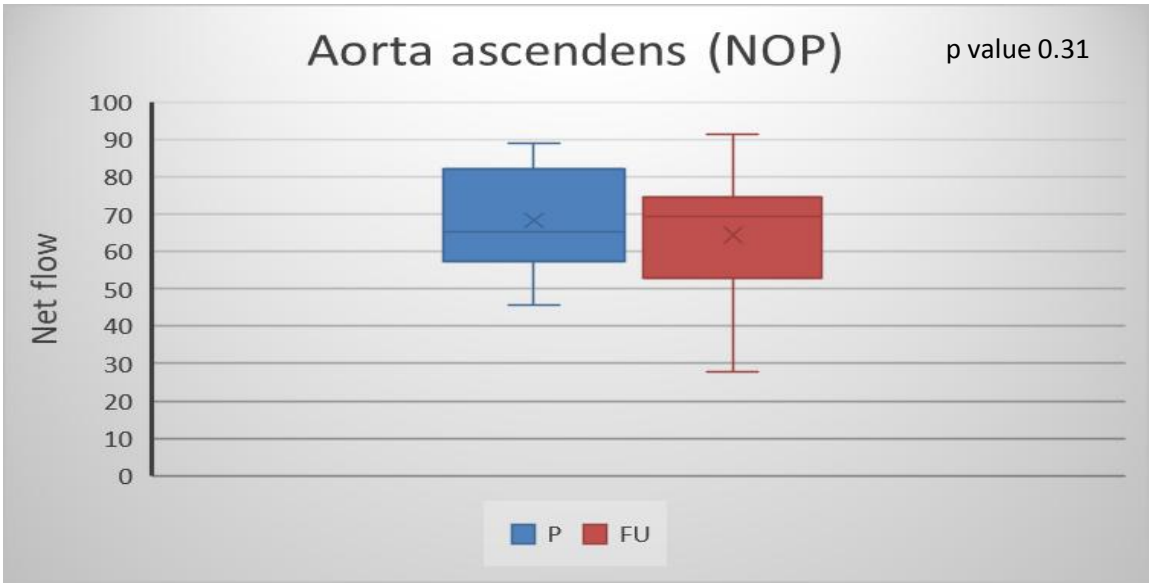

Figure 27. The difference between P and FU regarding the mean net flow in the entire ascending aorta in NOP.

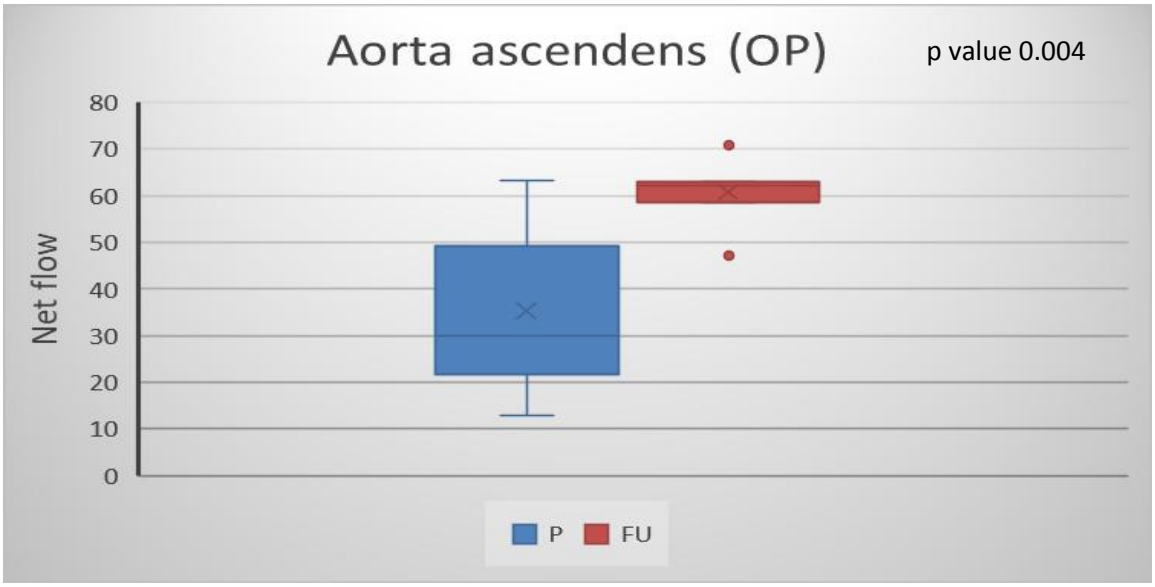

Figure 28. The difference between P and FU regarding the mean net flow in the entire ascending aorta in OP.

In both NOP and OP, the mean net flow in the aortic arch did not change significantly (NOP: P: 45.75±5.81 ml, FU: 49.01±2.48 ml, p value: 0.24; OP: P: 41.66±3.59 ml, FU: 43.5±3.31 ml, p value: 0.13).

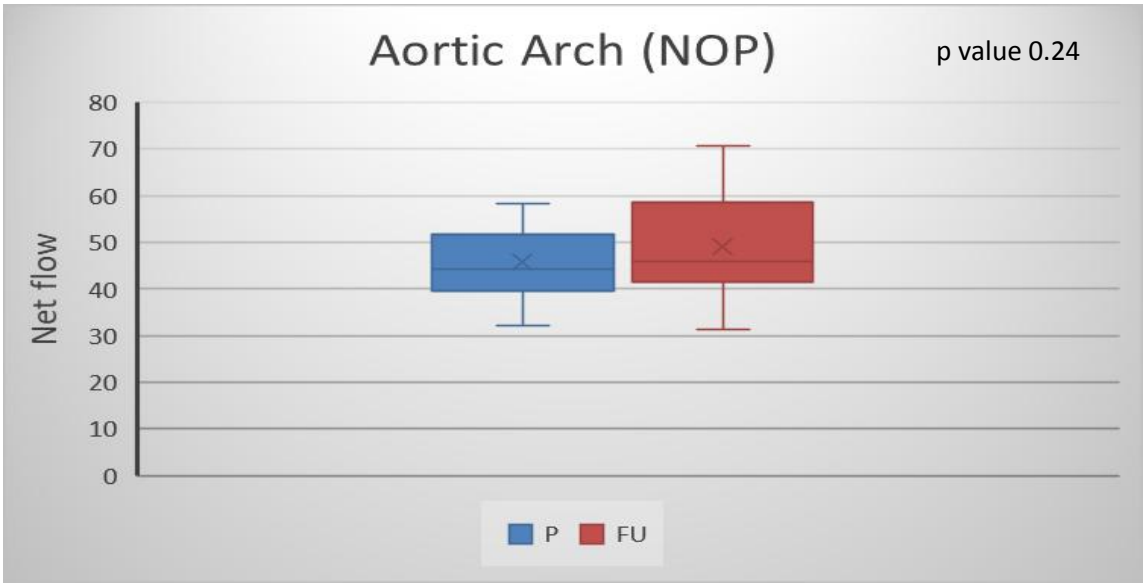

Figure 29. The difference between P and FU regarding the mean net flow in the entire aortic arch in NOP.

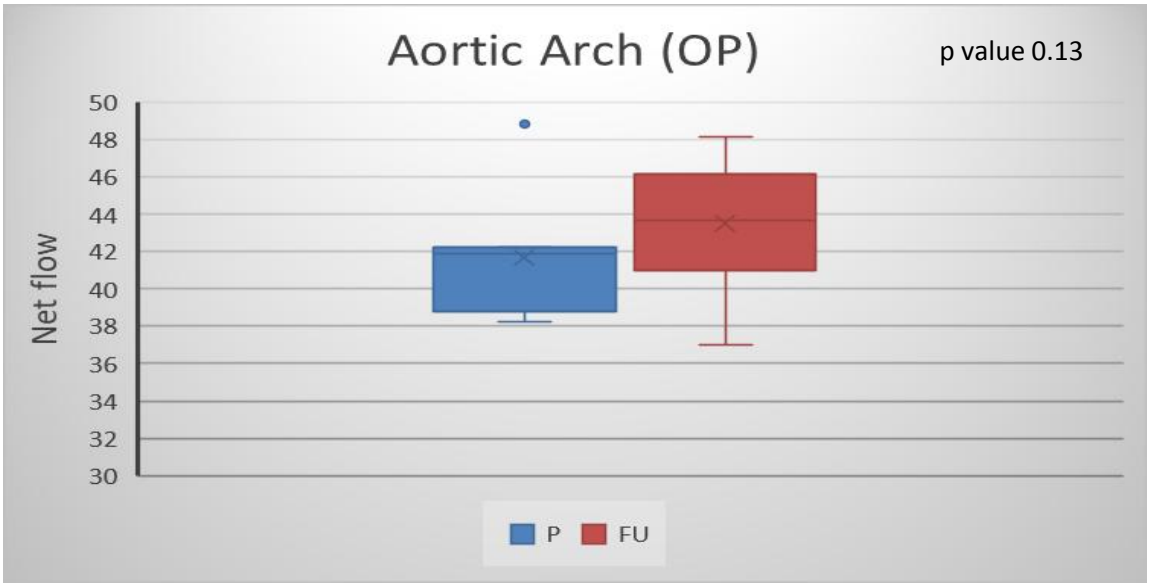

Figure 30. The difference between P and FU regarding the mean net flow in the entire aortic arch in OP.

Because plane 4 is in the transition zone between the ascending aorta and the aortic arch, a reanalysis was conducted, and plane 4 was considered to be the first part of the aortic arch. As a result, it was added to planes 5 and 6 to represent the aortic arch. In both NOP and OP, however, there was no significant change in the aortic arch net flow over time (NOP: P: 51.80±11.66 ml, FU: 55.13±11.10 ml, p value: 0.19; OP: P:47.74±10.98 ml, FU:49.33±10.40 ml, p value: 0.16).

In both NOP and OP, the mean net flow in the descending aorta did not differ significantly (NOP: P:42.86±4.33 ml, FU:40.29±7.65 ml, p value: 0.43; OP P:35.04±3.45 ml, FU:34.2±4.29 ml, p value: 0.74).

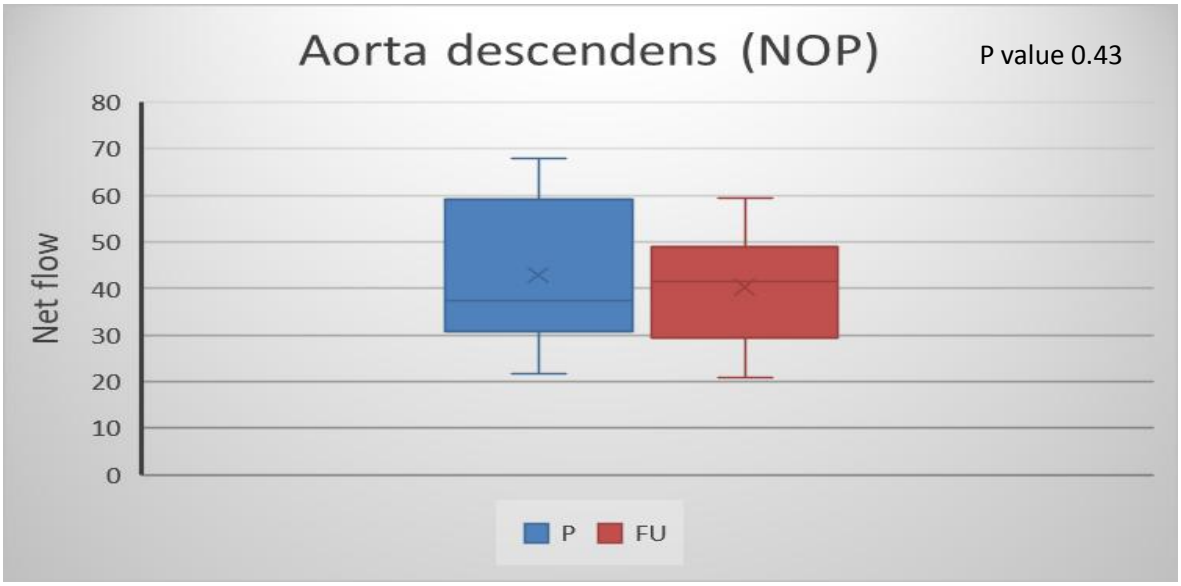

Figure 31. The difference between P and FU regarding the mean net flow in the entire descending aorta in NOP.

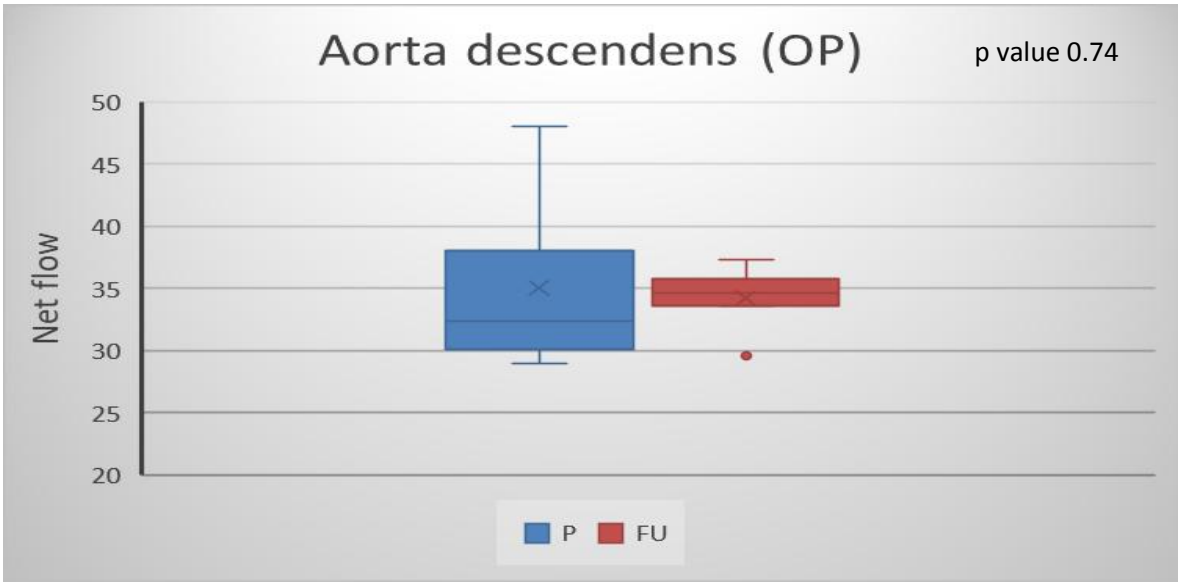

Figure 32. The difference between P and FU regarding the mean net flow in the entire descending aorta in OP.

Level 3 of analysis:

Net flow significantly increased in planes 1, 2 and 6 in OP (**plane 1:** P: 18.5±29.38 ml, FU: 55.36±12.7 ml, p value: 0.02; **plane 2:** P: 12.99±38.69 ml,

FU: 63.67±21.61ml, p value: 0.007; **plane 6:** P: 39.81±5.01 ml, FU: 42.64±4.6 ml, p value: 0.049). However, there were no significant changes in net flow in any plane in NOP.

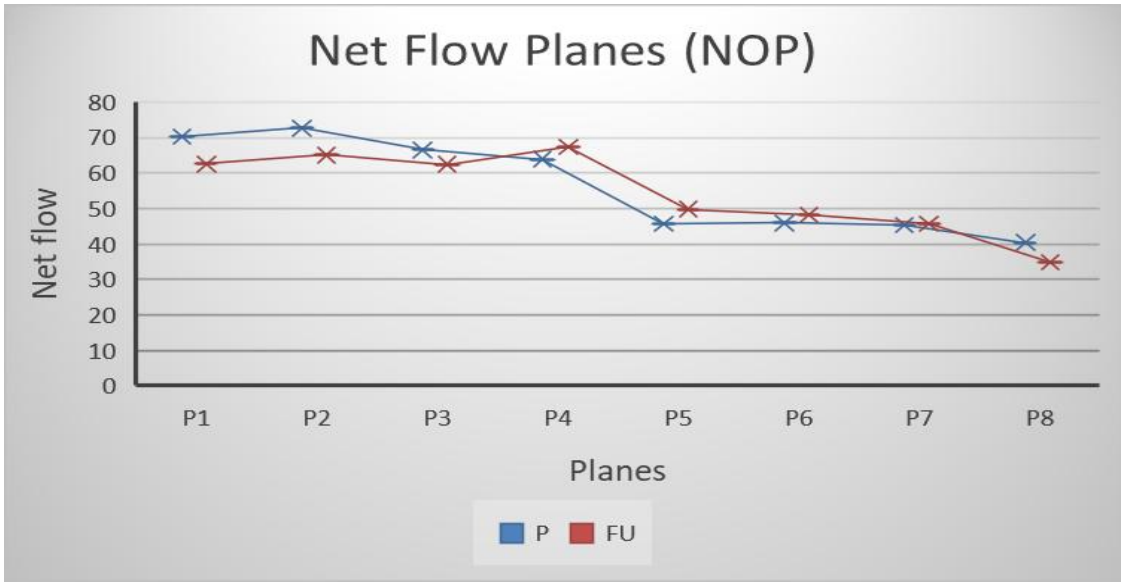

p value	
P1	0.13
P2	0.19
P3	0.51
P4	0.23
P5	0.25
P6	0.35
P7	0.88
P8	0.16

Figure 33. The difference between P and FU regarding the net flow at each individual plane throughout the thoracic aorta in NOP. There was no significant change in net flow over time.

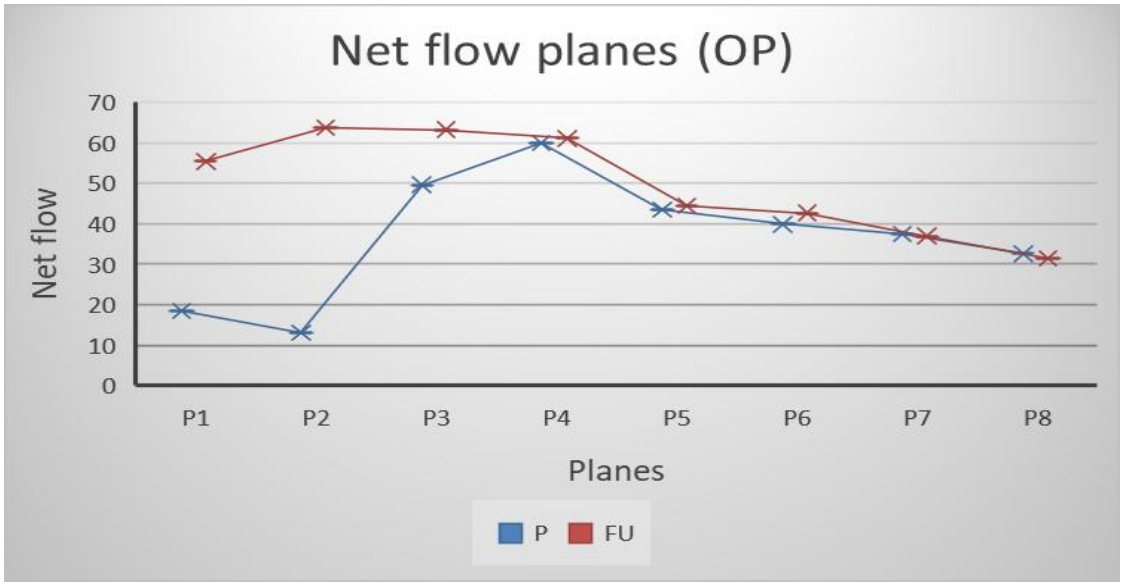

p value	
P1	0.01
P2	0.008
P3	0.09
P4	0.33
P5	0.38
P6	0.02
P7	0.40
P8	0.35

Figure 34. The difference between P and FU regarding the net flow in each individual plane throughout the thoracic aorta in OP. A significant increase was observed in net flow in planes 1, 2, and 6 over time.

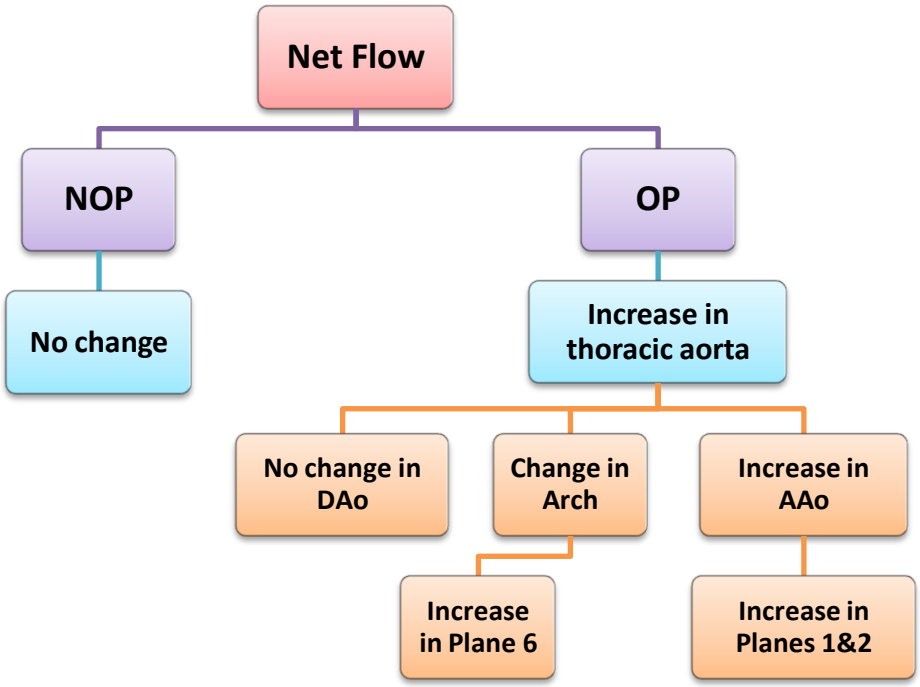

Figure 35. Summary of the results of net flow in both NOP and OP. AAo = ascending aorta, Arch = aortic arch, DAo = descending aorta.

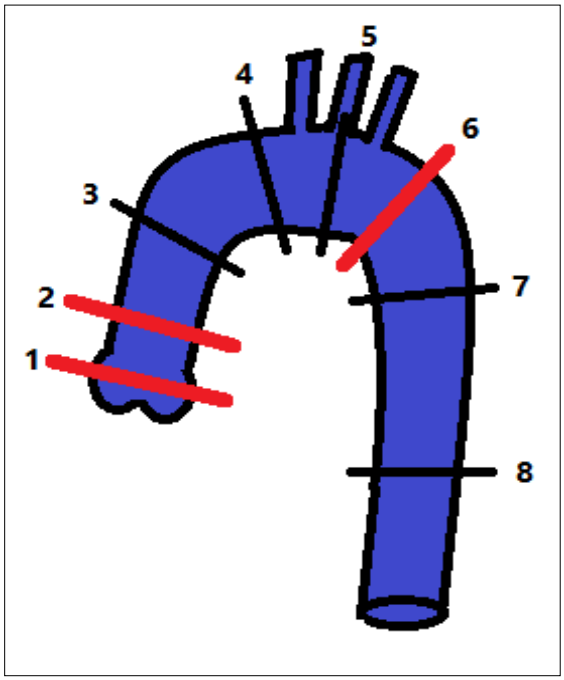

Figure 36. There is an increase in the mean net flow in planes 1, 2 and 6 (the red colored ones) in OP.

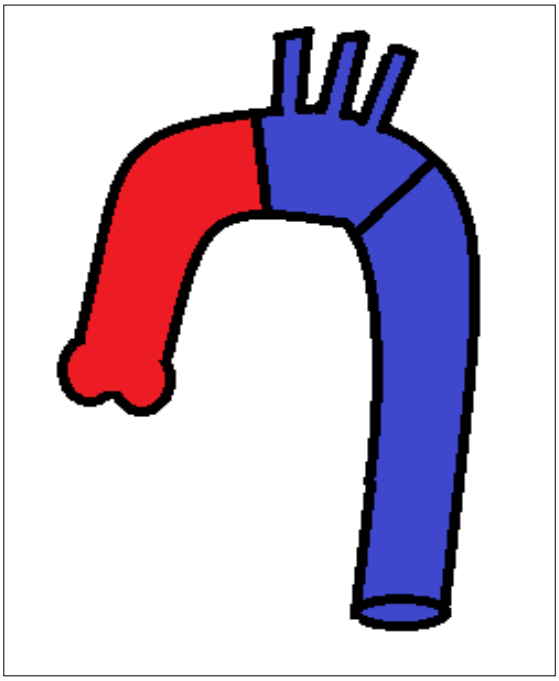

Figure 37. An increase in the mean net flow in OP's ascending aorta (the red-colored segment).

Net flow and WSS

A significant negative correlation was observed between the net flow in the ascending aorta and the WSS (all patients together, NOP and OP). The WSS increases when the net flow decreases (as in aortic stenosis). FU showed a trend toward a negative correlation; however, it was not statistically significant. This may be related to the fact that almost all the patients in FU have normal blood flow, either because there is no relevant aortic valve stenosis or because the blood flow after surgery has been normalized.

In the aortic arch, there was a trend toward a significant positive correlation between net flow and WSS in P, while in FU, the positive correlation became statistically significant.

In the descending aorta, a statistically significant positive correlation was observed between net flow and WSS in both P and FU.

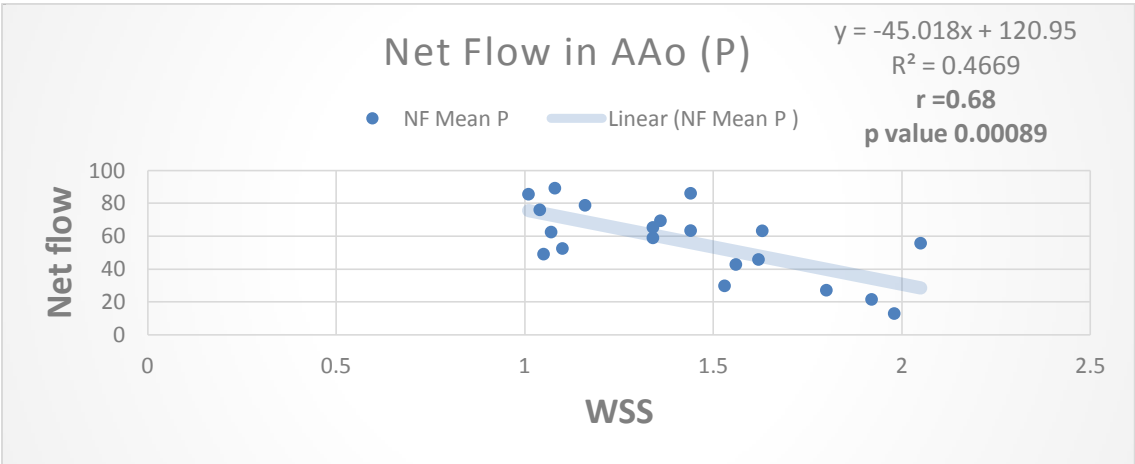

Figure 38. The negative correlation between the net flow and the WSS in the ascending aorta in P. NF = Net Flow, AAo = ascending aorta.

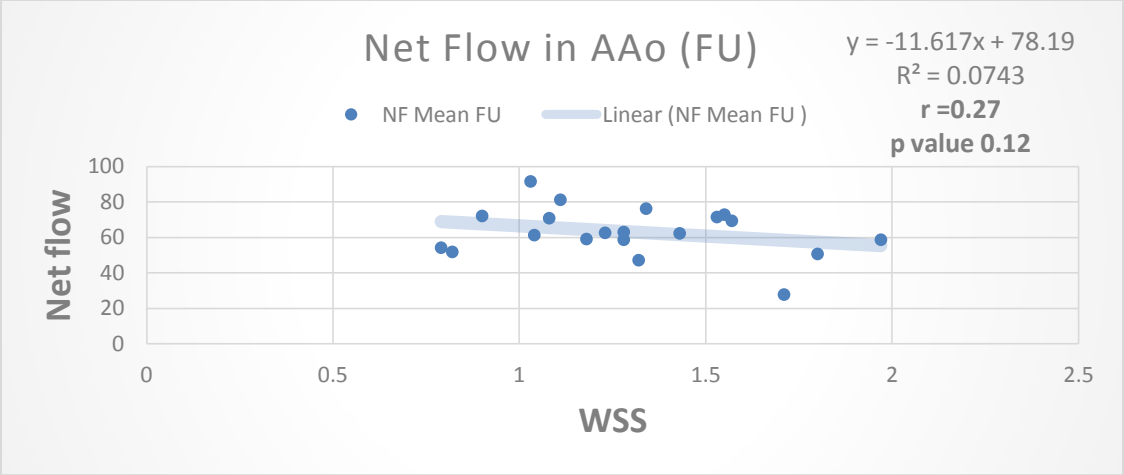

Figure 39. The correlation between the net flow and the WSS in the ascending aorta in FU. NF = Net Flow, AAo = ascending aorta.

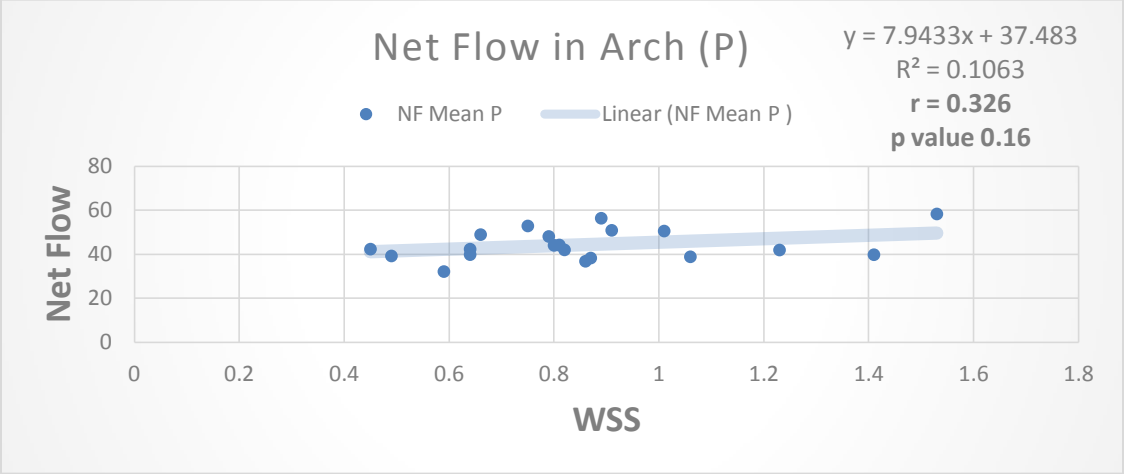

Figure 40. The correlation between the net flow and the WSS in the aortic arch in P.

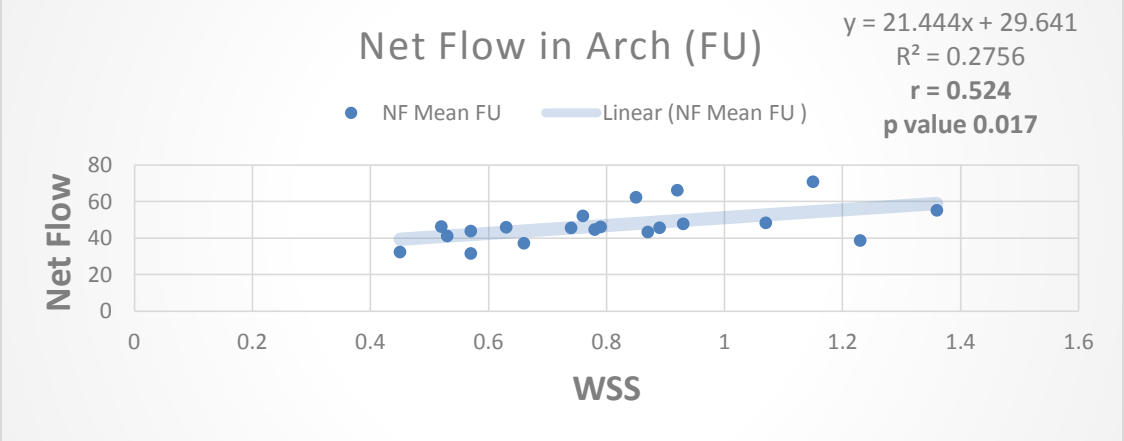

Figure 41. The correlation between the net flow and the WSS in the aortic arch in FU.

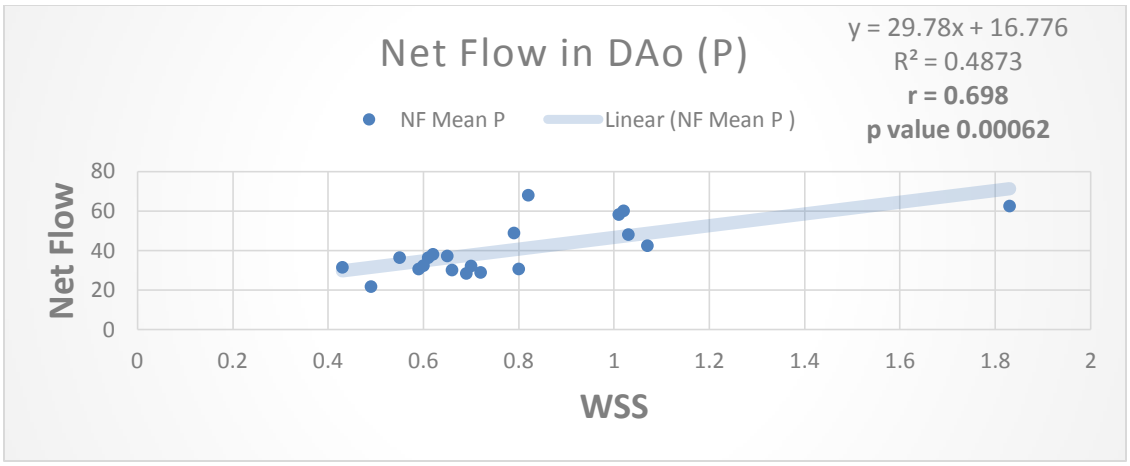

Figure 42. The correlation between the net flow and the WSS in the descending aorta in P. DAo = descending aorta.

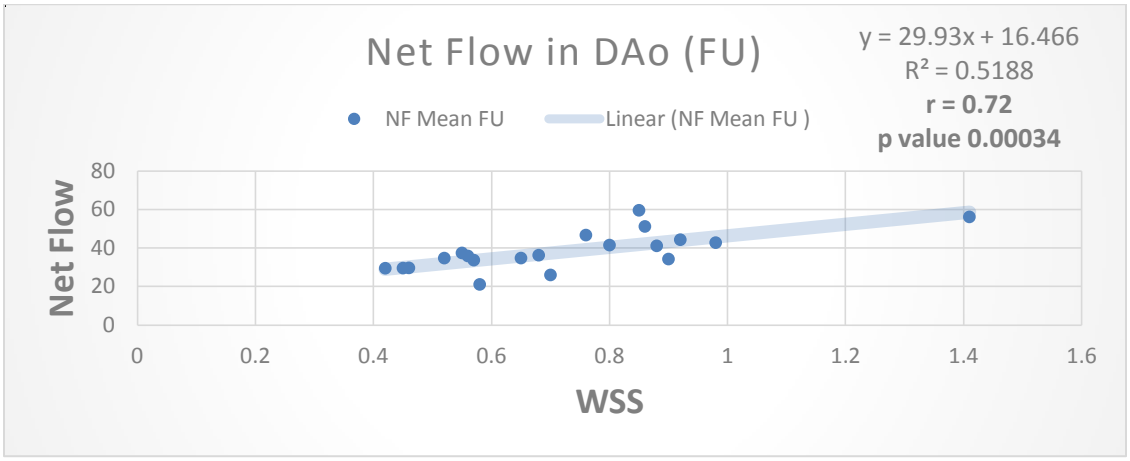

Figure 43. The correlation between the net flow and the WSS in the descending aorta in FU. DAo = descending aorta.

11.3. Wall shear stress (WSS) in thoracic aorta

For the purpose of analyzing the WSS, the thoracic aorta was divided into 18 segments. Ascending aorta, aortic arch, and descending aorta were divided into 6 segments each. The WSS was calculated at four levels. In the first level of analysis, the results of 18 segments were added together to calculate the mean WSS for the entire thoracic aorta. In the second level of analysis, the thoracic aorta was divided into ascending, arch, and descending aorta. A mean WSS in the ascending aorta was obtained by adding the results of segments 1 to 6. A mean WSS for the aortic arch was obtained by adding the WSS results of

segments 7 to 12. The mean WSS in the descending aorta was obtained by adding the results of segments 13 to 18. At the third level of analysis, WSS results for segments with odd numbers (1,3,5,7,9,11,13,15,17) were added to derive the mean WSS for the outer aortic curvature and WSS results for segments with even numbers (2,4,6,8,10,12,14,16,18) were added to derive the mean WSS for the inner aortic curvature. The addition of segments (1,3,5) yielded a mean WSS for ascending aorta outer curvature. Adding the WSS results of segments (7,9,11) yielded a mean WSS in the aortic arch outer curvature. Adding the WSS results of segments (13,15,17) gave a mean WSS in the descending aorta outer curvature. The mean WSS in ascending aorta inner curvature was obtained by adding WSS results from segments (2,4,6). A mean WSS in the aortic arch inner curvature was calculated by adding the WSS results of segments (8,10,12). Adding the WSS results of segments (14,16,18) resulted in the mean WSS in the descending aorta. The fourth level was to calculate WSS at each segment separately.

Level 1 of analysis:

The mean WSS in the entire thoracic aorta significantly decreases in OP (P: 1.07±0.54 N/m^2, FU:0.88±0.39 N/m^2, p value: 0.02), with no significant change in NOP (P: 0.998±0.36 N/m^2, FU:0.978±0.34 N/m^2, p value: 0.61) over time.

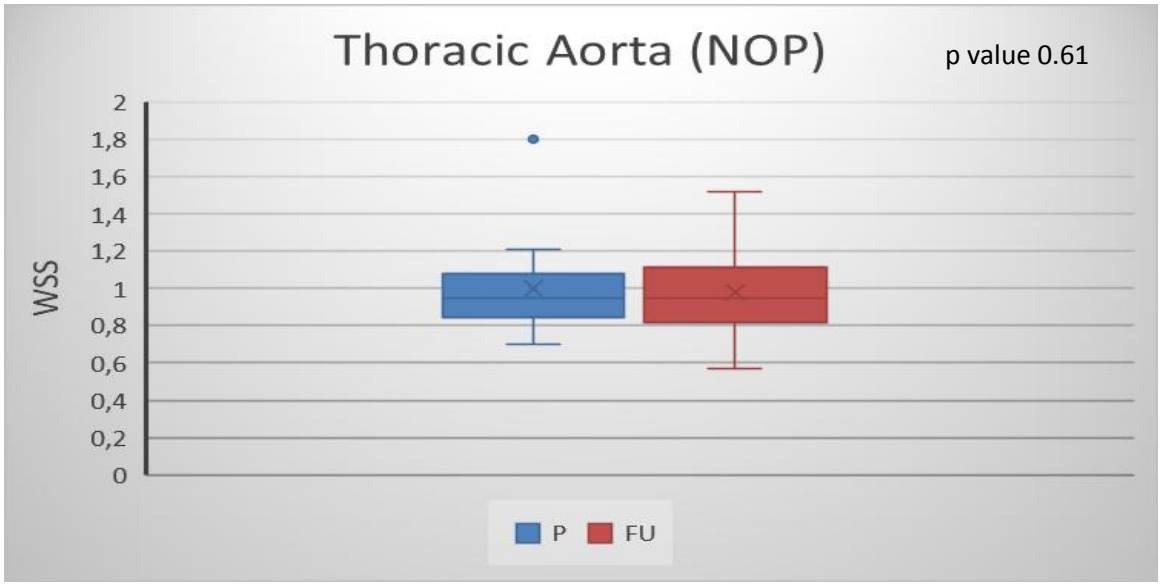

Figure 44. The difference between P and FU regarding the WSS in the whole thoracic aorta in NOP.

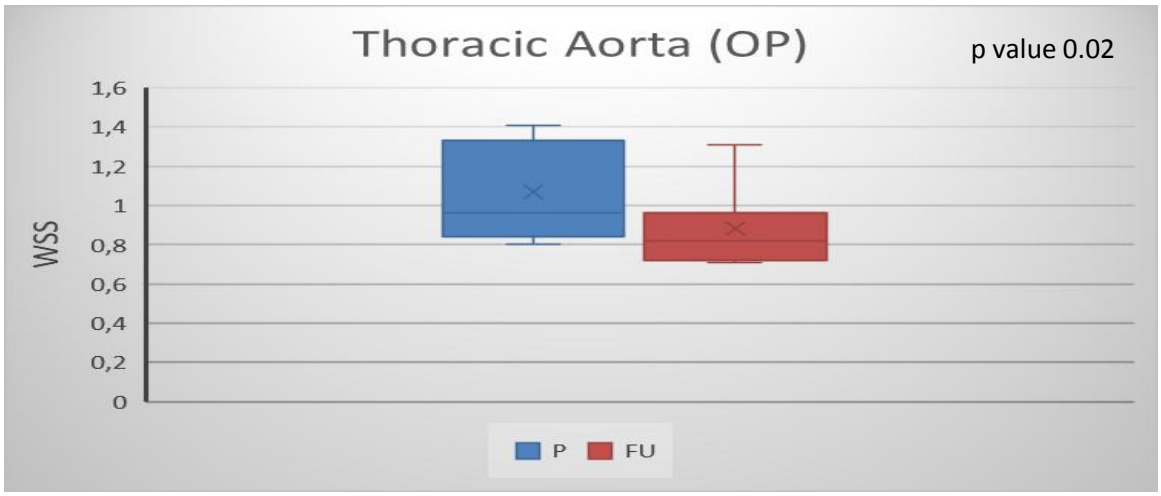

Figure 45. The difference between P and FU regarding the WSS in the whole thoracic aorta in OP.

Level 2 of analysis:

WSS significantly decreased in OP group in the ascending aorta (P: 1.61±0.57 N/m^2, FU: 1.33±0.32 N/m^2, p value: 0.03). There was a borderline decrease in the aortic arch (P: 0.93±0.15 N/m^2, FU: 0.71±0.09 N/m^2, p value: 0.05) and a significant decrease in the descending aorta (P: 0.67±0.13 N/m^2, FU: 0.6±0.11 N/m^2, p value: 0.03). In NOP, there was no significant change in WSS over time in either ascending aorta (P: 1.33±0.39 N/m^2, FU: 1.28±0.33 N/m^2, p value: 0.39), aortic arch (P: 0.82±0.13 N/m^2, FU: 0.87±0.15 N/m^2, p value: 0.55) or descending aorta (P: 0.85±0.14 N/m^2, FU: 0.79±0.14 N/m^2, p value: 0.13).

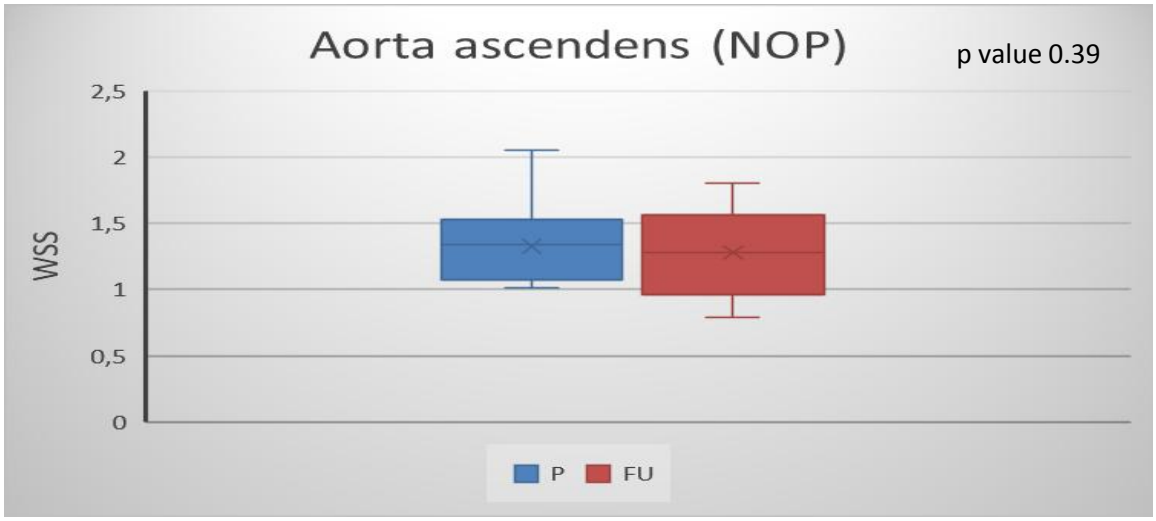

Figure 46. The difference between P and FU regarding the WSS in the ascending aorta in NOP.

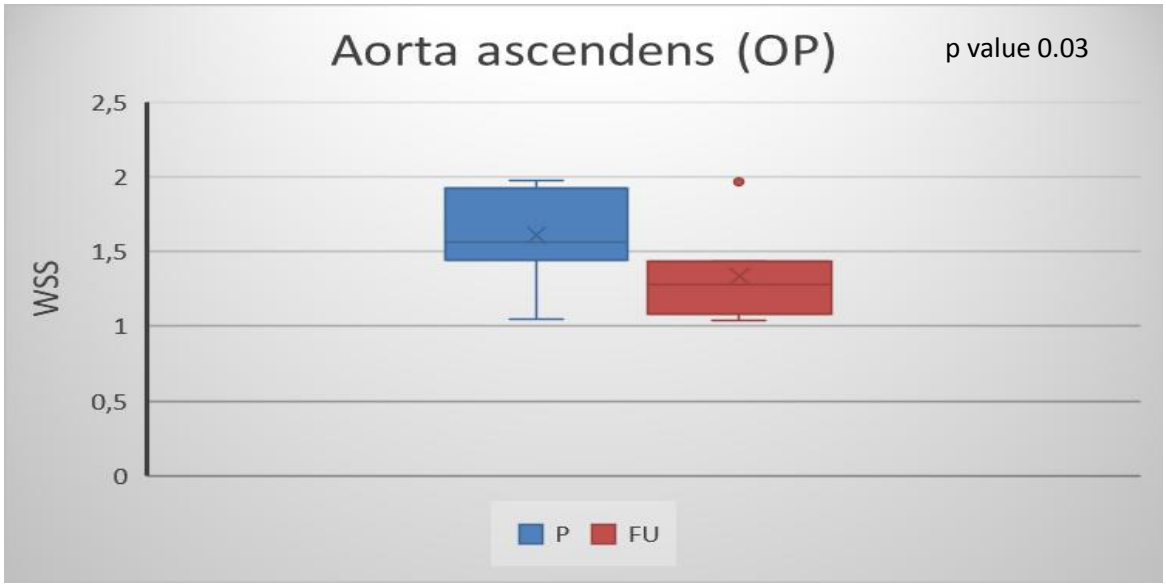

Figure 47. The difference between P and FU regarding the WSS in the ascending aorta in OP.

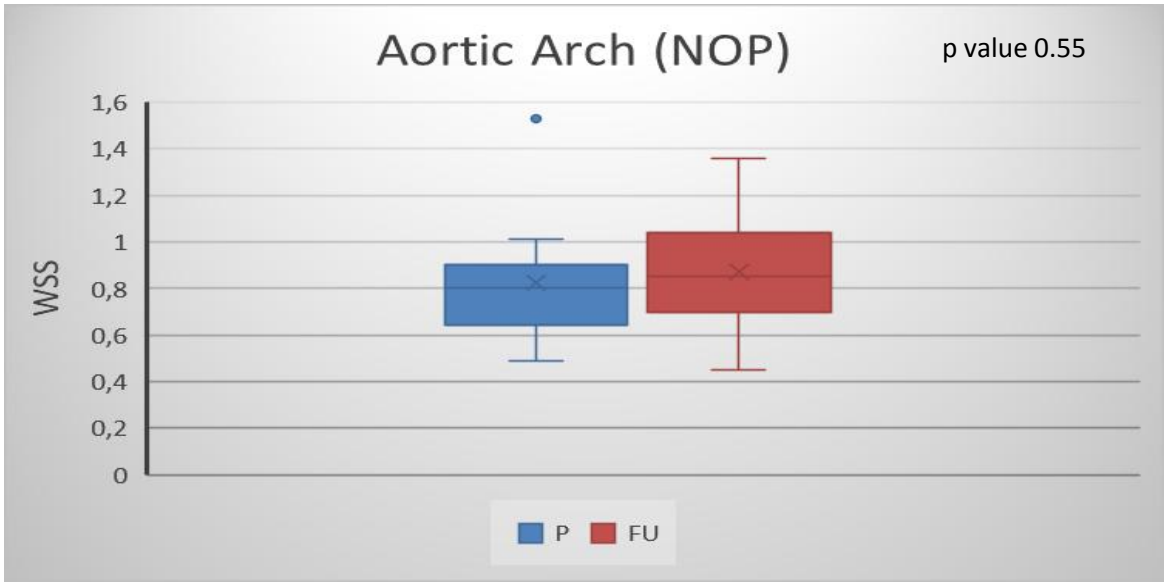

Figure 48. The difference between P and FU regarding the WSS in the aortic arch in NOP.

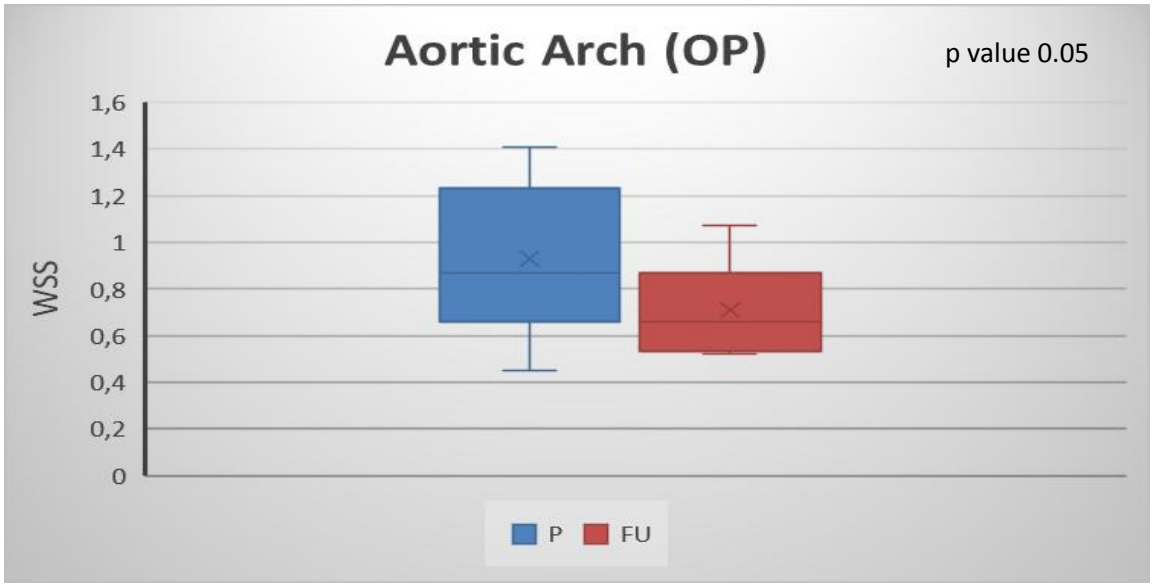

Figure 49. The difference between P and FU regarding the WSS in the aortic arch in OP.

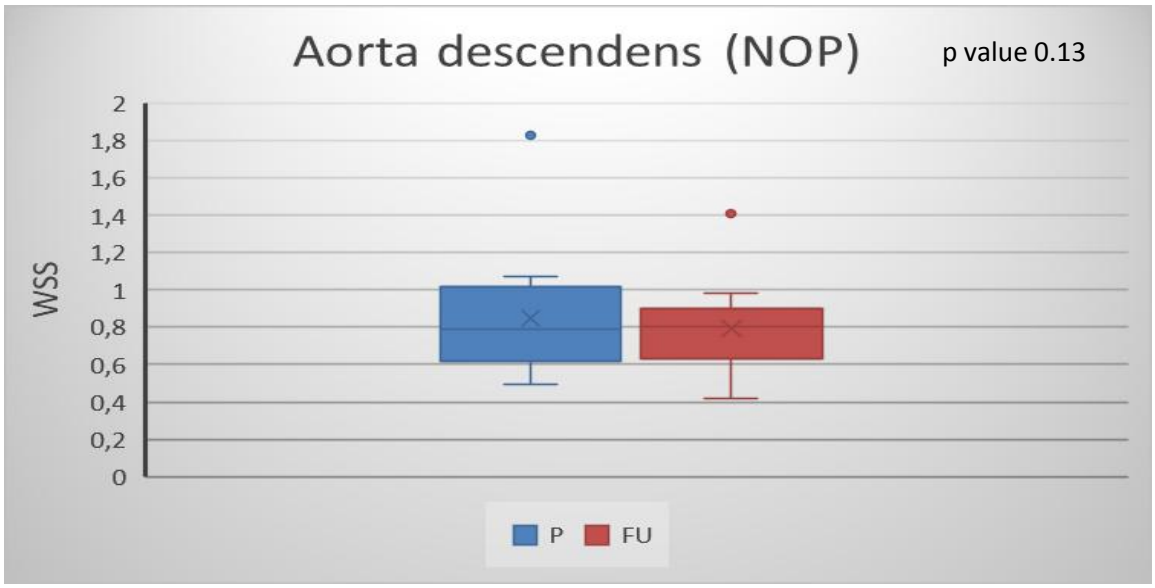

Figure 50. The difference between P and FU regarding the WSS in the descending aorta in NOP.

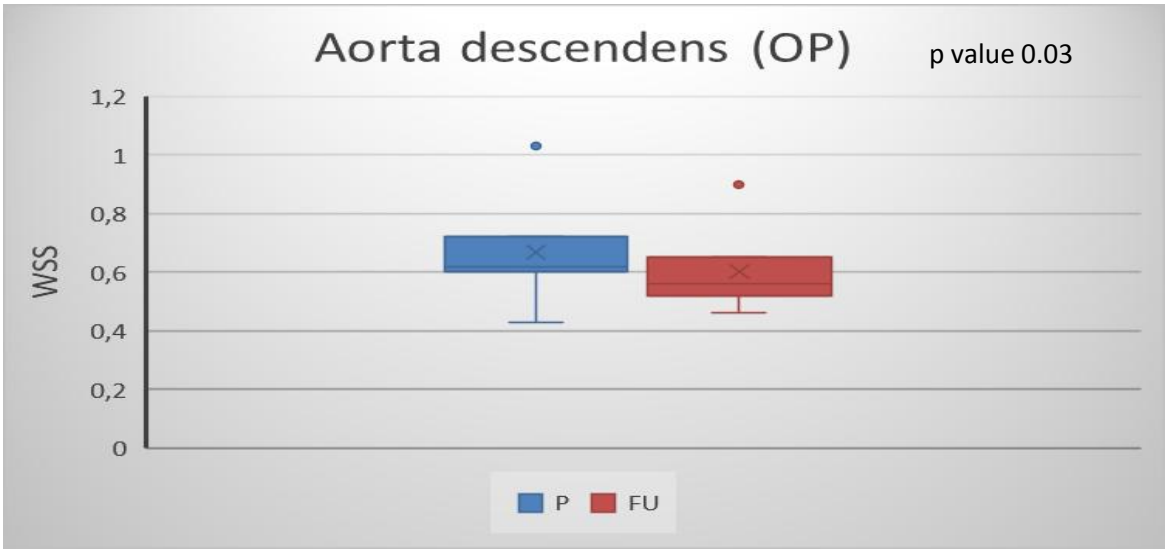

Figure 51. The difference between P and FU regarding the WSS in the descending aorta in OP.

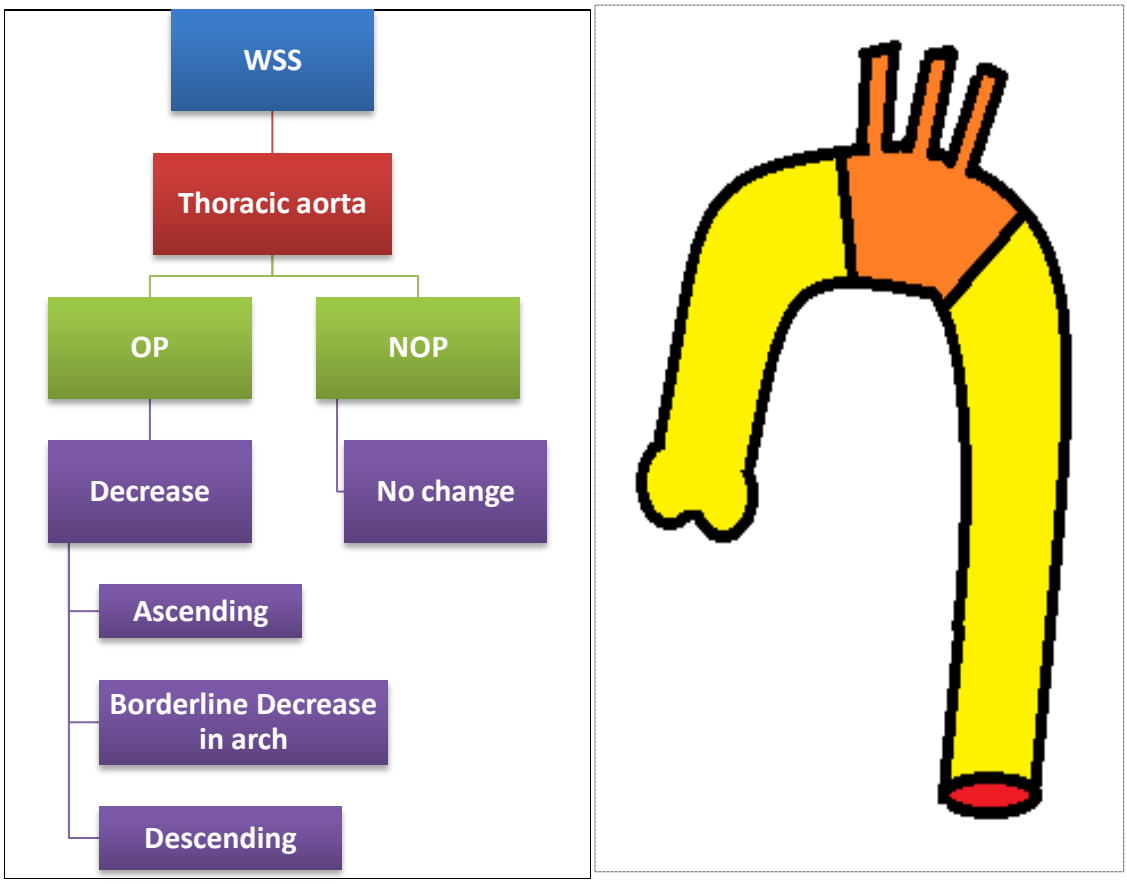

Figure 52. On the left side: summary of WSS results in thoracic aorta in both NOP and OP. On the right side: Color-coded representation of the WSS changes in OP; a significant decrease in the mean WSS in ascending and descending aorta (yellow-colored segments) with a borderline significant decrease in WSS in the aortic arch (the orange-colored segment).

NOP did not show a significant change in the mean WSS throughout the thoracic aorta's outer curvature (P: 0.96±0.34 N/m^2, FU: 0.98±0.35 N/m^2, p value: 0.75). There was, however, a significant decrease in the mean WSS throughout the outer curvature of the thoracic aorta in OP (P: 1.11±0.59 N/m^2, FU: 0.89±0.42 N/m^2, p value: 0.02).

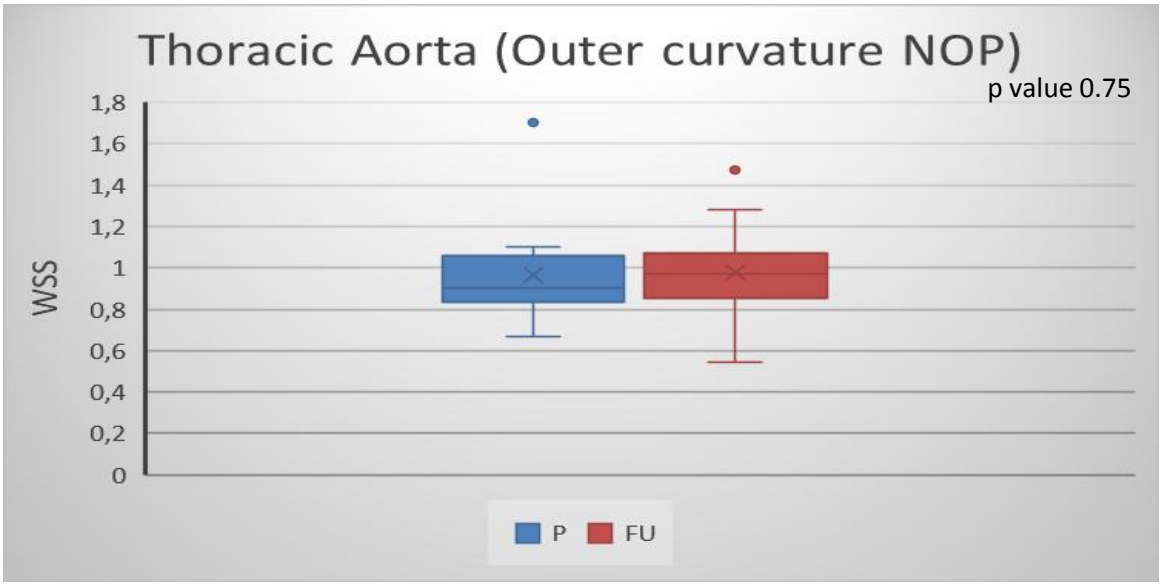

Figure 53. The difference between P and FU regarding the mean WSS throughout the outer curvature of the whole thoracic aorta in NOP.

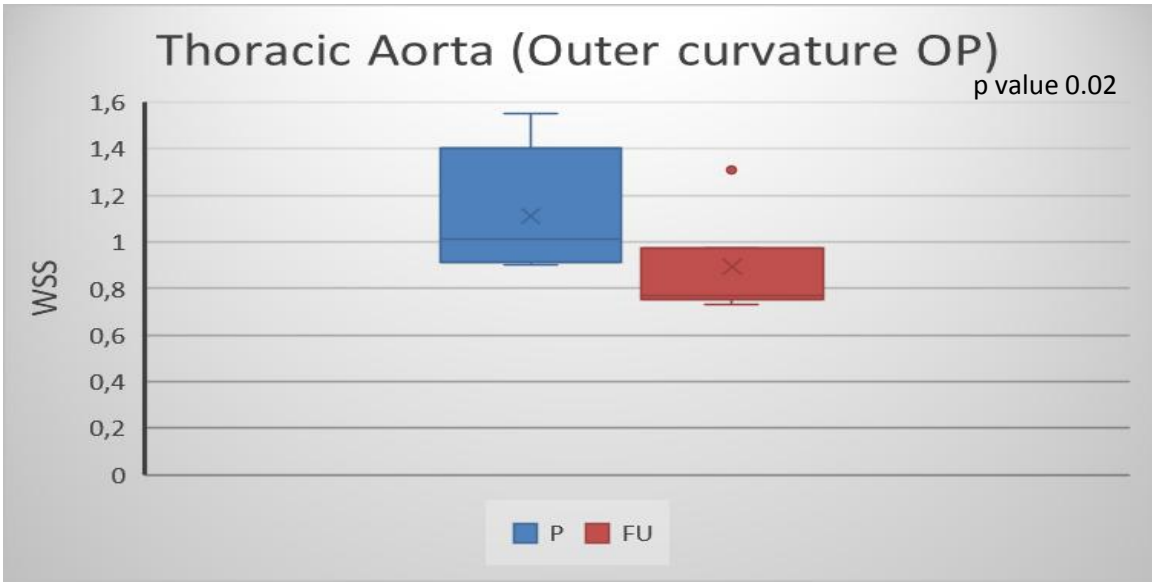

Figure 54. The difference between P and FU regarding the mean WSS throughout the outer curvature of the whole thoracic aorta in OP.

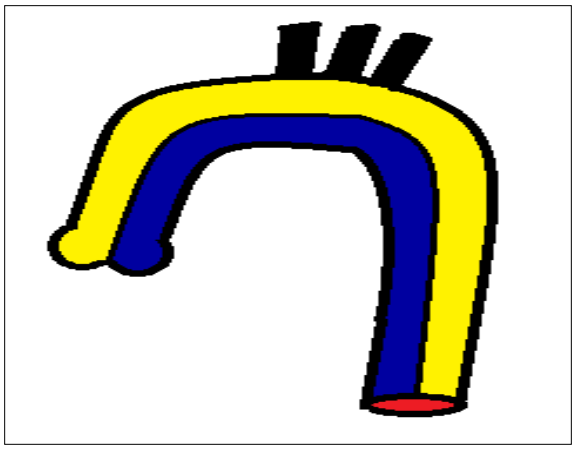

Figure 55. In OP, a significant decrease in the mean WSS along the outer aortic curvature (the yellow-colored segment) was observed.

The mean WSS throughout the inner curvature of the thoracic aorta did not change significantly in NOP (P: 1.04±0.38 N/m^2, FU: 0.98±0.34 N/m^2, p value: 0.16). On the other hand, there was a borderline decrease in the mean WSS throughout the inner curvature of the whole thoracic aorta in OP (P: 1.02±0.48 N/m^2, FU: 0.87±0.37 N/m^2, p value: 0.06).

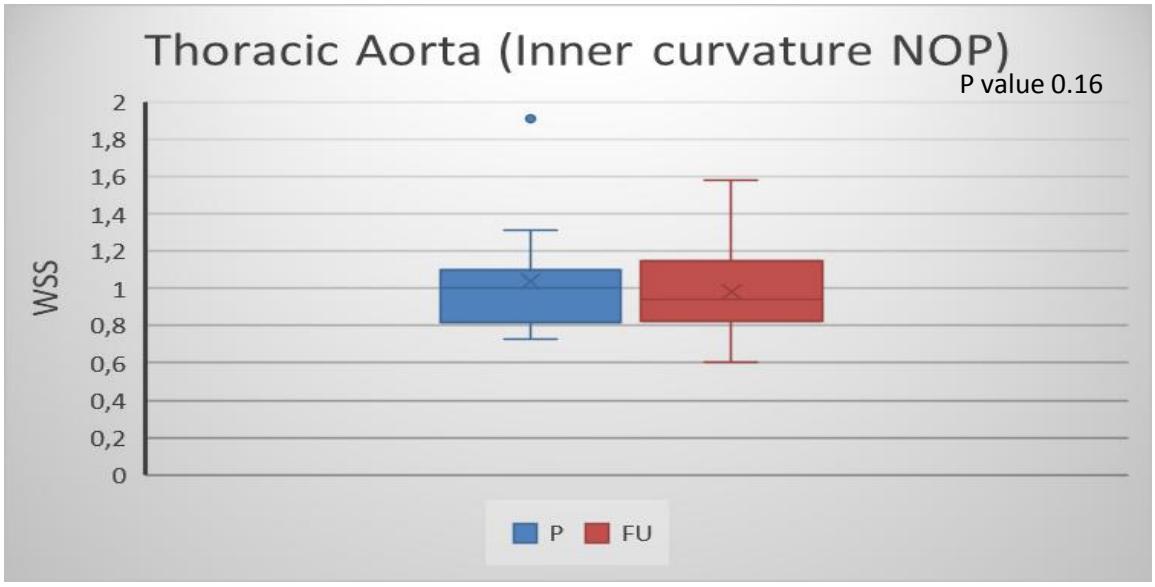

Figure 56. The difference between P and FU regarding the mean WSS throughout the inner curvature of the whole thoracic aorta in NOP.

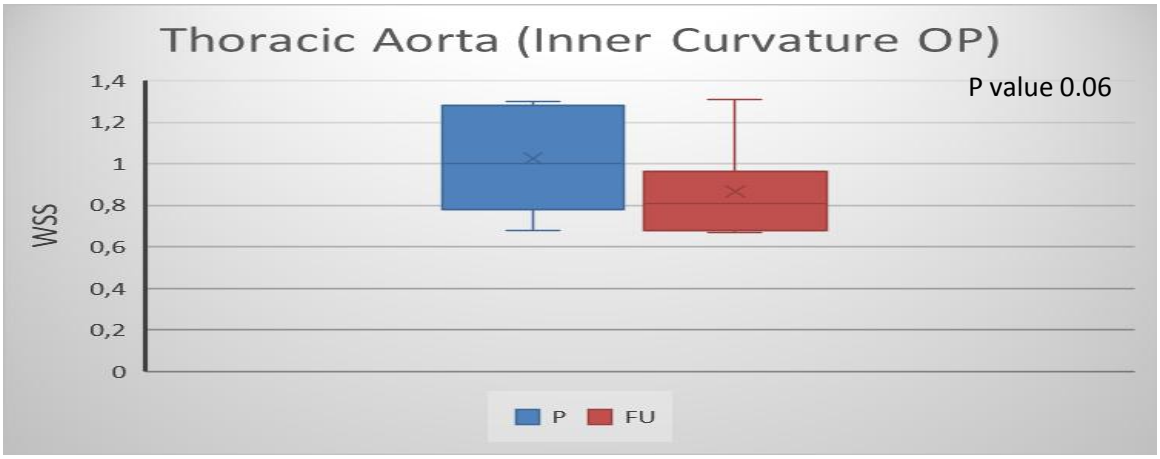

Figure 57. The difference between P and FU regarding the mean WSS throughout the inner curvature of the whole thoracic aorta in OP.

In NOP, the mean WSS in the outer curvature of the ascending aorta did not change significantly (P: 1.29±0.26 N/m^2, FU: 1.3±0.24 N/m^2, p value: 0.86). There was, however, a significant decrease in mean WSS in the outer curvature of the ascending aorta in OP (P: 1.76±0.49 N/m^2, FU: 1.39±0.33 N/m^2, p value: 0.02). Interestingly, there was a significant decrease in mean WSS in the inner curvature of the ascending aorta in NOP (P: 1.37±0.48 N/m^2, FU: 1.25±0.42 N/m^2, p value: 0.048). In contrast, the mean WSS in the inner curvature of the ascending aorta in the OP did not significantly change (P: 1.46±0.53 N/m^2, FU: 1.27±0.32 N/m^2, p value: 0.17).

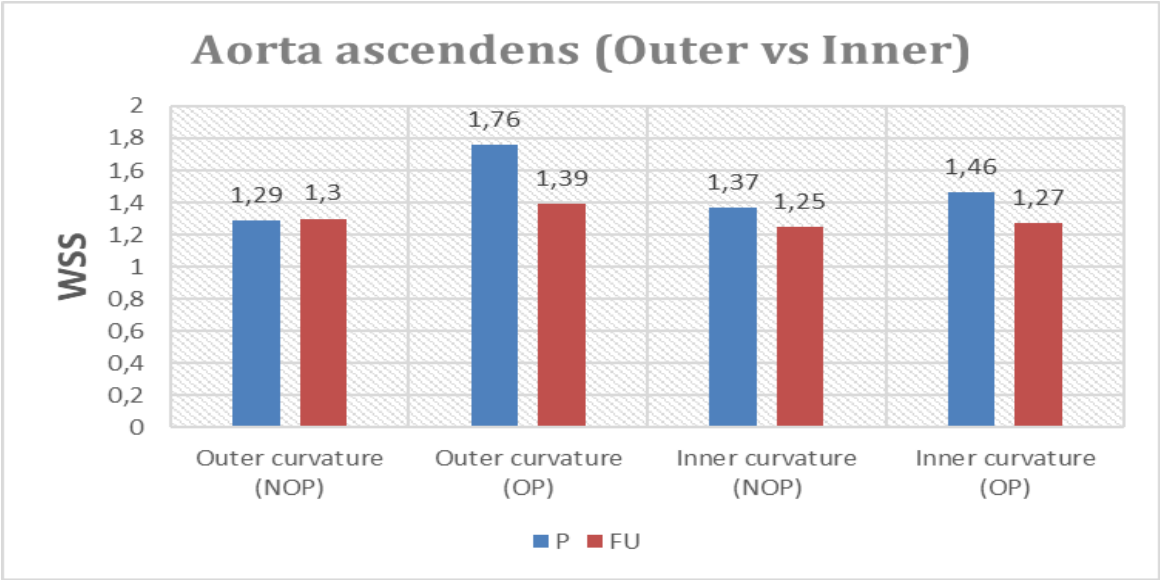

Figure 58. The difference between P and FU as well as the difference between outer and inner aortic curvature regarding the mean WSS in the ascending aorta in both NOP and OP. Outer = outer aortic curvature, Inner = inner aortic curvature.

There was no significant change in mean WSS in the outer curvature of the aortic arch in NOP (P: 0.77±0.13 N/m^2, FU: 0.85±0.18 N/m^2, p value: 0.17). However, a significant decrease in mean WSS was found in the outer curvature of the aortic arch in OP (P: 0.93±0.17 N/m^2, FU: 0.7±0.10 N/m^2, p value: 0.03).

There was no significant change in mean WSS in the inner curvature of the aortic arch in NOP (P: 0.87±0.09 N/m^2, FU: 0.89±0.08 N/m^2, p value: 0.75). Likewise, there was no significant change in mean WSS in the inner curvature of the aortic arch in OP (P: 0.92±0.12 N/m^2, FU: 0.72±0.08 N/m^2, p value: 0.09).

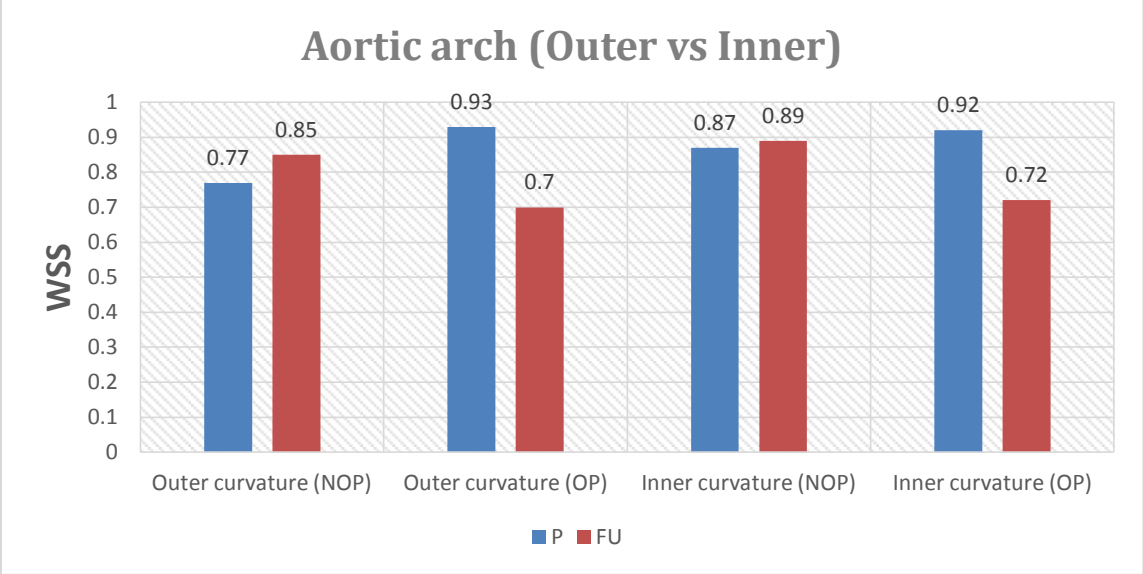

Figure 59. The difference between P and FU as well as the difference between outer and inner aortic curvature regarding the mean WSS in the aortic arch in both NOP and OP.

NOP showed no significant change in mean WSS in the outer curvature of the descending aorta (P: 0.83±0.14 N/m^2, FU: 0.78±0.16 N/m^2, p value: 0.22). Likewise, there was no significant change in mean WSS in the outer curvature of the descending aorta in OP (P: 0.64±0.11 N/m^2, FU: 0.59±0.10 N/m^2, p value: 0.08). In addition, there was no significant change in mean WSS in the inner curvature of the descending aorta in NOP (P: 0.86±0.15 N/m^2, FU: 0.80±0.13 N/m^2, p value: 0.13). However, the mean WSS in the inner curvature of the descending aorta significantly decreased in OP (P: 0.70±0.14 N/m^2, FU: 0.61±0.11 N/m^2, p value: 0.04).

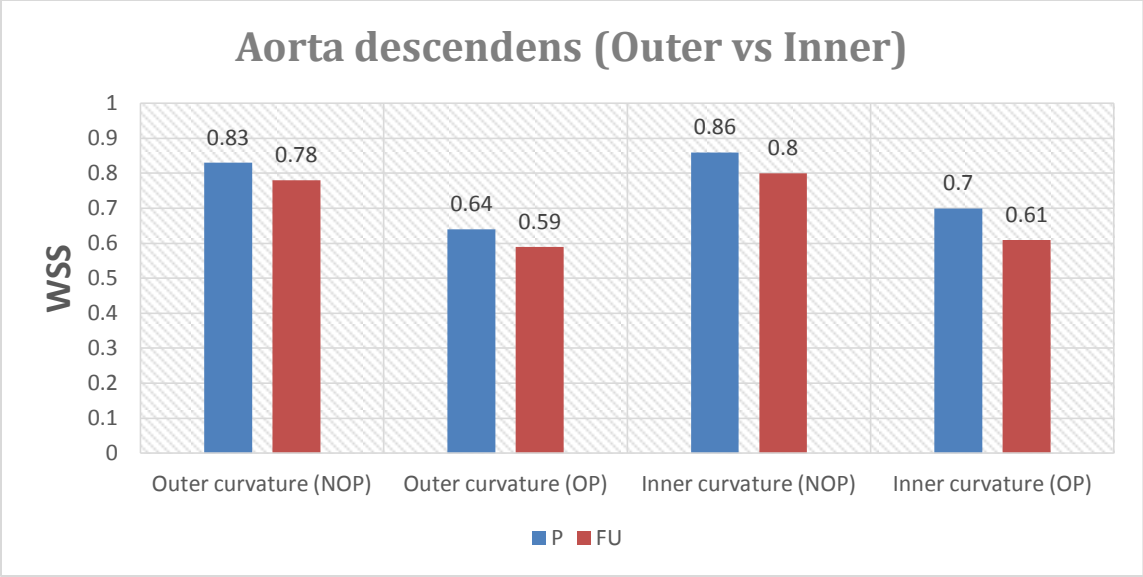

Figure 60. The difference between P and FU as well as the difference between outer and inner aortic curvature regarding the mean WSS in the descending aorta in both NOP and OP.

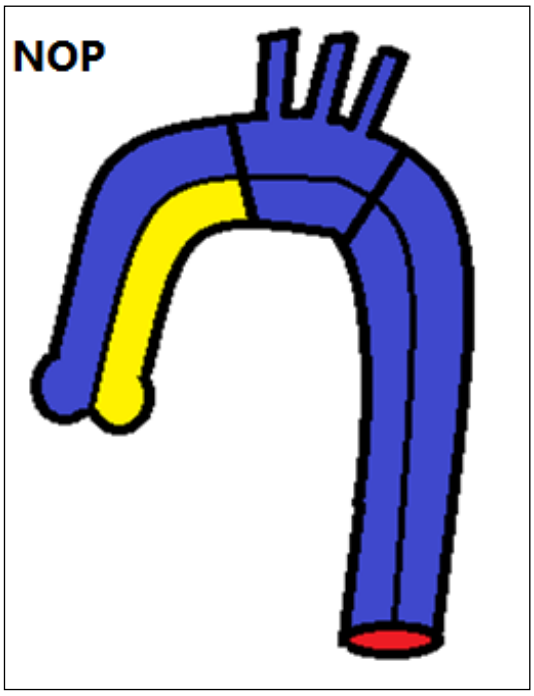

Figure 61. In NOP, a significant decrease in the mean WSS along the inner curvature of the ascending aorta (yellow-colored segment) was observed.

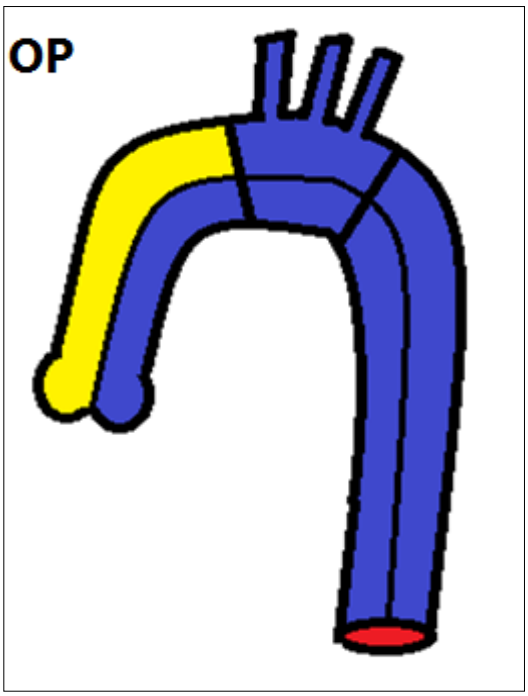

Figure 62. In OP, a significant decrease in the mean WSS along the outer curvature of the ascending aorta (yellow-colored segment) was observed.

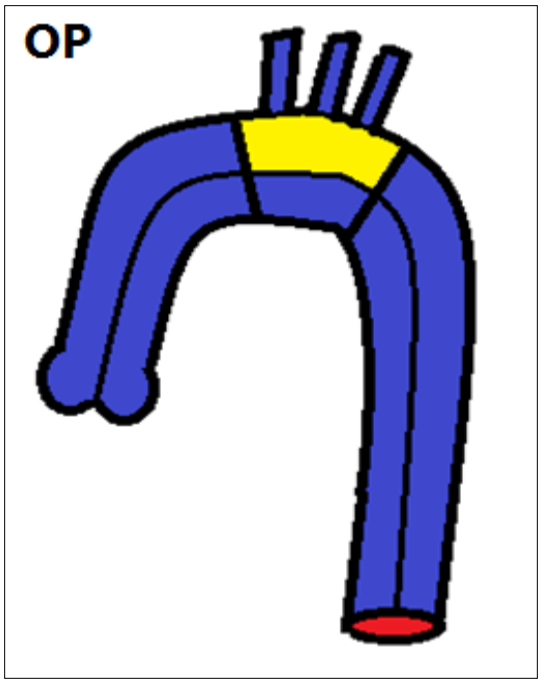

Figure 63. In OP, a significant decrease in the mean WSS in the outer curvature of aortic arch was observed.

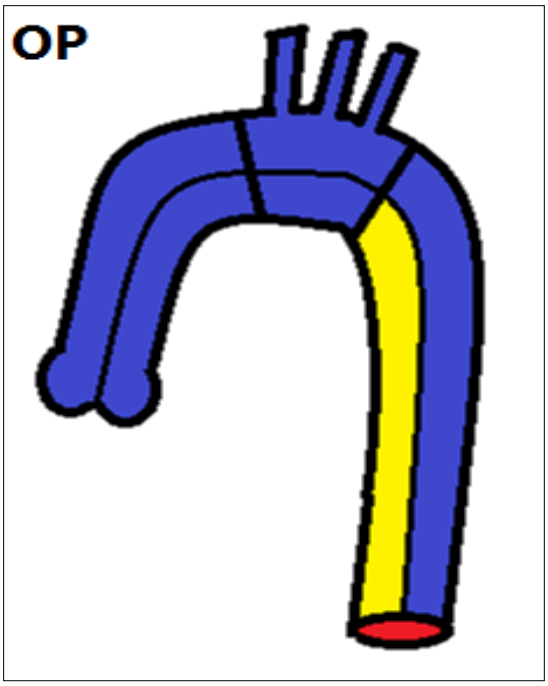

Figure 64. In OP, a significant decrease in mean WSS in the inner curvature of the descending aorta was observed.

In the ascending aorta, WSS along the outer curvature was significantly higher than the inner curvature as the aortic valve disease progressed (OP group in the primary study) (p value: 0.09). However, there was no difference between outer and inner curvatures in the aortic arch or descending aorta.

	Out (NOP)	Inn (NOP)	p value	Out (OP)	Inn (OP)	p value
AAo (P)	1.29±0.26	1.37±0.48	0.2	1.76±0.49	1.46±0.53	0.09
AAo (FU)	1.3±0.24	1.25±0.42	0.4	1.39±0.33	1.27±0.32	0.2
Arch (P)	0.77±0.13	0.87±0.09	0.18	0.93±0.17	0.92±0.12	0.5
Arch (FU)	0.85±0.18	0.89±0.08	0.4	0.7±0.10	0.72±0.08	0.4
DAo (P)	0.83±0.14	0.86±0.15	0.4	0.64±0.11	0.7±0.14	0.3
DAo (FU)	0.78±0.16	0.8±0.13	0.4	0.59±0.10	0.61±0.11	0.4

Table 10. The comparison between the outer and inner aortic curvatures regarding the mean WSS in the ascending aorta, aortic arch and descending aorta in P and FU. Out = outer curvature, Inn = inner curvature, AAo = ascending aorta, Arch = aortic arch, DAo = descending aorta.

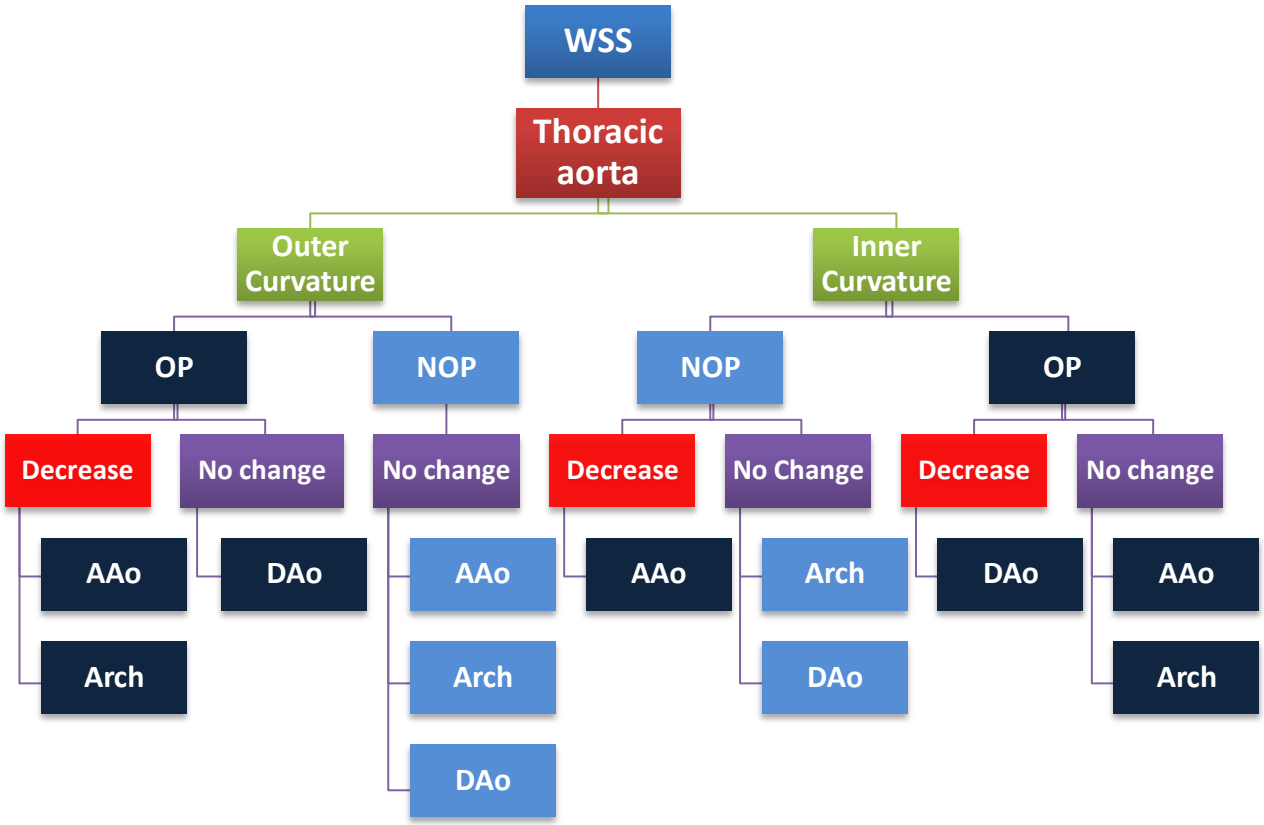

Figure 65. A summary of WSS results in the thoracic aorta in both outer and inner aortic curvatures in NOP and OP.

Analysis of the WSS of each segment in the 18-segment model revealed the following results:

In NOP, there was a change in 2 out of 18 segments over time. There was a significant increase in mean WSS in segment 7 (P: 0.82±0.29 N/m^2, FU: 1.01±0.38 N/m^2, p value: 0.03) and a significant decrease in mean WSS in segment 14 (P: 1.00±0.46 N/m^2, FU: 0.90±0.37 N/m^2, p value: 0.03) (Table 11). In OP, there was a significant decrease in 5 out of 18 segments, all of them along the outer aortic curvature. There was a significant decrease in mean WSS in segment 3 (P: 2.14±0.59 N/m^2, FU: 1.57±0.47 N/m^2, p value: 0.01), segment 7 (P: 1.06±0.32 N/m^2, FU: 0.78±0.17 N/m^2, p value: 0.02), segment 9 (P: 0.96±0.32 N/m^2, FU: 0.70±0.25 N/m^2, p value: 0.04), segment 11 (P: 0.78±0.24 N/m^2, FU: 0.62±0.19 N/m^2, p value: 0.03), and segment 15 (P: 0.62±0.23 N/m^2, FU: 0.55±0.19 N/m^2, p value: 0.04) (Table 12).

WSS (NOP) Segments	Mean P	Mean FU	SD P	SD FU	p value
1	1.38	1.39	0.43	0.40	0.92
2	1.83	1.69	0.62	0.58	0.33
3	1.29	1.26	0.39	0.40	0.80
4	1.27	1.09	0.40	0.39	0.14
5	1.19	1.25	0.34	0.45	0.47
6	1.01	0.97	0.35	0.27	0.62
7	0.82	1.01	0.29	0.38	**0.03**
8	0.87	0.91	0.35	0.36	0.51
9	0.74	0.78	0.21	0.23	0.45
10	0.85	0.89	0.29	0.31	0.44
11	0.76	0.77	0.28	0.23	0.85
12	0.89	0.85	0.28	0.24	0.38
13	0.93	0.89	0.63	0.55	0.35
14	1.00	0.90	0.46	0.37	**0.03**
15	0.84	0.75	0.36	0.22	0.23
16	0.86	0.81	0.42	0.28	0.51
17	0.72	0.69	0.19	0.17	0.39
18	0.74	0.70	0.18	0.16	0.07

Table 11. Mean WSS along the thoracic aorta in 18-segment model in NOP. WSS = wall shear stress, NOP = non-operated group, P = primary, FU = follow-up, SD = standard deviation.

WSS (OP) segments	Mean P	Mean FU	SD P	SD FU	p value
1	1.44	1.32	0.57	0.26	0.21
2	1.80	1.50	0.77	0.33	0.20
3	2.14	1.57	0.59	0.47	**0.01**
4	1.52	1.37	0.36	0.56	0.28
5	1.70	1.29	0.57	0.39	0.06
6	1.06	0.95	0.48	0.30	0.27
7	1.06	0.78	0.32	0.17	**0.02**
8	0.99	0.74	0.48	0.24	0.09
9	0.96	0.70	0.32	0.25	**0.04**
10	0.90	0.73	0.40	0.26	0.15
11	0.78	0.62	0.24	0.19	**0.03**
12	0.88	0.68	0.31	0.18	0.05
13	0.72	0.65	0.24	0.28	0.23
14	0.82	0.69	0.28	0.17	0.09
15	0.62	0.55	0.23	0.19	**0.04**
16	0.62	0.54	0.20	0.08	0.09
17	0.57	0.59	0.18	0.16	0.37
18	0.65	0.60	0.17	0.12	0.24

Table 12. Mean WSS along the thoracic aorta in 18-segment model in OP. WSS = wall shear stress, OP = operated group, P = primary, FU = follow-up, SD = standard deviation.

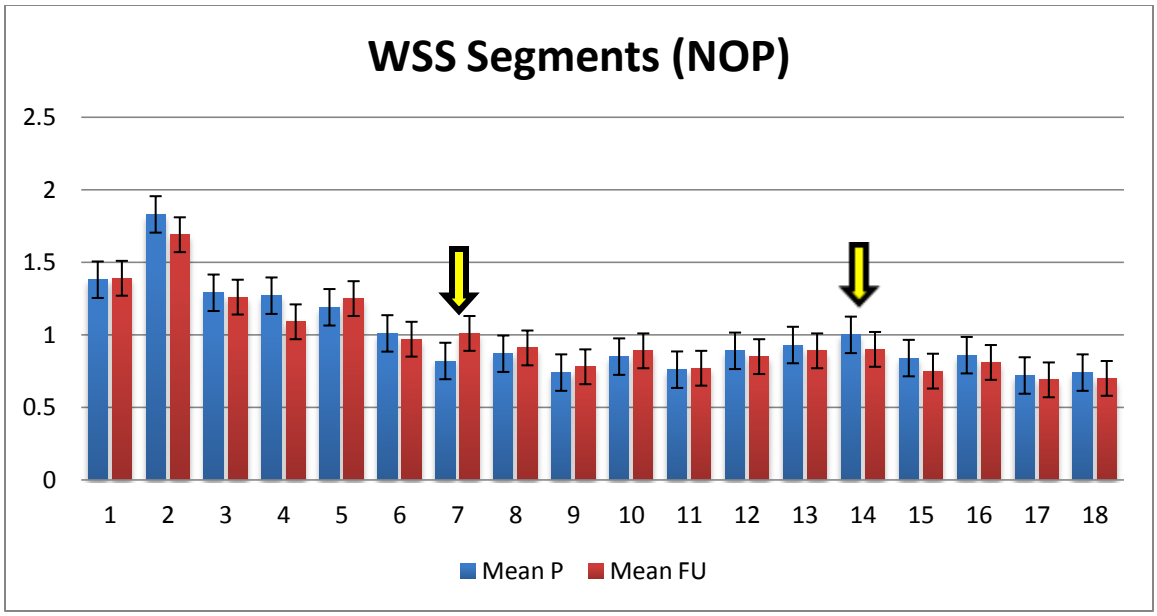

Figure 66. The difference between P and FU regarding the mean WSS along the thoracic aorta in 18-segment model in NOP. Yellow arrows depict segments that have undergone statistically significant change over time.

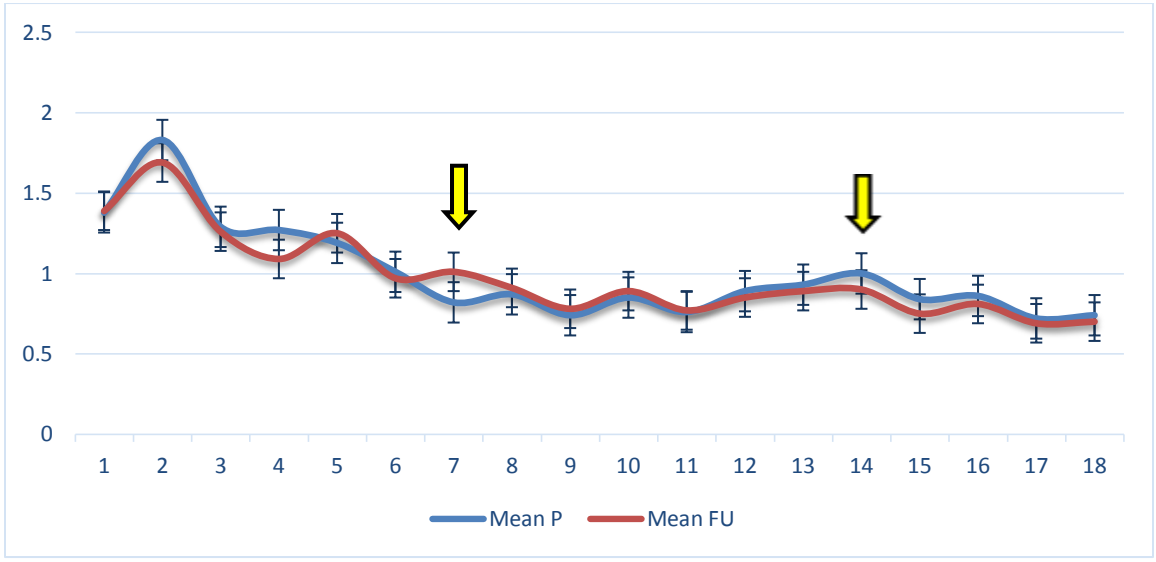

Figure 67. The difference between P and FU regarding the mean WSS along the thoracic aorta in 18-segment model in NOP. There was a significant increase in the mean WSS in segment 7 and a significant decrease in segment 14. Yellow arrows depict segments that have undergone statistically significant change over time.

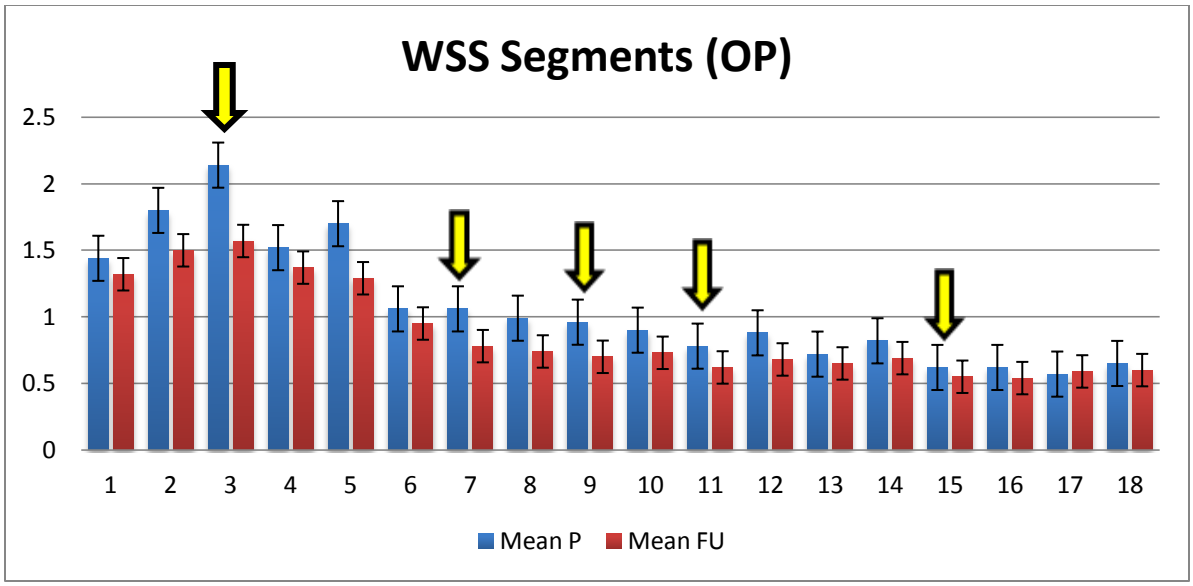

Figure 68. The difference between P and FU regarding the mean WSS along the thoracic aorta in 18-segment model in OP. Yellow arrows depict segments that have undergone statistically significant change over time.

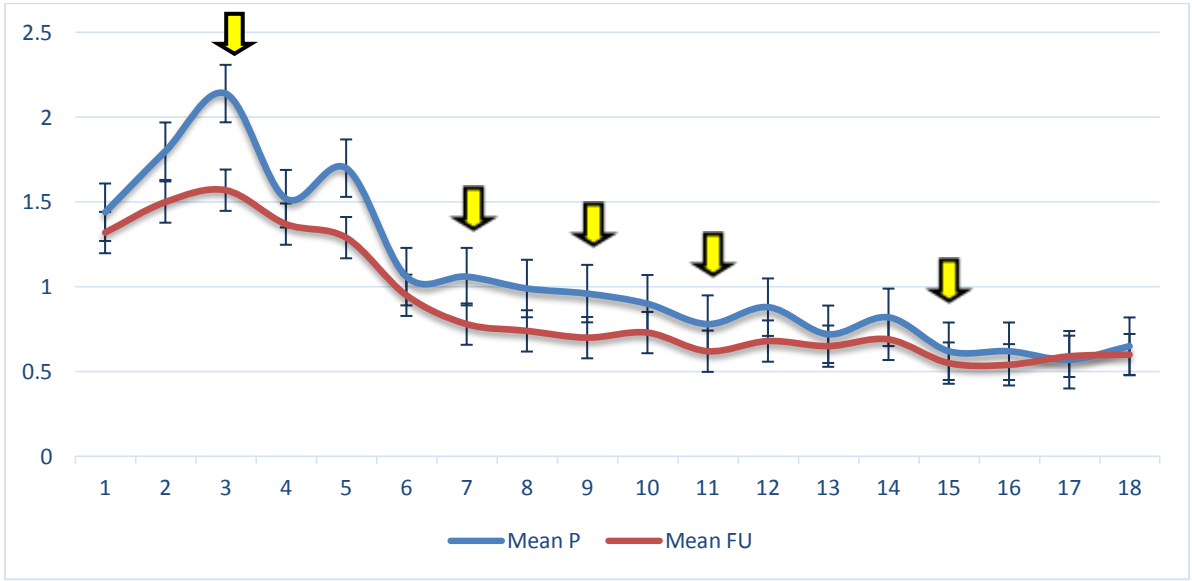

Figure 69. The difference between P and FU regarding the mean WSS along the thoracic aorta in 18-segment model in OP. There was a significant decrease in the mean WSS in segments 3, 7, 9, 11 and 15. Yellow arrows depict segments that have undergone statistically significant change over time.

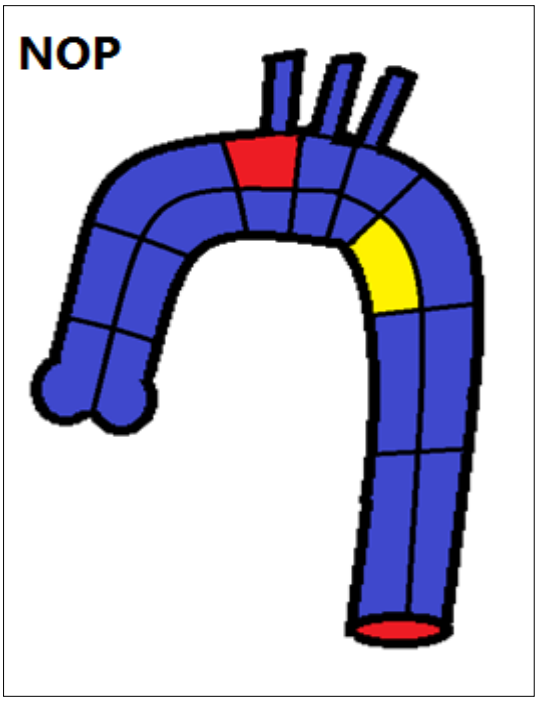

Figure 70. In NOP, there was a significant increase in mean WSS in segment 7 (the red-colored segment) and a decrease in mean WSS in segment 14 (the yellow-colored segment).

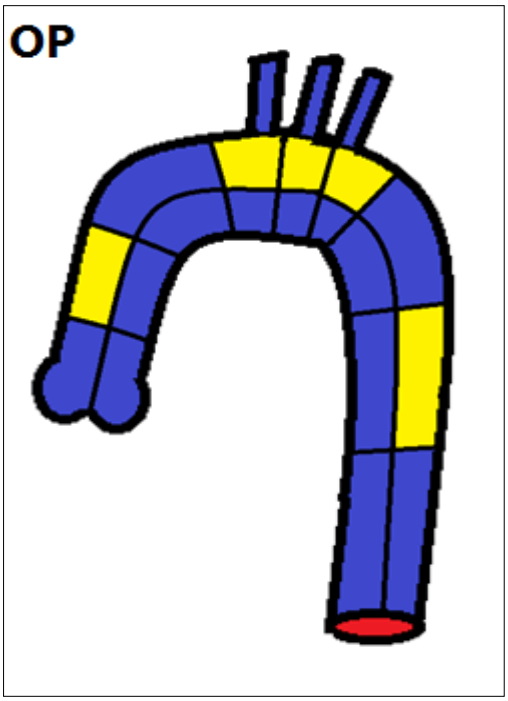

Figure 71. In OP, there was a significant decrease in mean WSS in segments 3, 7, 9, 11, and 15 (yellow-colored segments).

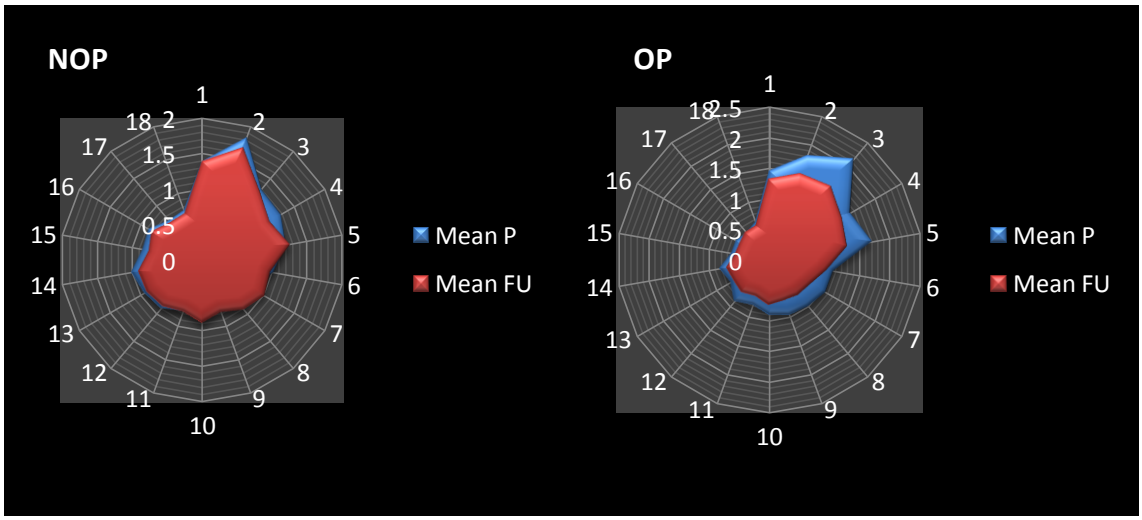

Figure 72. The difference between P and FU regarding the mean WSS along the thoracic aorta in 18-segment model in both NOP and OP. The blue color represents the mean WSS in P, and the red represents the mean WSS in FU. There was no significant change in mean WSS in NOP, and a significant decrease in OP over time is noted.

WSS distribution

Tables 13 and 14 show the distribution of the WSS and the segments with the highest and lowest WSS values. In NOP in P, the top 6 segments with the highest WSS values are arranged from highest to lowest: 2,1,3,4,5,6. Note that the top 6 segments are the same 6 segments representing the ascending aorta. Segment 2 represents the proximal aortic inner curvature and has the highest WSS value. In comparison, the lowest 6 segments are 15, 7, 11, 9, 18, and 17. Segment 17 - representing the outer curvature of the distal descending aorta - has the lowest WSS value. The segments with the lowest WSS values are all along the outer curvature of the aortic arch and descending aorta. In NOP in FU, the top 6 segments with the highest WSS values arranged from highest to lowest are: 2,1,3,5,4,7. Five out of the six segments are in the ascending aorta, and the sixth segment represents the proximal outer aortic arch, while the lowest 6 segments are 16,9,11,15,18,17. The segment with the lowest WSS value remains the same as in P: 17.

In OP at P, the top 6 segments with the highest WSS values arranged from highest to lowest are: 3,2,5,4,1,6. Note that the top 6 segments are the 6 representing the ascending aorta. The segments are the same as in NOP, but the distribution is different. The segment with the highest WSS value is segment 3, representing the mid-outer curvature of ascending aorta, while the lowest 6 segments are 11,13, 18,15,16,17. The segment with the lowest WSS value is segment 17, representing the outer curvature of the distal descending aorta. All the segments with the lowest WSS values are in the descending aorta, except segment 11, representing the distal outer curvature of the aortic arch. In OP in FU, the top 6 segments with the highest WSS values arranged from highest to lowest are: 3,2,4,1,5,6. They are the same segments as at P but with different rankings. Note that the top 2 segments with the highest WSS remained the same after surgery, while the lowest 6 segments were 13,11,18,17,15,16. Once again, these were the same segments as at P but with a different distribution. The segment with the lowest WSS value is segment 16.

	WSS (NOP)					WSS (OP)			
Rank	**Seg P**	**Mean P**	**Seg FU**	**Mean FU**	***Rank***	**Seg P**	**Mean P**	**Seg FU**	**Mean FU**
1	***S 2***	1.83	***S 2***	1.69	***1***	***S 3***	2.14	***S 3***	1.57
2	***S 1***	1.38	***S 1***	1.39	***2***	***S 2***	1.8	***S 2***	1.5
3	***S 3***	1.29	***S 3***	1.26	***3***	***S 5***	1.7	***S 4***	1.37
4	***S 4***	1.27	***S 5***	1.25	***4***	***S 4***	1.52	***S 1***	1.32
5	***S 5***	1.19	***S 4***	1.09	***5***	***S 1***	1.44	***S 5***	1.29
6	***S 6***	1.01	***S 7***	1.01	***6***	***S 6***	1.06	***S 6***	0.95
7	***S 14***	1.00	***S 6***	0.97	***7***	***S 7***	1.06	***S 7***	0.78
8	***S 13***	0.93	***S 8***	0.91	***8***	***S 8***	0.99	***S 8***	0.74
9	***S 12***	0.89	***S 14***	0.9	***9***	***S 9***	0.96	***S 10***	0.73
10	***S 8***	0.87	***S 10***	0.89	***10***	***S 10***	0.9	***S 9***	0.7
11	***S 16***	0.86	***S 13***	0.89	***11***	***S 12***	0.88	***S 14***	0.69
12	***S 10***	0.85	***S 12***	0.85	***12***	***S 14***	0.82	***S 12***	0.68
13	***S 15***	0.84	***S 16***	0.81	***13***	***S 11***	0.78	***S 13***	0.65
14	***S 7***	0.82	***S 9***	0.78	***14***	***S 13***	0.72	***S 11***	0.62
15	***S 11***	0.76	***S 11***	0.77	***15***	***S 18***	0.65	***S 18***	0.6
16	***S 9***	0.74	***S 15***	0.75	***16***	***S 15***	0.62	***S 17***	0.59
17	***S 18***	0.74	***S 18***	0.7	***17***	***S 16***	0.62	***S 15***	0.55
18	***S 17***	0.72	***S 17***	0.69	***18***	***S 17***	0.57	***S 16***	0.54

Table 13. Ranking of the 18 segments representing the thoracic aorta regarding the WSS values. Seg = segment, S = segment, P = primary, FU = follow-up, NOP = non-operated group, OP = operated group.

WSS (NOP)						WSS (OP)					
AAo	**R**	**S P**	**Mean P**	**S FU**	**Mean FU**	**AAo**	**R**	**S P**	**Mean P**	**S FU**	**Mean FU**
	1	***S 2***	1.83	***S 2***	1.69		**1**	***S 3***	2.14	***S 3***	1.57
	2	***S 1***	1.38	***S 1***	1.39		**2**	***S 2***	1.8	***S 2***	1.5
	3	***S 3***	1.29	***S 3***	1.26		**3**	***S 5***	1.7	***S 4***	1.37
	4	***S 4***	1.27	***S 5***	1.25		**4**	***S 4***	1.52	***S 1***	1.32
	5	***S 5***	1.19	***S 4***	1.09		**5**	***S 1***	1.44	***S 5***	1.29
	6	***S 6***	1.01	***S 6***	0.97		**6**	***S 6***	1.06	***S 6***	0.95
Arch	**1**	***S 12***	0.89	***S 7***	1.01	**Arch**	**1**	***S 7***	1.06	***S 7***	0.78
	2	***S 8***	0.87	***S 8***	0.91		**2**	***S 8***	0.99	***S 8***	0.74
	3	***S 10***	0.85	***S 10***	0.89		**3**	***S 9***	0.96	***S 10***	0.73
	4	***S 7***	0.82	***S 12***	0.85		**4**	***S 10***	0.9	***S 9***	0.7
	5	***S 11***	0.76	***S 9***	0.78		**5**	***S 12***	0.88	***S 12***	0.68
	6	***S 9***	0.74	***S 11***	0.77		**6**	***S 11***	0.78	***S 11***	0.62
DAo	**1**	***S 14***	1.00	***S 14***	0.9	**DAo**	**1**	***S 14***	0.82	***S 14***	0.69
	2	***S 13***	0.93	***S 13***	0.89		**2**	***S 13***	0.72	***S 13***	0.65
	3	***S 16***	0.86	***S 16***	0.81		**3**	***S 18***	0.65	***S 18***	0.6
	4	***S 15***	0.84	***S 15***	0.75		**4**	***S 15***	0.62	***S 17***	0.59
	5	***S 18***	0.74	***S 18***	0.7		**5**	***S 16***	0.62	***S 15***	0.55
	6	***S 17***	0.72	***S 17***	0.69		**6**	***S 17***	0.57	***S 16***	0.54

Table 14. Ranking of the segments representing the ascending aorta, aortic arch and descending aorta regarding the WSS values. S = segment, AAo = ascending aorta, Arch = aortic arch, DAo = descending aorta.

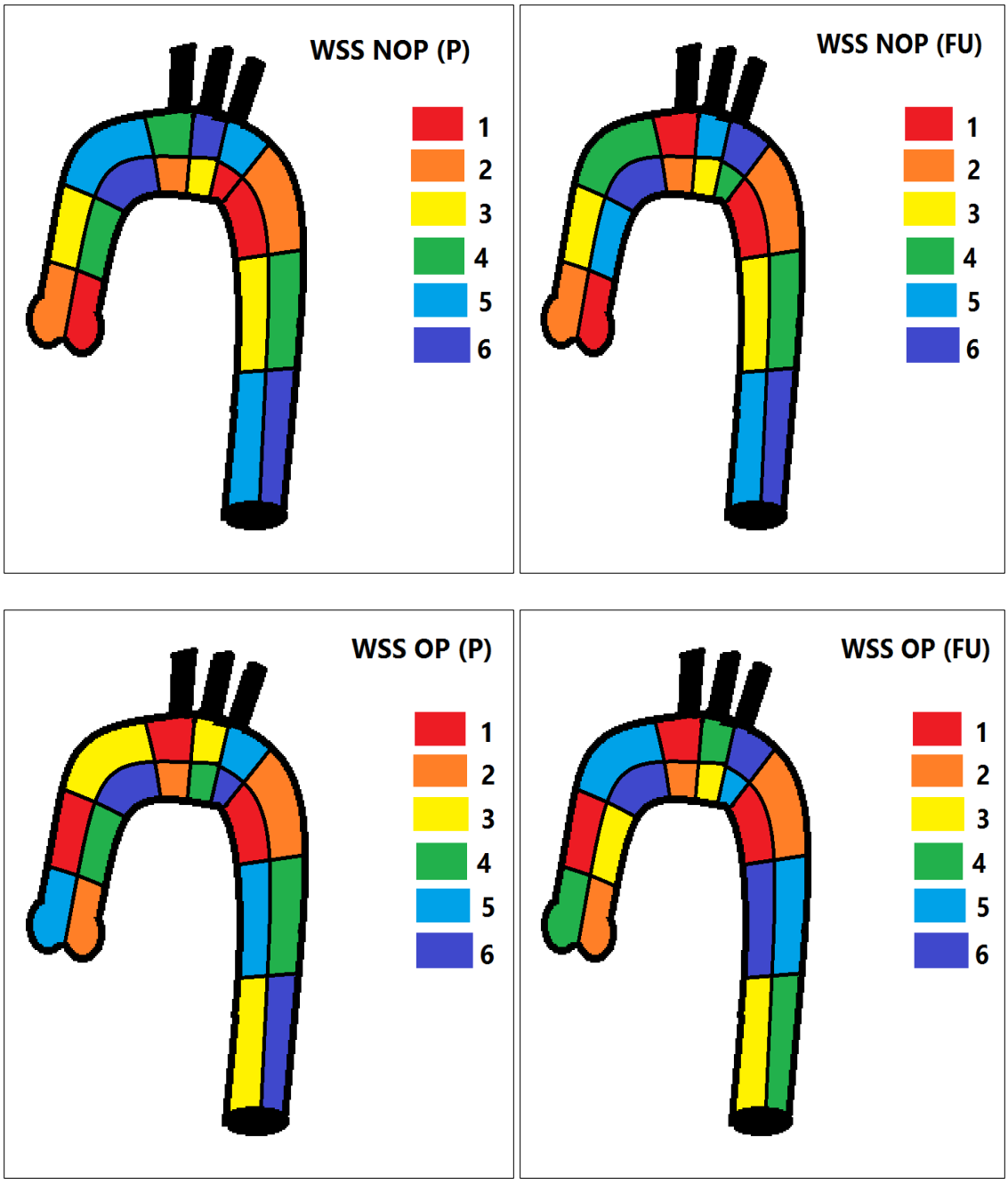

Figure 73. The figure shows the WSS distribution in the 18-segment model for the WSS analysis, drawn manually in Microsoft Paint. The aorta is divided into 3 parts: ascending aorta, aortic arch, and descending aorta. Each part is divided into six segments. The segments in each part are color-coded to represent the segments with the highest and those with the lowest WSS (red color represents the segment with the highest WSS, and dark blue represents the segment with the lowest WSS). Red = rank 1, orange = rank 2, yellow = rank 3, green = rank 4, sky blue = rank 5, dark blue = rank 6.

It should be taken into account that we actually have four groups: NOP (P) is composed of patients with mild to moderate aortic stenosis, NOP (FU) is composed of the same patients with almost no significant progression in aortic valve disease except for only one patient, OP (P) is composed of patients with severe aortic stenosis, and OP (FU) includes the same patients after surgery. We can consider that those four groups represent different aortic valve disease course stages. NOP (P) represents patients with mild to moderate aortic valve stenosis. NOP (FU) represents the same patients at follow-up with overall stable valvular disease, OP (P) represents patients with severe aortic valve stenosis before surgery, and OP (FU) represents the same patients after surgery.

In NOP, the distribution of the top 3 WSS segments in the ascending aorta was identical in both P and FU. The top 3 segments were confined to the proximal and mid ascending aorta (the top 2 segments represent the proximal ascending aorta, with segment 2 representing the inner proximal ascending aorta in first place and segment 3 in third place representing the outer mid ascending aorta). The distribution of the bottom 3 segments in ascending aorta changed in FU, where segments 4 and 5 exchanged their places, leading to a slightly higher WSS in the distal outer ascending aorta than in P.

The only change between P and FU in the aortic arch was that segments 7 and 12 had exchanged their places (the segment with the highest WSS in the aortic arch changed from the inner distal to the outer proximal aortic arch). The second and third place segments remained unchanged. In the descending aorta, the distribution of both the top and bottom three segments was precisely the same in both P and FU. Note that the top 2 segments in the descending aorta were 14 and then 13.

In the OP group in P, the distribution of the top 3 WSS segments in the ascending aorta was markedly changed compared to the NOP group in P. The top 3 OP (P) segments were distributed along the entire ascending aorta, whereas in NOP (P), they were confined only to the proximal and mid ascending aorta. The first place segment was segment 3 (outer mid ascending aorta), the second segment was segment 2 (inner proximal ascending aorta), and the third place went to segment 5 (outer distal ascending aorta). We can refer to the change in the distribution of WSS top 3 segments in the ascending aorta from being confined to the proximal and mid ascending aorta in NOP (P) to extending to the distal ascending aorta in OP (P) as a distal displacement of the WSS distribution. This distal displacement of the WSS distribution might signify aortic valvular disease progression.

The WSS distribution changed once again in OP in FU (i.e., after aortic valve replacement). We noticed an apparent regression of the previously described distal displacement of the WSS distribution. The top 3 segments after surgery were once again confined to the proximal and mid ascending aorta instead of reaching the distal ascending aorta. Interestingly, the top 2 segments kept their places even after surgery, with lower WSS values. The regression of the WSS distribution distal displacement (WDDD) may signify hemodynamic improvement after surgery.

In the aortic arch in the OP in P, the top 3 segments were confined to the proximal and mid arch. In comparison to the other three groups, we found that: segment 8, representing the inner proximal aortic arch, kept second place in all four groups. The difference in the top 3 segments in the aortic arch was confined to segments 1 and 3. In NOP (P), the top 3 segments in the aortic arch were 12, 8 and 10, respectively. All of the top 3 WSS segments in NOP (P) were confined to the inner aortic arch curvature. In NOP (FU), we observed that segment 7 (outer proximal arch) took the lead from segment 12 (inner distal arch), while segments 10 and 8 (inner mid and proximal arch) kept their places. In OP (P), both the first and second segments kept their places, while segment 9 (mid outer arch) took third place. That means that two out of the three top 3 segments are located in the outer aortic arch (outer proximal and mid arch). Comparing this WSS distribution in NOP to WSS distribution in OP, we observed a tendency to an outer displacement of WSS distribution (outer aortic arch) over time (i.e., with disease progression). Therefore, WSS distribution outer displacement (WDOD) might also signify aortic valve disease progression. Another interesting finding in the WSS distribution of the aorta arch was WSS in segment 7 (the outer proximal aortic arch). In NOP (P), it was in fourth place. In NOP (FU), even though the patients in this group showed no obvious overall aortic valve disease progression, segment 7 showed a marked increase in the WSS, taking the lead in the aortic arch from segment 12, and it also kept the lead in OP (P) and (FU). Therefore, increasing WSS in segment 7 might be an early sign of aortic valve disease progression.

In descending aorta OP, in both P and FU, the most interesting finding was that segments 14 and 13 kept their places as the top 2 segments in descending aorta not only in OP (P) and (FU) but also in NOP (P) and (FU). The third top segment (segment 18) kept its place in OP in both P and FU.

11.4. Peak systolic velocity in thoracic aorta

Analysis of the peak systolic velocity in 8 planes along the thoracic aorta using the EnSight program provided the following results:

In NOP, there was no significant change in peak systolic velocity in any plane (P1: P: 2.19±0.54m/s, FU: 2.34±0.57m/s, p value: 0.23), (P2: P: 2.17±0.55m/s, FU: 2.23±0.55m/s, p value: 0.58), (P3: P: 1.77±0.67m/s, FU: 1.66±0.42m/s, p value: 0.61), (P4: P: 1.42±0.54m/s, FU: 1.25±0.31m/s, p value: 0.20), (P5: P: 1.13±0.55m/s, FU: 1.14±0.56m/s, p value: 0.89), (P6: P: 0.92±0.27m/s, FU: 1.07±0.45m/s, p value: 0.06), (P7: P: 0.93±0.52m/s, FU: 0.90±0.37m/s, p value: 0.69), (P8: P: 0.88±0.50m/s, FU: 0.78±0.22m/s, p value: 0.40).

In OP, there was a statistically significant decrease in peak systolic velocity in two planes (P3 and P4) and borderline significant decrease in one plane (P5), with otherwise no significant change in the other planes over time (P1: P: 2.66±0.77m/s, FU: 2.44±0.47m/s, p value: 0.27), (P2: P: 2.63±0.65m/s, FU: 2.36±0.58m/s, p value: 0.22), (P3: P: 2.23±0.71m/s, FU: 1.74±0.46m/s, p value: 0.04), (P4: P: 1.76±0.77m/s, FU: 1.16±0.34m/s, p value: 0.04), (P5: P: 1.13±0.44m/s, FU: 0.89±0.42m/s, p value: 0.05), (P6: P: 0.73±0.24m/s, FU: 0.73±0.25m/s, p value: 0.47), (P7: P: 0.63±0.25m/s, FU: 0.62±0.27m/s, p value: 0.40), (P8: P: 0.74±0.49m/s, FU: 0.59±0.13m/s, p value: 0.22).

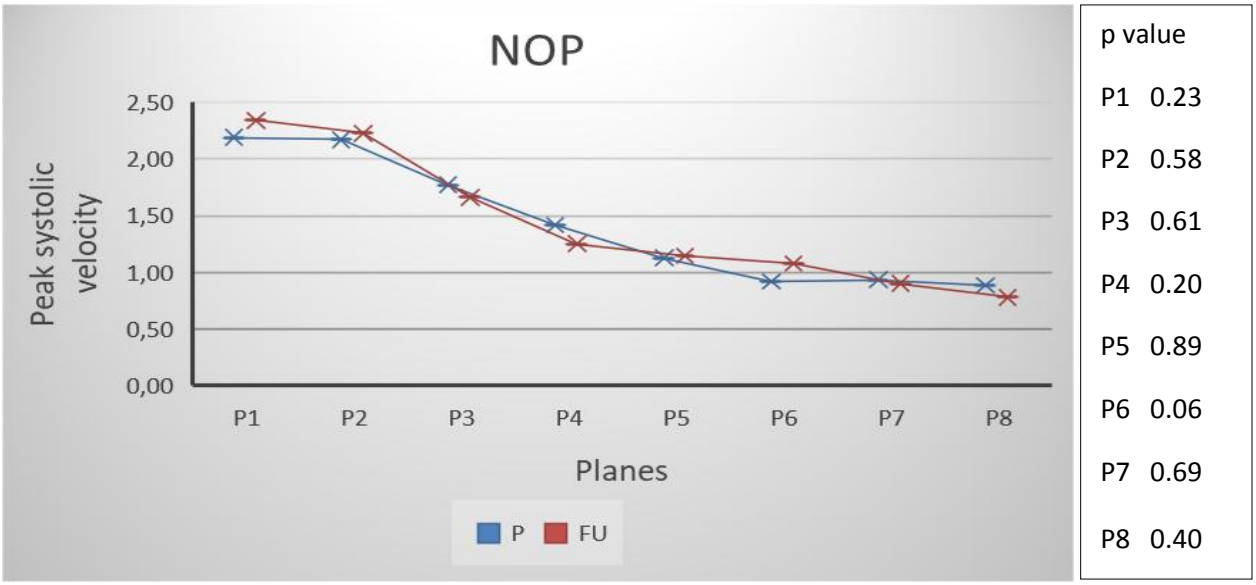

Figure 74. The mean peak systolic velocity in 8 planes along the thoracic aorta in NOP.

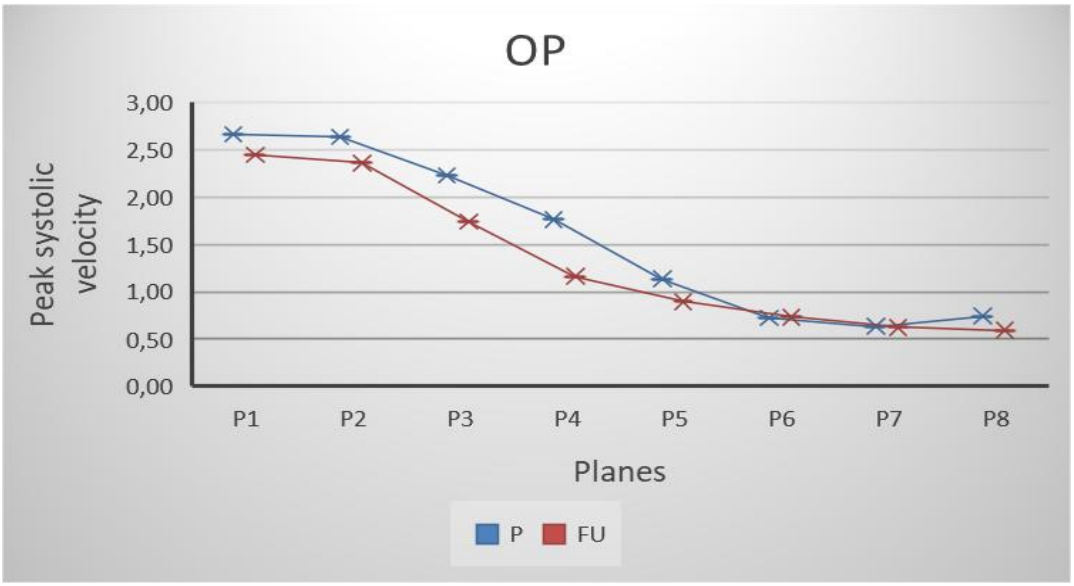

p value	
P1	0.27
P2	0.22
P3	0.04
P4	0.04
P5	0.05
P6	0.47
P7	0.40
P8	0.22

Figure 75. The mean peak systolic velocity in 8 planes along the thoracic aorta in OP.

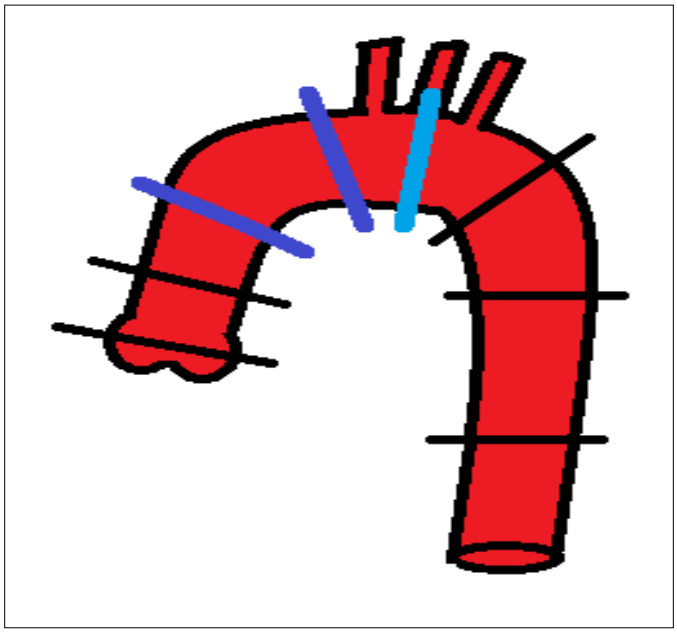

Figure 76. In OP, there was a significant decrease in the peak systolic velocity in P3 & 4 (blue-colored planes) and a borderline decrease in P5 (sky-blue-colored plane).

Adding the results of planes 1 to 4 to get a mean peak systolic velocity in the ascending aorta showed the following results:

In OP, a significant decrease in the peak systolic velocity was found in the ascending aorta, but not in NOP. (NOP: P: 1.89±0.47m/s, FU: 1.87±0.56m/s, p value: 0.86), (OP: P: 2.32±0.72m/s, FU: 1.93±0.64m/s, p value: 0.02).

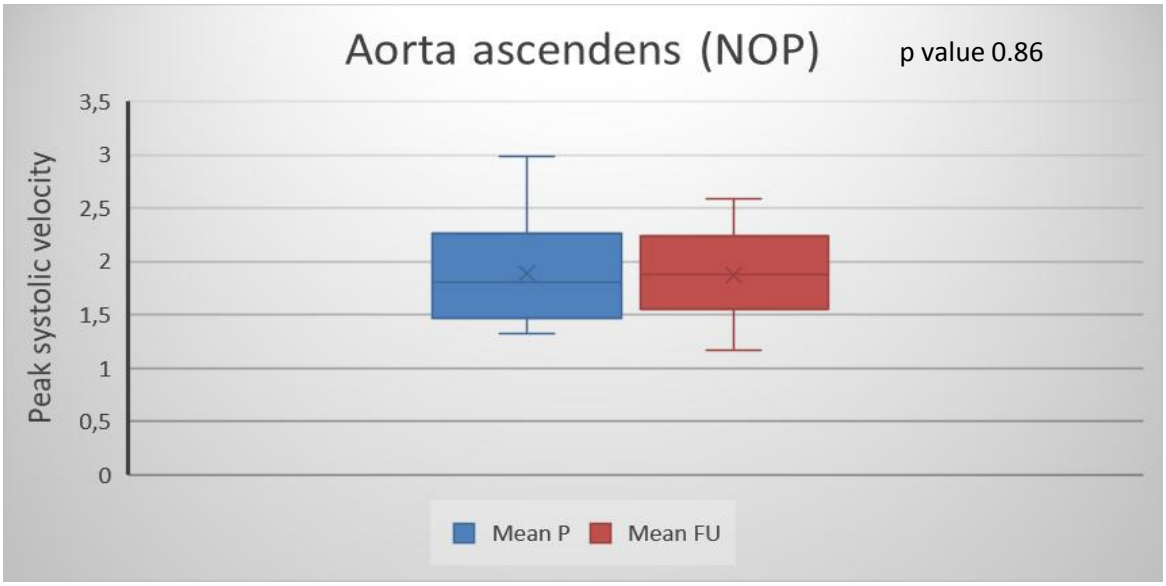

Figure 77. The mean peak systolic velocity of the 4 planes along the ascending aorta in NOP.

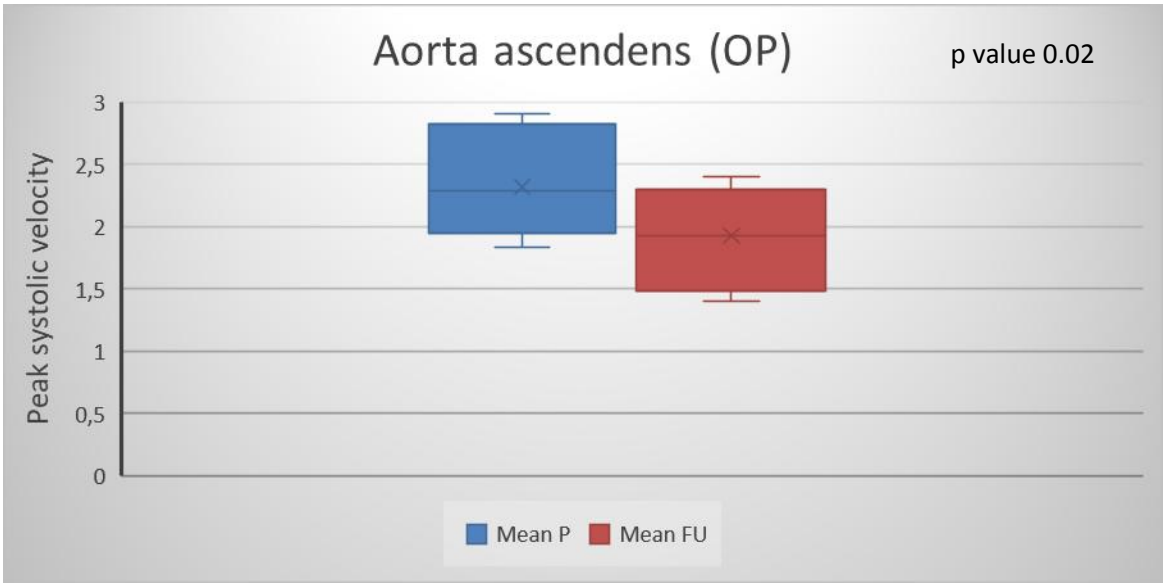

Figure 78. The mean peak systolic velocity of the 4 planes along the ascending aorta in OP.

Adding the results of planes 5 and 6 to get a mean peak systolic velocity in the aortic arch gave the following results:

In both NOP and OP, the mean peak systolic velocity in the aortic arch was not statistically significantly different (NOP: P: 1.02±0.16m/s, FU: 1.11±0.18m/s, p value: 0.3), (OP: P: 0.93±0.29m/s, FU: 0.81±0.14m/s, p value: 0.14).

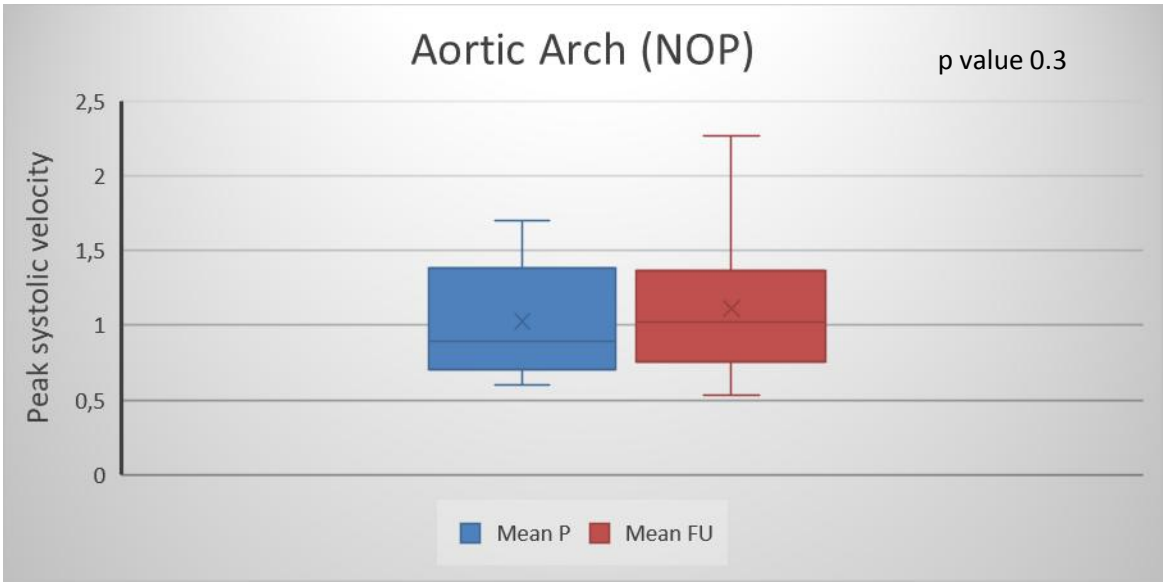

Figure 79. The mean peak systolic velocity of the 2 planes along the aortic arch in NOP.

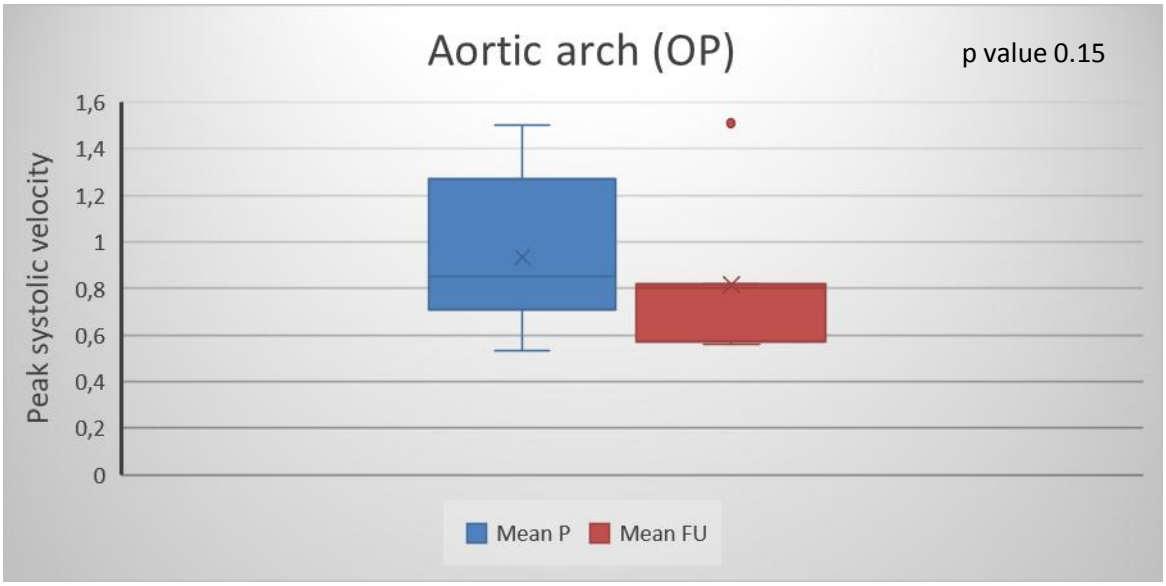

Figure 80. The mean peak systolic velocity of the 2 planes along the aortic arch in OP.

As for the net flow analysis in planes, once again, we considered that plane four is placed in the transitional zone between the ascending aorta and aortic arch. We performed a second analysis considering plane four as the first part of the aortic arch and then adding it to planes 5 and 6 to represent the aortic arch. Despite that, there was no significant change in peak systolic velocity in the aortic arch over time in NOP and a borderline significant decrease in peak systolic velocity in OP (NOP P: 1.15±0.29, FU: 1.16±0.25, p-value 0.96; OP P:1.21±0.53, FU:0.93±0.24, p value 0.05).

Adding the results of planes 7 and 8 to get a mean peak systolic velocity in the descending aorta gave the following results:

In both NOP and OP, the mean peak systolic velocity in the descending aorta did not change statistically significantly (NOP: P: 0.91±0.20m/s, FU: 0.84±0.14m/s, p value: 0.89), (OP: P: 0.69±0.13m/s, FU: 0.61±0.15m/s, p value: 0.19).

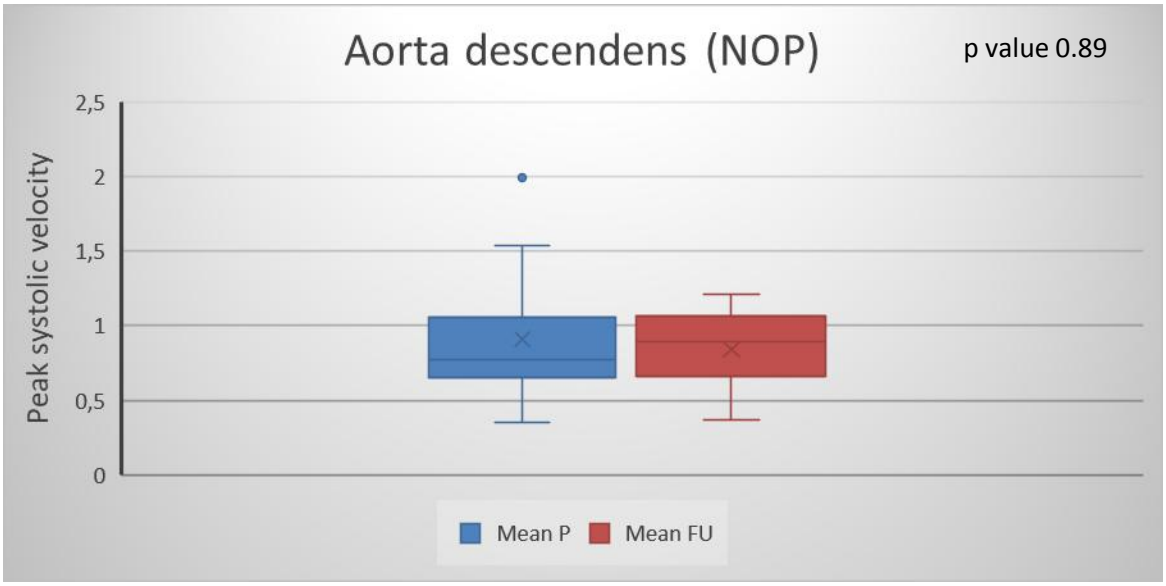

Figure 81. The mean peak systolic velocity of the 2 planes along the descending aorta in NOP.

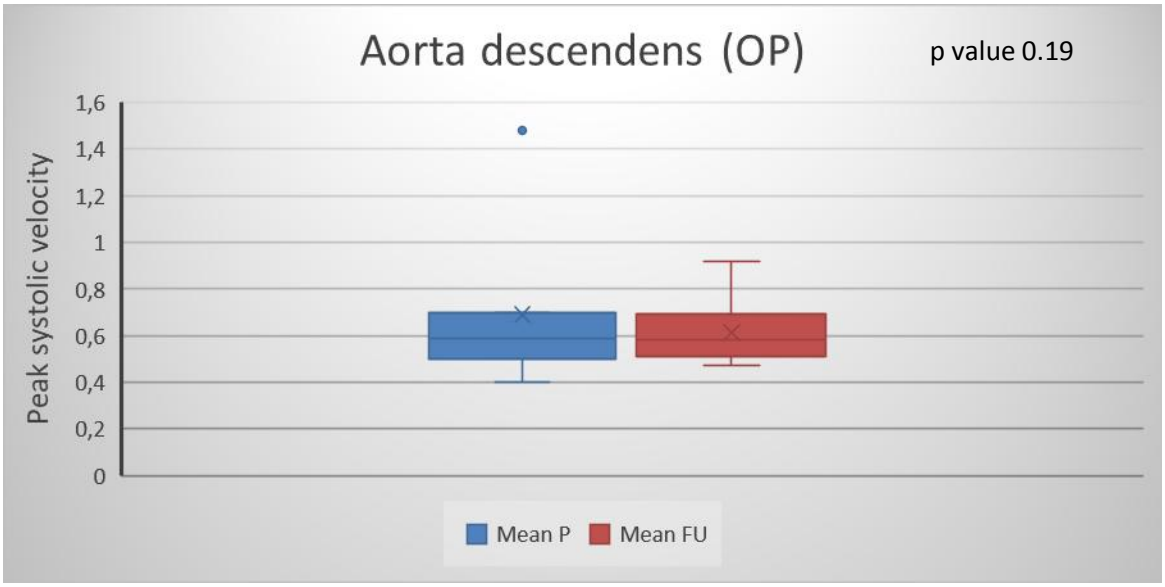

Figure 82. The mean peak systolic velocity of the 2 planes along the descending aorta in OP.

Analysis of the peak systolic velocity in segments using Matlab-based tool.

Analysis of the peak systolic velocity by dividing the thoracic aorta into three segments (ascending aorta, aortic arch, and descending aorta) gave the following results:

There was no significant change in the peak systolic velocity in the ascending aorta in NOP, while a statistically significant decrease in the peak systolic velocity in the ascending aorta was observed in OP (NOP: P: 2.53±0.77m/s, FU: 2.50±0.62m/s, p value: 0.84), (OP: P: 3.22±0.49m/s, FU: 2.65±0.45m/s, p value: 0.01).

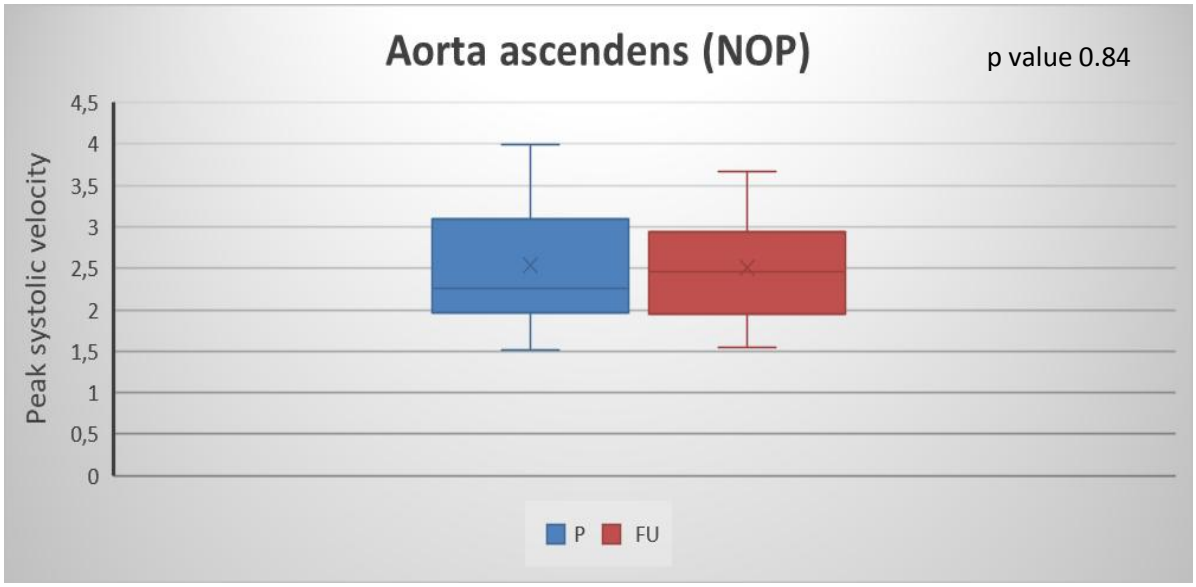

Figure 83. The mean peak systolic velocity in the ascending aorta in NOP.

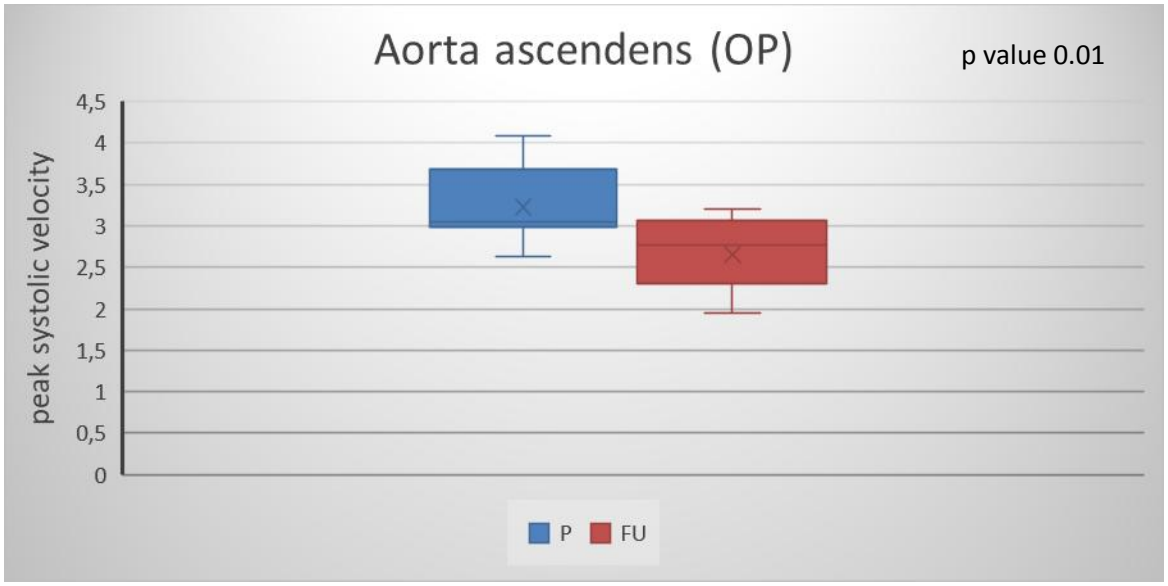

Figure 84. The mean peak systolic velocity in the ascending aorta in OP.

In NOP, the peak systolic velocity in the aortic arch did not change significantly, but in OP, the peak systolic velocity was significantly reduced (NOP: P: 1.23±0.37m/s, FU: 1.3±0.34m/s, p value: 0.44), (OP: P: 1.38±0.32m/s, FU: 1.01±0.22m/s, p value: 0.02).

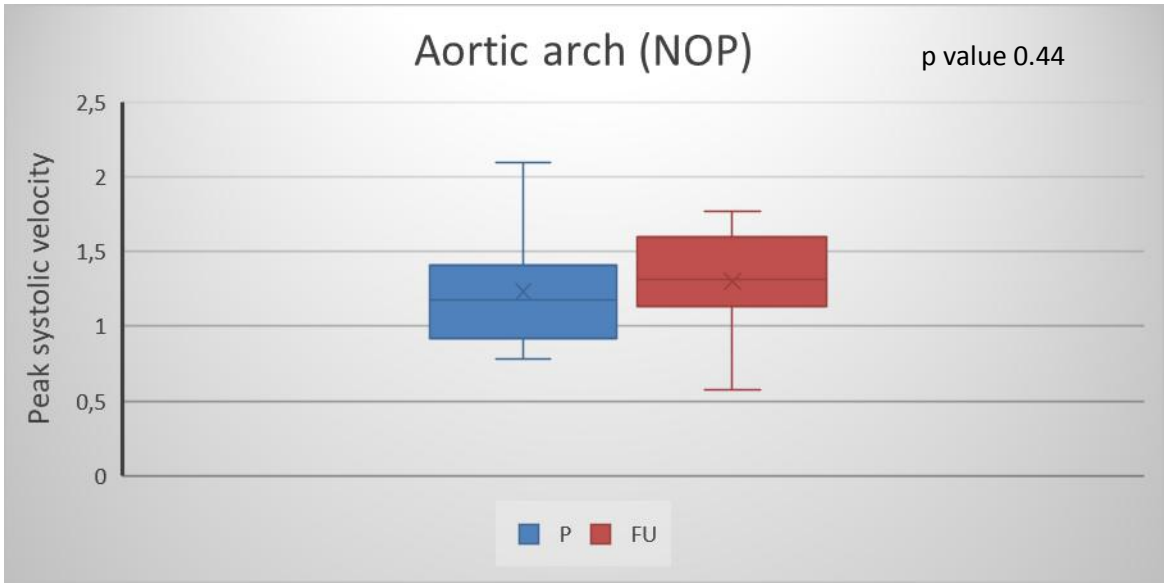

Figure 85. The mean peak systolic velocity in the aortic arch in NOP.

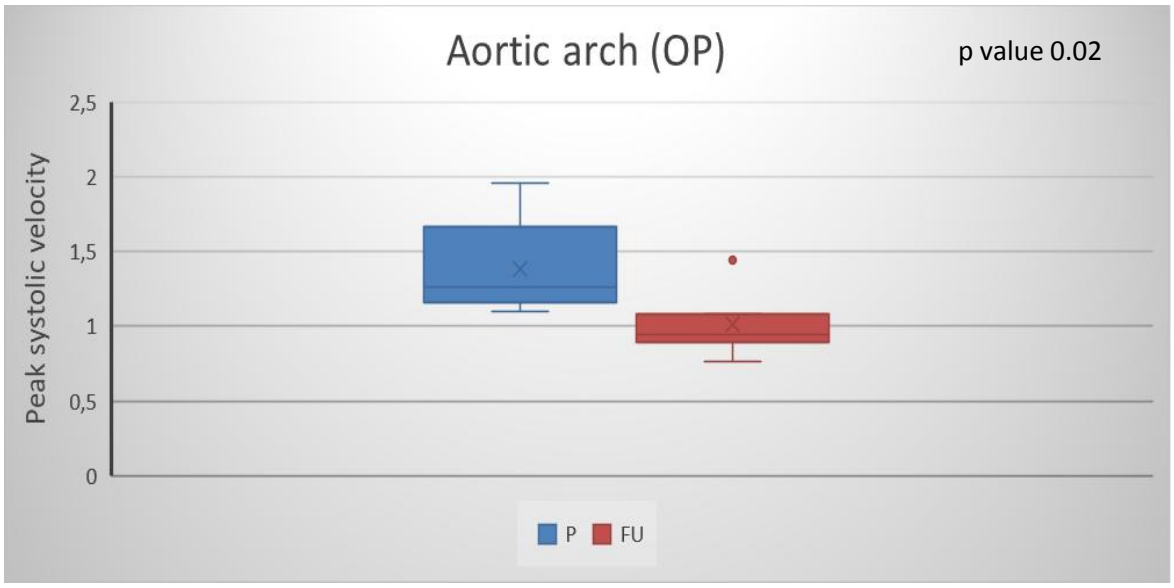

Figure 86. The mean peak systolic velocity in the aortic arch in OP.

There was no significant change in the peak systolic velocity in the descending aorta in both NOP and OP (NOP: P: 1.09±0.48m/s, FU: 1.06±0.43m/s, p value: 0.81), (OP: P: 0.85±0.24m/s, FU: 0.81±0.18m/s, p value: 0.29).

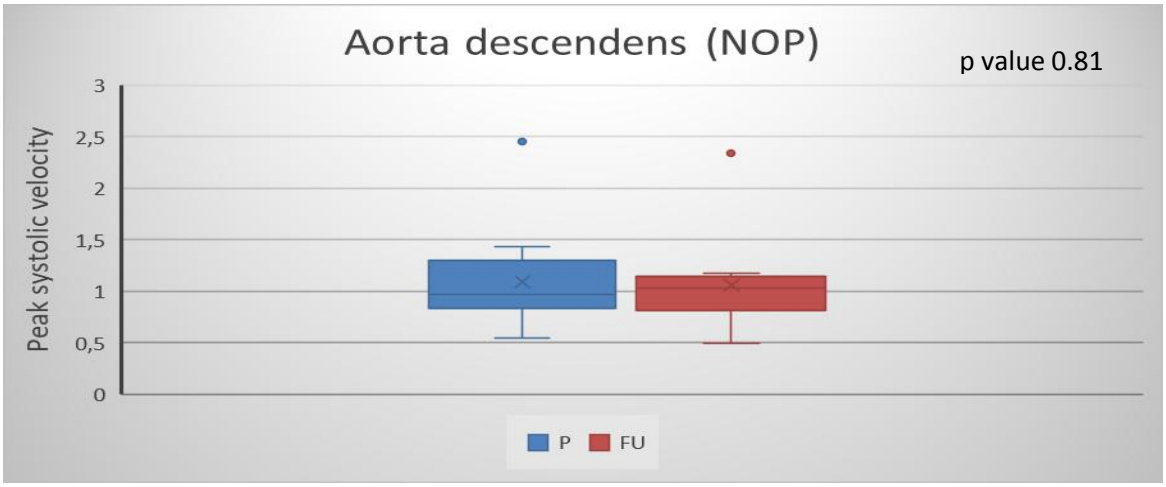

Figure 87. The mean peak systolic velocity in the descending aorta in NOP.

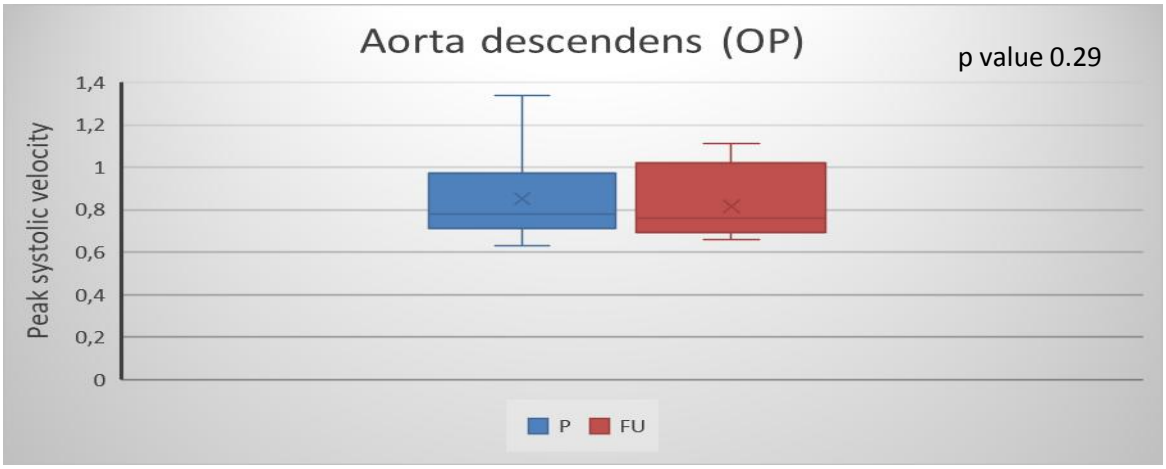

Figure 88. The mean peak systolic velocity in the descending aorta in OP.

Comparison of the two analysis modalities used to calculate the peak systolic velocity (peak velocity in planes using EnSight vs. peak velocity in segments using Matlab-based tool)

In Matlab, we get only one value of peak systolic velocity in the whole segment: ascending aorta, aortic arch, and descending aorta. With EnSight, we get a peak systolic velocity in each plane. We chose the plane with the highest peak systolic velocity in each segment and regarded it as the peak systolic velocity for the entire segment: ascending aorta, aortic arch, and descending aorta. Comparing EnSight with Matlab-based tool results provided the following:

Results obtained using EnSight, and the Matlab-based tool do not differ statistically significantly (Table 15).

PV AAo (NOP)	Mean P (P)	Mean P (S)	Mean FU (P)	Mean FU (S)	PV Arch (NOP)	Mean P (P)	Mean P (S)	Mean FU (P)	Mean FU (S)	PV DAo (NOP)	Mean P (P)	Mean P (S)	Mean FU (P)	Mean FU (S)
1	1.6	1.7	1.6	1.5	**1**	0.7	0.8	0.6	0.6	**1**	0.6	0.7	0.6	0.8
2	2.3	3.0	3.3	2.9	**2**	0.7	1.2	0.8	1.5	**2**	0.4	0.5	0.4	0.5
3	2.8	3.0	2.5	3.0	**3**	0.9	1.1	1.0	1.3	**3**	0.8	0.9	0.8	0.9
4	2.7	3.7	2.5	2.6	**4**	1.4	1.4	1.1	1.4	**4**	1.2	1.3	1.1	1.2
5	2.2	2.1	2.0	2.1	**5**	0.7	0.8	0.8	0.8	**5**	0.7	0.9	0.8	0.8
6	2.2	2.1	3.0	3.2	**6**	0.9	1.0	1.2	1.6	**6**	0.8	1.0	0.9	1.1
7	2.6	3.2	2.9	2.9	**7**	0.9	1.6	1.3	1.6	**7**	0.8	1.0	0.8	0.9
8	2.0	2.3	2.3	2.3	**8**	0.7	0.8	0.8	1.3	**8**	0.7	0.8	0.8	0.8
9	3.5	4.0	3.2	3.7	**9**	1.7	2.1	2.0	1.8	**9**	2.3	2.5	1.7	2.3
10	1.8	1.9	1.6	1.7	**10**	1.0	1.2	0.9	1.1	**10**	1.0	1.3	1.0	1.2
11	2.6	2.5	2.3	2.5	**11**	2.0	1.4	2.6	1.1	**11**	1.1	1.0	1.3	1.1
12	1.5	1.5	2.2	1.8	**12**	0.9	1.2	1.4	1.6	**12**	0.8	1.0	1.1	1.1
13	3.2	2.1	2.8	2.4	**13**	2.3	1.4	1.4	1.2	**13**	2.4	1.4	1.0	1.0
Mean	2.4	2.5	2.5	2.5	**Mean**	1.1	1.2	1.2	1.3	**Mean**	1.1	1.1	0.9	1.1
SD	0.6	0.8	0.6	0.6	**SD**	0.5	0.4	0.6	0.3	**SD**	0.6	0.5	0.3	0.4
p-value		0.3		0.4	**p value**		0.3		0.3	**p value**		0.4		0.2
PV AAO (OP)					**PV Arch (OP)**					**PV DAo (OP)**				
1	2.7	2.6	1.9	1.9	1	0.9	1.2	0.7	0.9	1	0.6	0.7	0.6	0.7
2	2.7	3.0	2.6	2.3	2	1.6	2.0	0.6	0.8	2	0.6	1.0	0.6	0.8
3	3.7	3.7	3.2	2.8	3	1.0	1.3	0.9	1.1	3	0.7	0.8	0.8	1.0
4	3.4	3.1	1.9	2.4	4	0.9	1.1	0.9	0.9	4	0.7	0.8	0.7	0.8
5	2.8	3.0	2.9	3.1	5	1.0	1.4	0.9	1.1	5	0.5	0.7	0.5	0.7
6	2.6	3.0	2.9	3.2	6	0.7	1.2	0.6	0.9	6	0.4	0.6	0.6	0.7
7	3.1	4.1	2.9	2.9	7	1.9	1.7	1.8	1.4	7	1.8	1.3	1.2	1.1
Mean	3.0	3.2	2.6	2.7	Mean	1.1	1.4	0.9	1.0	Mean	0.8	0.9	0.7	0.8
SD	0.4	0.5	0.5	0.4	SD	0.4	0.3	0.4	0.2	SD	0.5	0.2	0.2	0.2
p-value		0.2		0.5	**p value**		0.1		0.3	**p value**		0.4		0.2

Table 15. A comparison of the peak systolic velocity values obtained with EnSight and the Matlab-based tool. AAo = ascending aorta, Arch = aortic arch, DAo = descending aorta, PV = peak velocity, (P) = planes, (S) = segments, P = primary, FU = follow-up, NOP = non-operated, OP = operated. The two methods did not show any statistically significant differences.

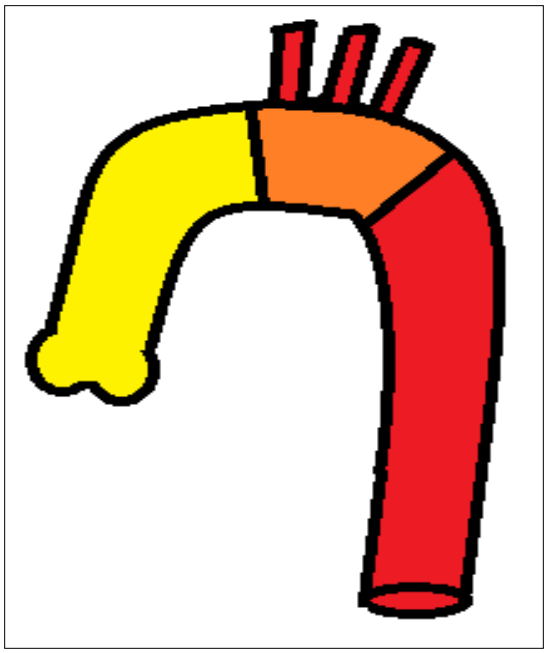

Figure 89. An increase in peak systolic velocity was observed in the ascending aorta (yellow segment) and a borderline decrease in the aortic arch (orange segment) in OP (peak velocity in planes with EnSight).

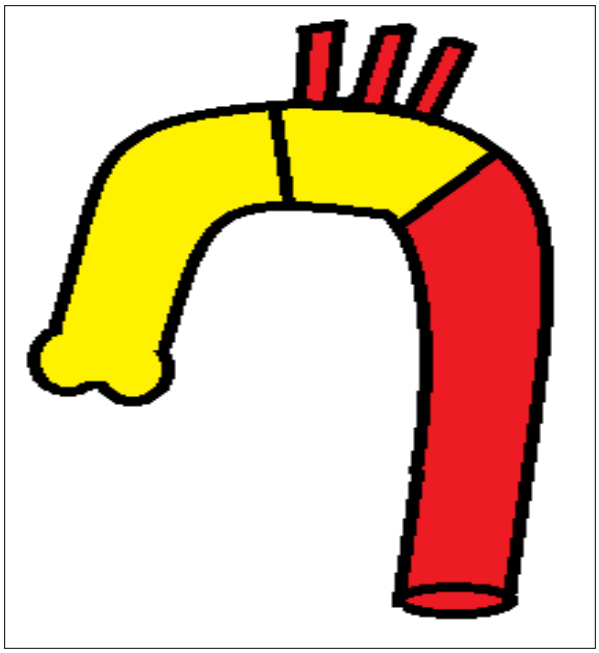

Figure 90. The peak systolic velocity decreased significantly in the ascending aorta and aortic arch (yellow-colored segments) in OP (peak velocity in segments with Matlab-based tool).

Peak systolic velocity and WSS

There was a strong positive correlation between the peak velocity and WSS across the ascending aorta, aortic arch, and descending aorta in both P and FU.

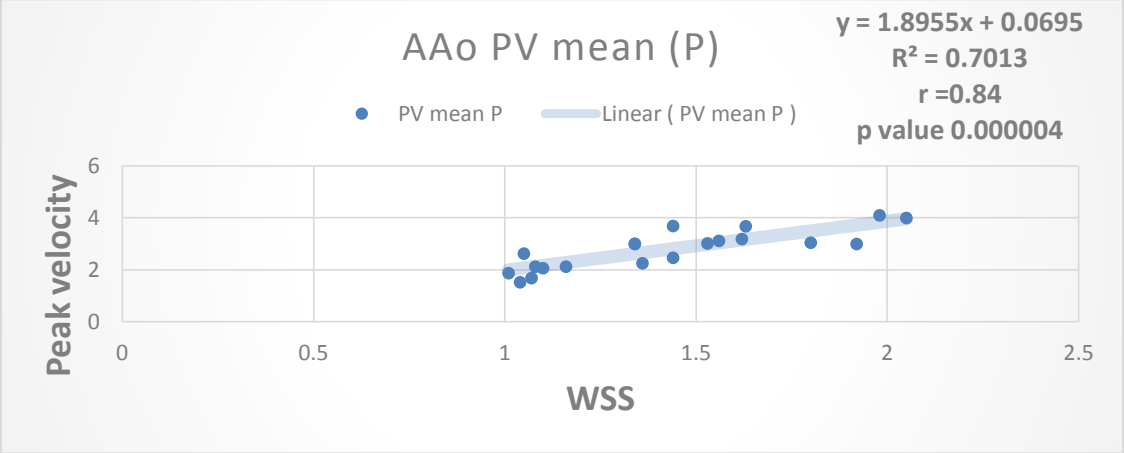

Figure 91. The correlation between the peak systolic velocity in the ascending aorta and WSS magnitude in P. Note the very strong positive correlation. AAo = ascending aorta, PV = peak velocity, P = primary.

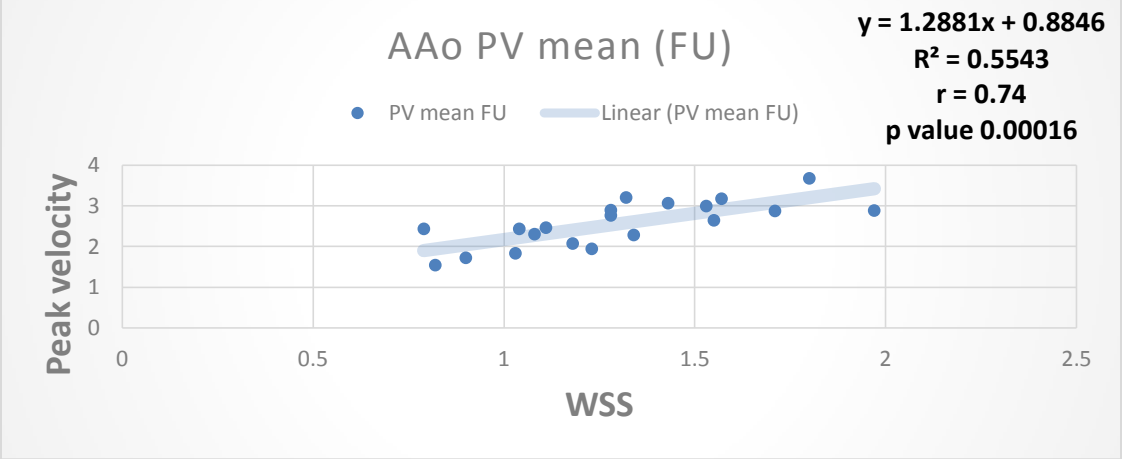

Figure 92. The correlation between the peak systolic velocity in the ascending aorta and WSS magnitude in FU. Note the strong positive correlation. AAo = ascending aorta, PV = peak velocity, FU = follow-up.

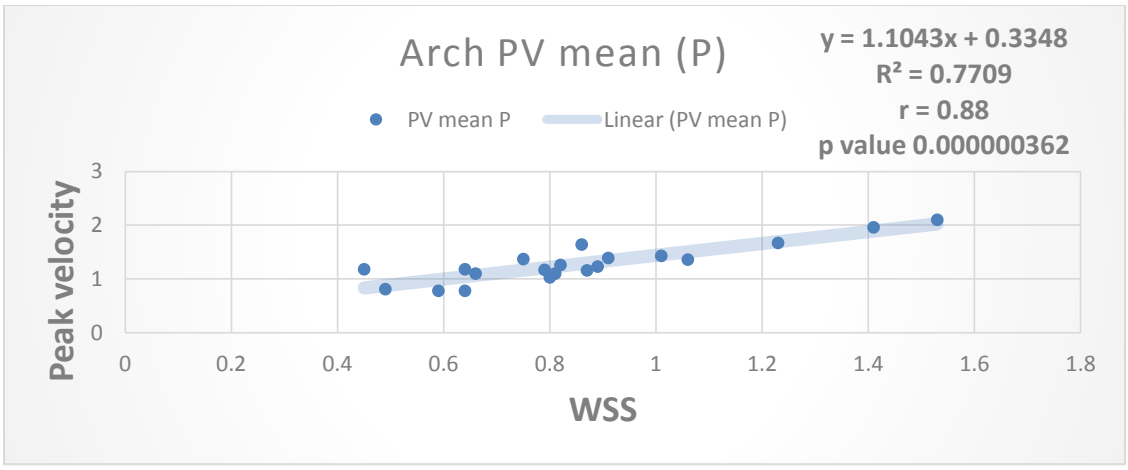

Figure 93. The correlation between the peak systolic velocity in the aortic arch and WSS magnitude in P. Note the strong positive correlation. Arch = aortic arch, PV = peak velocity, P = primary.

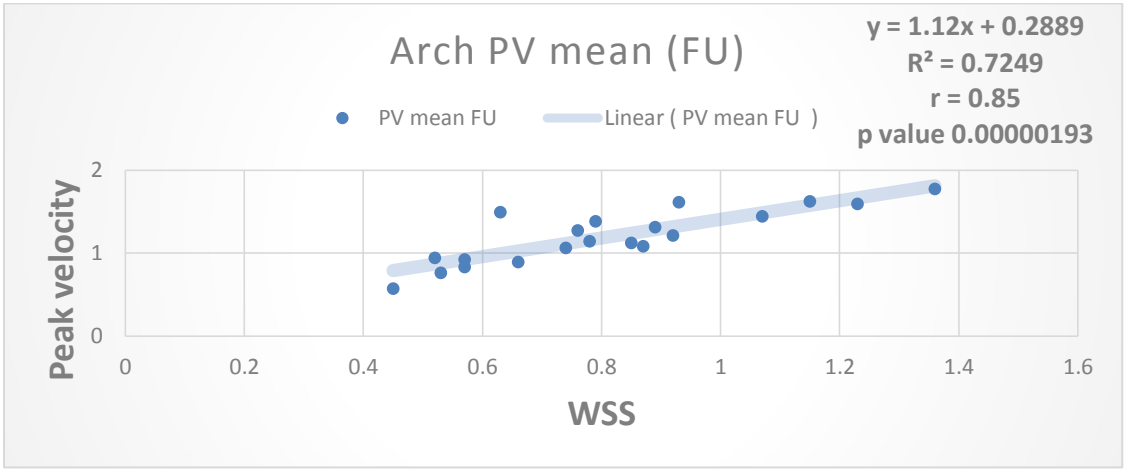

Figure 94. The correlation between the peak systolic velocity in the aortic arch and WSS magnitude in FU. Note the strong positive correlation. Arch = aortic arch, PV = peak velocity, FU = follow-up.

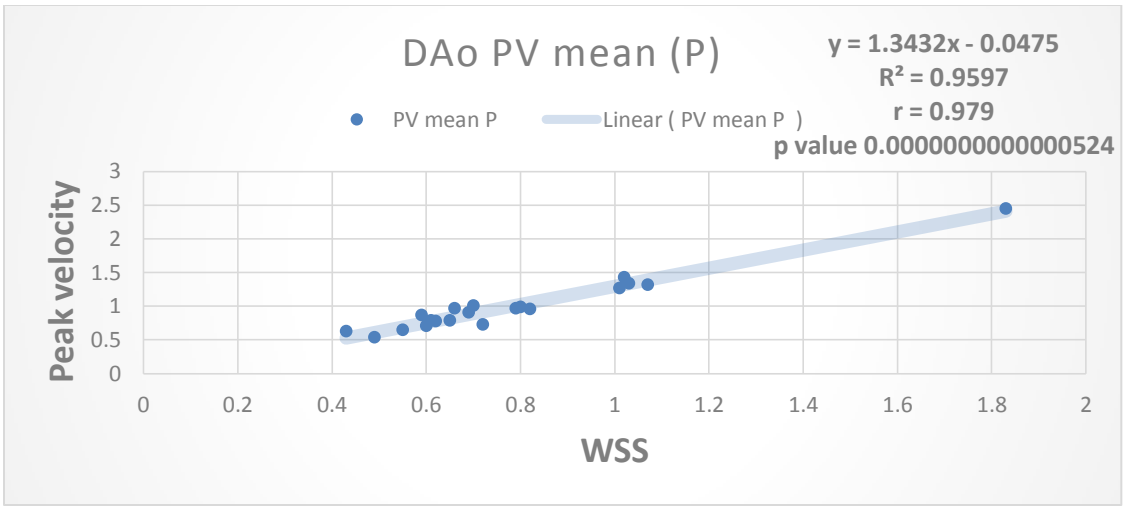

Figure 95. The correlation between the peak systolic velocity in the descending aorta and WSS magnitude in P. Note the very strong positive correlation. DAo = descending aorta, PV = peak velocity, P = primary.

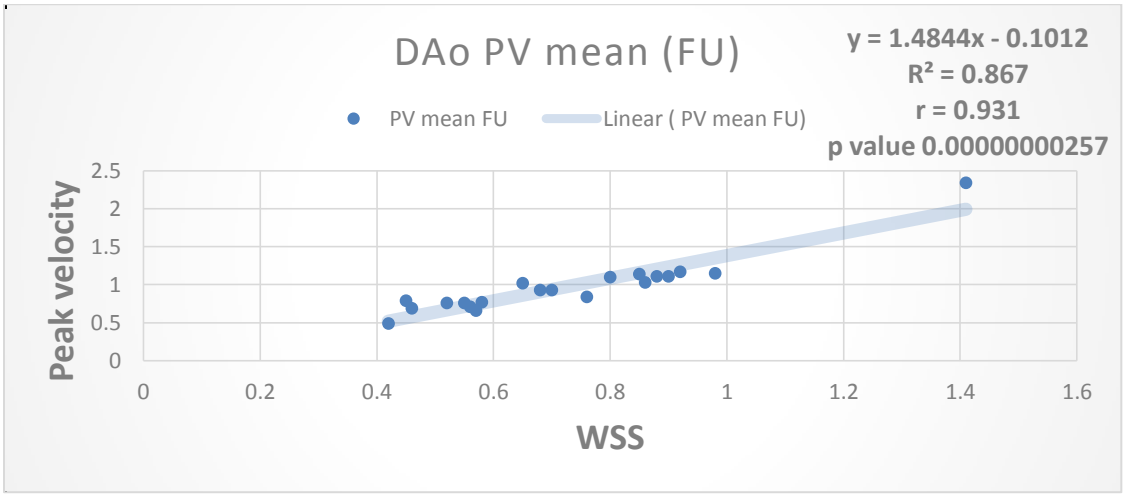

Figure 96. The correlation between the peak systolic velocity in the descending aorta and WSS magnitude in FU. Note the very strong positive correlation. DAo = descending aorta, PV = peak velocity, FU = follow-up. In Figures 78 and 79, only one patient's descending aortic velocity is significantly higher than all the others because of aortic coarctation.

Additionally, there was no significant correlation between peak velocity, blood pressure and heart rate, given that all the patients were normotensive and had normal heart rates during the examination (mean systolic blood pressure: 129.3±17.87 mmHg, mean diastolic blood pressure: 74.5 ±11.57 mmHg, mean heart rate: 67±12.03 bpm).

11.5. Helical and vortical flow in thoracic aorta

The helical and vortical flow formations in NOP and OP did not change statistically significantly over time (Table 17). However, we observed changes in helical and vortical flow in individual cases. There were 13 patients in the NOP group, 5 with TAV and 8 with BAV. Over time, there was no change in the helical and vortical flow formation in the five patients with TAV. However, while there was no change in vortices over time for the eight patients with BAV, helical flow increased from grade 1 to grade 2 in one patient and decreased from grade 2 to grade 1 in another. Otherwise, helical flow remained unchanged in the remaining patients.

The vortical flow in OP changed in 2 of the 7 patients. After surgery, one patient developed a new vortical flow formation, and in the other, the vortical flow formation disappeared. Regarding the helical flow formation, four out of seven patients showed a change. Helical flow intensity decreased in one patient from grade 3 to 1, in one patient from grade 3 to 2, and in one patient from grade 2 to 1, while one patient showed an increase from grade 1 to 2 (Table 16).

Statistically, the helical flow was more intense in patients with BAV than those with TAV in primary and follow-up studies (p value of 0.002 and 0.009, respectively). The intensity of helical flow formation does not correlate with the presence of vortical flow formation. There is helical flow in all patients, but not all have vortical flow.

Change over time	Helical flow NOP	Helical flow OP	Vortical flow NOP	Vortical flow OP
Increase	1B	1B	0	1B
Decrease	1B	3B	0	1B

Table 16. The change in helical and vortical flow over time. B = BAV, NOP = non-operated group, OP = operated group.

(NOP) TAV	Hx(P)	Hx(FU)	p value	Vx(P)	Vx(FU)	p value
1	1	1		0	0	
2	1	1		1	1	
3	2	2		1	1	
4	1	1		0	0	
5	1	1	1	1	1	1
BAV						
1	1	2		0	0	
2	3	3		0	0	
3	3	3		0	0	
4	3	3		0	0	
5	1	1		1	1	
6	2	1		1	1	
7	1	1		1	1	
8	1	1	1	1	1	1
(OP)						
1 T	1	1		1	1	
2	3	1		0	0	
3	3	3		1	1	
4	2	1		0	1	
5	1	2		1	0	
6	3	2		1	1	
7	3	3	0.29	1	1	1

Table 17. The difference between P and FU regarding the helical and vortical flow formations. Hx = helix, Vx = vortex, T = TAV, BAV = bicuspid aortic valve, P = primary, FU = follow-up.

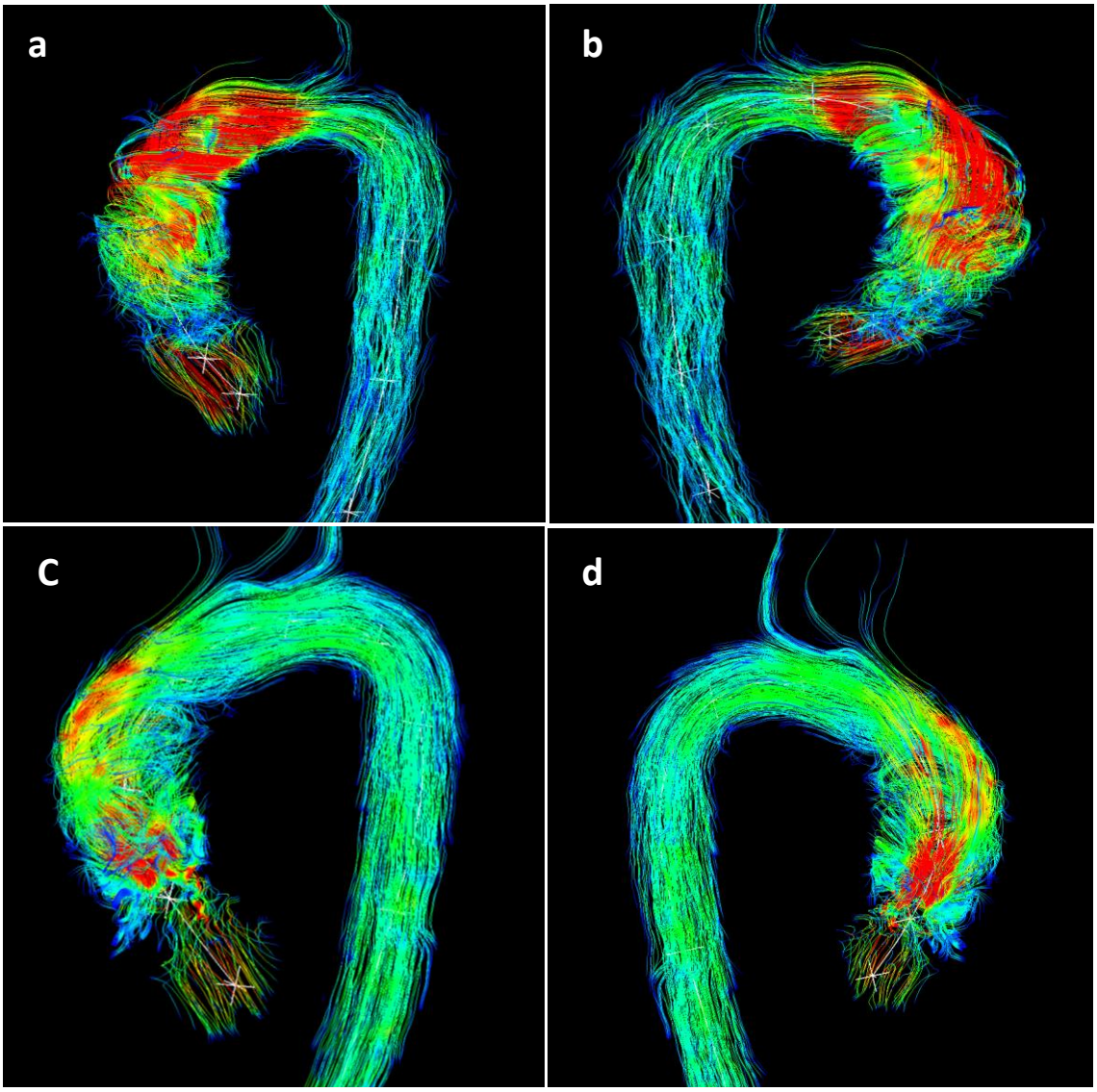

Figure 97. Here is an example of a patient whose helical flow intensity decreased after surgery. Images a and b are anterior and posterior views of the thoracic aorta depicting the helical flow intensity with streamlines in the primary study; c and d are the same views of the thoracic aorta showing regression of the helical flow intensity in the follow-up study.

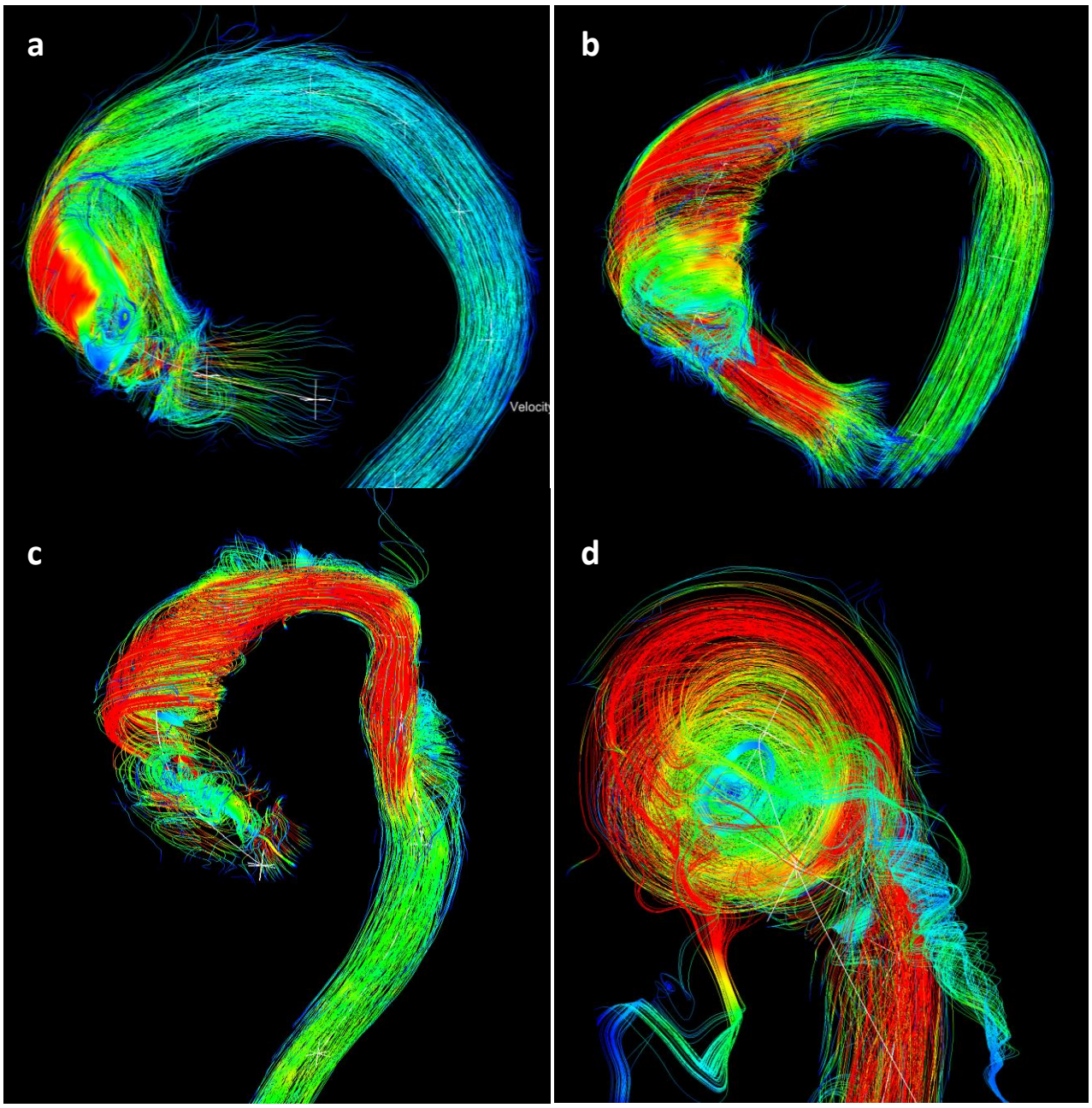

Figure 98. Examples of the different grades of helical flow intensity. a) mild helical flow (grade 1), b) moderate helical flow (grade 2), and c) severe helical flow (grade 3). d) cross-sectional view of the mid ascending aorta showing helical flow.

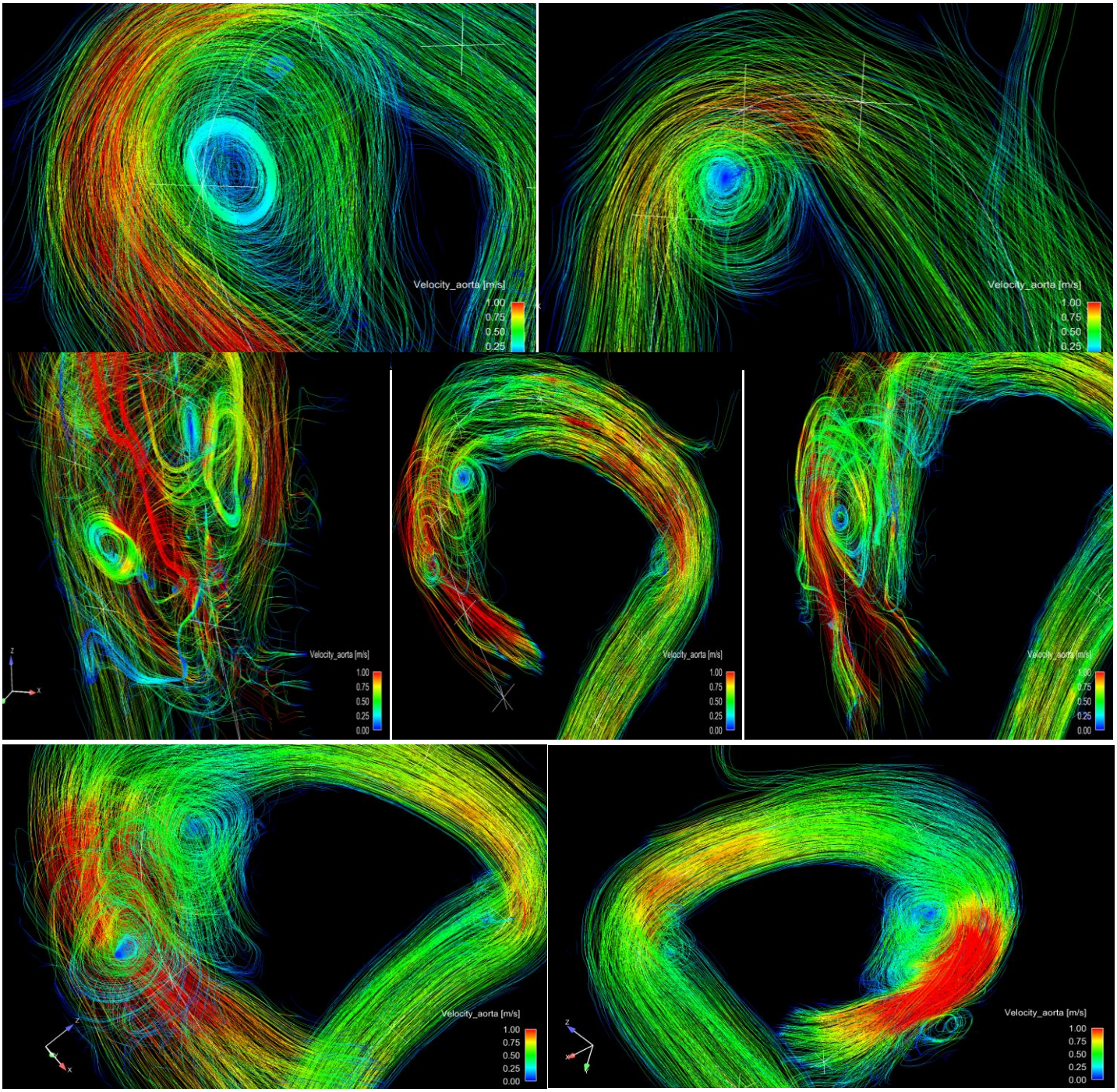

Figure 99. Examples of the most stunning vortical flow formations in our study.

Helical flow and vortical flow and WSS

There was a significant positive correlation between helical flow formation intensity and WSS in both P and FU.

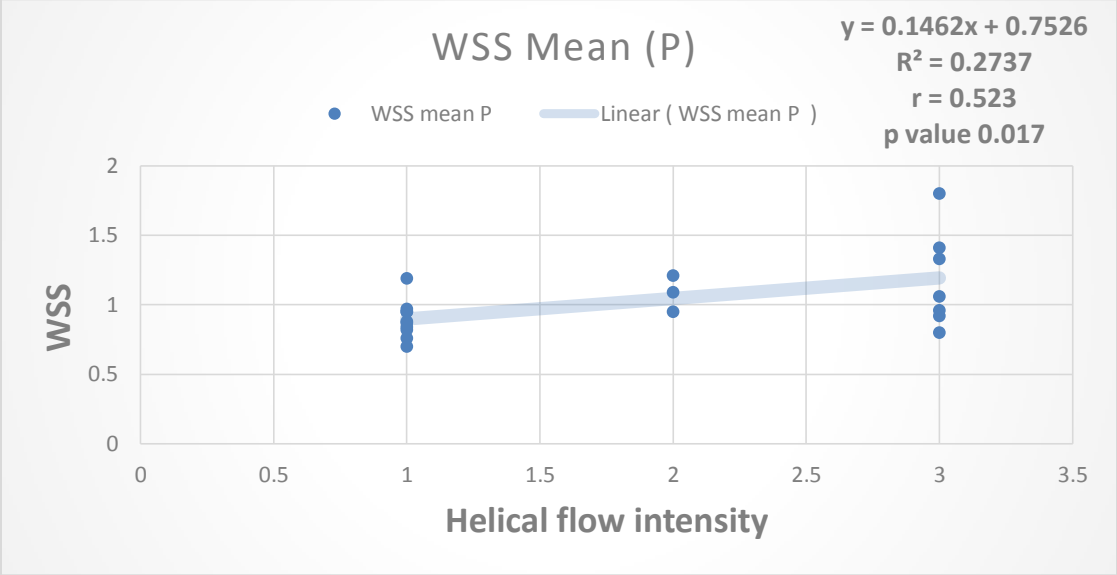

Figure 100. The correlation between the helical flow intensity and the WSS in P. Note the positive correlation. WSS = wall shear stress, P = primary.

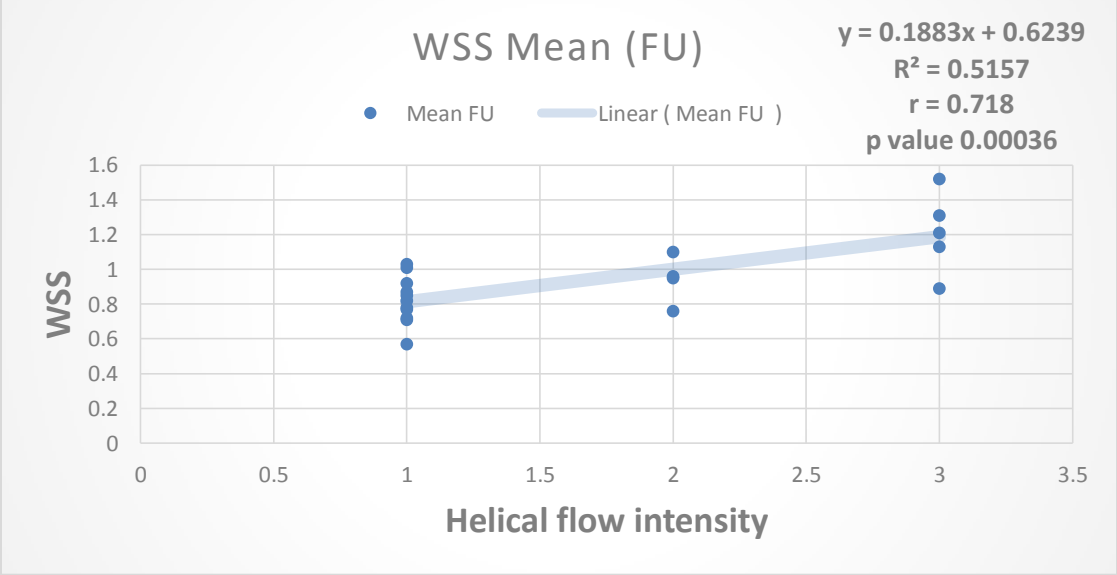

Figure 101. The correlation between the helical flow intensity and the WSS in FU. Note the positive correlation. WSS = wall shear stress, FU = follow-up.

There was a significant correlation between aortic valve morphology and helical flow intensity. BAV patients had more intense helical flow.

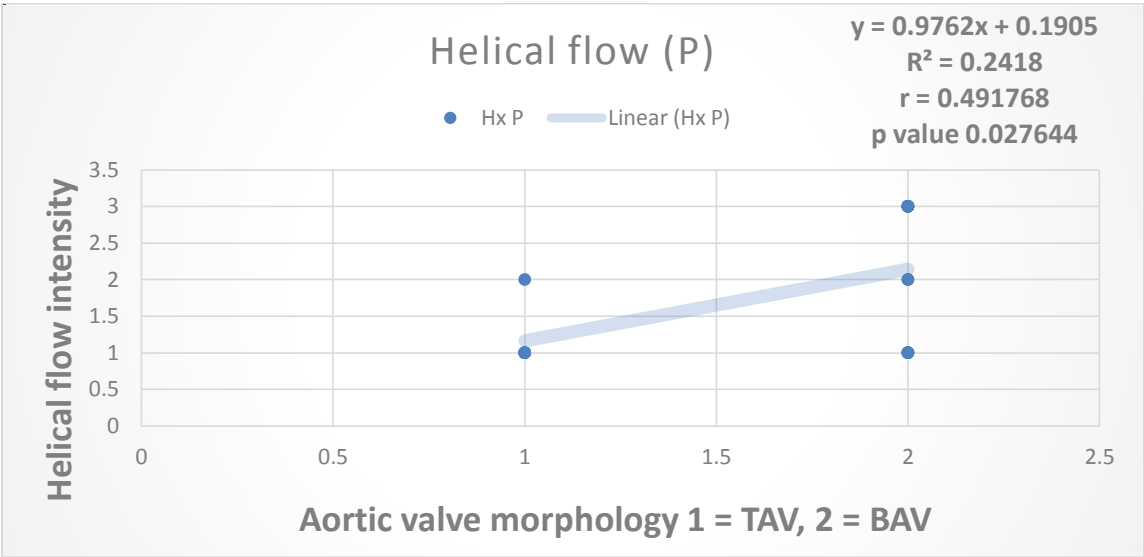

Figure 102. The correlation between the helical flow intensity and the aortic valve morphology. Note the positive correlation between the presence of BAV and the helical flow intensity. Hx = helical flow, P = primary.

There was no significant correlation between the aortic valve morphology and the presence of vortical flow (r = 0.09, p value = 0.71). In addition, there was no significant correlation between the intensity of helical flow and the presence of vortical flow (P: r = 0.25, p value 0.29; FU: r = 0.29, p value 0.21). Helical flow intensity tended to be related to the severity of aortic valve stenosis (Hx P (NOP): 1.6±0.87, Hx P (OP): 2.3±0.95, p value 0.06). There was no significant correlation between the presence of vortical flow and WSS (P: r = 0.087, p value 0.71; FU: r = 0.13, p value 0.59). There was no correlation between the aortic diameter and the presence of vortical flow (P: r = 0.29, p value 0.21; FU: r = 0.14, p value 0.57). In addition, there was no significant correlation between the aortic diameter and the intensity of helical flow (P: r = 0.27, p value 0.25; FU: r = 0.15, p value 0.52).

There was no significant correlation between the presence of vortical flow and age (r = 0.01, p value 0.96), gender (r = 0.13, p value 0.57), blood pressure (r = 0.002, p value 0.99), heart rate (r = 0.21, p value 0.37) and aortic valve morphology (TAV or BAV) (r = 0.09, p value 0.71). There was no significant correlation between helical flow and age (r = 0.1, p value 0.69), gender (r = 0.15, p value 0.51), blood pressure (r = 0.07, p value 0.77) and heart rate (r = 0.25, p value 0.28).

12. Discussion

Our follow-up study successfully enrolled 20 patients, divided into two groups: NOP and OP. This is one of the few follow-up studies evaluating aortic hemodynamics in patients with aortic valve disease. We longitudinally evaluated left ventricular parameters and hemodynamic parameters using 4D flow MRI. This study was focused on wall shear stress (WSS), its evolution over time, and its possible correlation to other parameters. On follow-up, the mean age was 57.5±15.9 years in NOP and 73.2±4.4 years in OP. The mean duration from P to FU was 4.4±1.5 years for NOP and 4.3±1.4 years for OP. There was a significant difference between OP and NOP in terms of age and BMI, with the OP group being older and having a lower BMI.

In our study, WSS and BMI were not significantly correlated ($r = 0.07$, $p = 0.77$). There was, however, a trend of a significant negative correlation between age and WSS (P: $r = 0.31$, p value 0.092, FU: $r = 0.41$, p value 0.038). There was a correlation between age and WSS in a few previous studies. An example is a study published in 2015 in which Lantz et al. measured aortic diameter and WSS using CMR in two groups of males: younger males ($n = 10$) and older males ($n = 8$) of various ages. The study found that WSS decreased with age due to an increase in aortic diameter and a decrease in stroke volume resulting in a decrease in aortic shear rate (77). Furthermore, Callaghan et al. published a study in 2018 in which they measured thoracic aortic WSS in 224 healthy subjects with normal anatomy (mean age 49.58± 17.97) using 4D flow MRI. The same conclusion was reached that WSS decreases with age (78).

The results of our study support the previously described observations that the WSS decreases with age. The decrease in WSS with time (i.e., with age) could be explained by the increase in aortic diameter over time in NOP and the decrease in LVEF and LVSV after surgery in OP.

12.1. LV mass, LV EF, and aortic diameter

We assessed the LV mass and mass index as an indicator of LV remodeling together with the other LV parameters: LVEDV, LVSV, and LVEF. In NOP, we evaluated the evolution of LV mass over time and predicted that it would decline in OP following surgery. There were no significant differences in LVEDV, LVSV, LVEF, and LV mass between P and FU in NOP. In contrast, in OP, there was a significant decline in LVSV, LVEF, and LV mass after surgery. Our study showed a reduction in LV mass and mass index of 24.6% after surgery. Reverse cardiac remodeling is clearly evident from the marked LV mass reduction after surgery.

The significant reduction in LVEF is probably due to a reduction in LVSV caused by the reduction in LV mass.

In previous studies, similar results were observed. An example is Rank et al.'s study published in 2021. In a prospective study, 27 patients undergoing aortic valve replacement were assessed by CMR for left ventricular function and structure (n = 19 with aortic stenosis and 8 with aortic regurgitation). CMR was performed before and 1, 5, and 10 years after aortic valve replacement. LV volumes, mass, and LVEF were evaluated. Their observations showed a decrease in LVMI, EDVI, and ESVI in both groups, and as a consequence, they concluded that aortic valve replacement might result in reverse cardiac remodeling (79). In addition, Thomas et al. published a study in 2018. A total of 181 patients with severe aortic stenosis were evaluated by echocardiography and CMR before undergoing aortic valve replacement (AVR). CMR was done one year after AVR for 116 patients who did not receive a pacemaker after AVR (age 70 ± 10 years; 54% male). It was observed that the LV mass index had decreased by 19% following surgery (80). Another follow-up study published in 2015 by Une et al. reported similar results after assessing 3112 patients with AVR by echocardiography (median follow-up: 6 years). The average age of the patients at the time of surgery was 67.8±13.4 years; almost 30% were females. There was a significant reduction in LV mass following surgery. The maximum LV mass regression took one year in patients with aortic stenosis and almost five years in patients with aortic regurgitation (81).

As for aortic diameter, the maximal aortic diameter showed a statistically significant increase over time in NOP (aortic diameter P: 39.8±6.8 mm, FU: 40.3±6.1 mm, p value: 0.045). The annual growth rate was approximately 0.1 mm/y. None of the patients included in our study was a fast grower. The maximal aortic diameter did not differ statistically significantly after surgery. However, in one case with BAV, we observed an increase in the aortic diameter even after the valve was replaced (aortic diameter P: 37 mm and FU: 40 mm).

There was a statistically significant correlation between LV mass and WSS in our current study. In other words, WSS regression after surgery may be considered a sign of reverse cardiac remodeling after surgery. The correlation between aortic diameter and WSS was insignificant in P, but it tended to be more significant in FU. (P: r = 0.09, p value 0.69; FU: r = 0.30, p value 0.19). Our current study may indicate a possible correlation between WSS and aortic dilatation over time; however, this relationship was not statistically confirmed.

12.2. Net flow

With 4D Flow CMR, flow measurements are similar to those in conventional 2D PC-CMR, but it is possible to retrospectively position planes for flow volume measurements at any location within the acquired data volume (82). According to our analysis, there was no significant change in the NOP's net flow over time. However, the mean net flow in the thoracic aorta in the OP increased significantly over time. According to the findings, the mean net flow in the ascending aorta increased, but the aortic arch and descending aorta did not show any statistically significant changes. At the level of planes, the net flow in OP increased significantly in 3 out of 8 planes: planes 1, 2, and 6 (planes 1 and 2 correspond to the proximal ascending aorta, and plane 6 represents the transition zone between the aortic arch and the descending aorta).

In the ascending aorta, we observed a statistically significant negative correlation between the net flow and the WSS in P ($r = 0.68$, p value 0.0008) and a less significant correlation in FU ($r = 0.27$, p value 0.12). The net flow decreases as the WSS increases (as in aortic stenosis). One possible explanation for this is that as WSS increases, there is more resistance to blood flow, which contributes to a decline in net blood flow in the ascending aorta. Additionally, as aortic valve stenosis progresses, the measured noninvasive hemodynamic parameters (flow and peak velocity) become more underestimated (92), causing a more significant negative correlation between net flow and WSS. Overall, FU showed a negative correlation, but it was not statistically significant. The reason might be that all patients in FU had relatively normal flow values, either because their aortic valve stenosis was not hemodynamically significant (in NOP) or because their flow had normalized after their surgery (in OP). In contrast, in the aortic arch, there was a trend toward a significant positive correlation between net flow and mean WSS ($r = 0.33$, p value 0.16). Moreover, a statistically significant positive correlation between net flow and mean WSS was observed in FU ($r = 0.51$, p value 0.017). In the descending aorta, a significant positive correlation was found between net flow and mean WSS both in P ($r = 0.7$, p-value 0.0006) and FU ($r = 0.7$, p-value 0.0003). The positive correlation between the WSS and net flow in the aortic arch and descending aorta could be explained by the fact that the aortic arch and descending aorta experience lower WSS values than the ascending aorta, and those values are not high enough to cause significant resistance to blood flow and a subsequent decrease in net flow. It also seems that the relation between WSS and net flow is, to a certain extent, a positive correlation, but as the WSS increases, the correlation becomes negative. The exact correlation between aortic net flow and WSS will have to be determined in more extensive studies in the future.

12.3. Wall shear stress (WSS)

Wall shear stress represents the force that the vessel wall exerts on the blood flow per unit area along the local tangent plane (83). Additionally, the WSS can be defined as the spatial gradient of the 3D velocity vector perpendicular to the vessel wall at each edge point. Recently, several methods have been developed to compute volumetric 3D WSS along the entire aorta using a 3D velocity field (84-88). However, it remains challenging to assess WSS *in vivo* with absolute accuracy. In 4D flow MRI, WSS is calculated from the gradient of the velocity adjacent to the wall and an assumed viscosity using the formula below (85).

$$WSS = \mu \frac{dv}{dy}$$

μ: blood viscosity, v: blood flow velocity, y: distance from the wall.

Due to the discrete nature of the measured velocity field in 4D flow MRI, WSS values are systematically underestimated. Wall shear stress (WSS) is commonly estimated from maximum velocity when a parabolic (Poiseuille) velocity profile is assumed; however, *in vivo*, the usually assumed fully developed velocity profile is seldom valid. Using a parabolic profile may result in errors of 20–50% and 30–60% in average and peak WSS, respectively. Furthermore, WSS estimates based on maximum velocity overlook significant circumferential variations (89). Despite that, the WSS magnitude and its expression pattern can be reliably assessed if a constant methodology is used for its estimation across samples. (90,91).

In healthy aging, WSS in the aorta undergoes significant changes, reinforcing the necessity of age-matched control cohorts in clinical studies for identifying patients with altered WSS (87,88). Unfortunately, the two groups represented in our follow-up study population differed significantly in age. WSS has been implicated in modifying gene expression and endothelial cell function, leading to vascular remodeling (92). Several studies have demonstrated that it can be a helpful tool for determining the effects of altered blood flow on the aortic wall. The WSS pattern and magnitude are significantly altered in both BAV and AS patients. Hope et al. (93) and Barker et al. (94) first referred to a link between eccentric flow patterns and elevated WSS in BAV patients. Several other studies have also confirmed these findings (95,96,97,98). The high-velocity transvalvular outflow jets seen in patients with aortic stenosis result in an eccentrically elevated WSS in the ascending aorta. Our previous study published in 2016 by von Knobelsdorff-Brenkenhoff et al. (n = 37) showed that patients with aortic valve stenosis have altered flow patterns and regionally elevated wall shear

stress (WSS) in the ascending aorta (1). The same findings were confirmed by a large study (n >500) using 4D flow MRI in patients with AS and ascending aortic dilatation. A 3D WSS analysis of ascending aortas demonstrates that AS is associated with a markedly increased regional WSS compared to patients with aortic dilation and normally functioning tricuspid aortic valves (99).

A study published in 2015 by Guzzardi et al. explored the correlation between abnormal 3D WSS and regional aortic tissue remodeling in BAV patients with AS. Preoperative 4D flow MRI was performed on 20 patients undergoing ascending aortic resection to map their 3D WSS, and the results were compared with histological examinations of the surgically resected tissues. In addition, a paired sample of the aortic wall (regions with elevated and normal WSS) was histologically examined. Medial elastin degradation was more pronounced in areas with increased WSS than in adjacent areas with normal WSS. These findings suggest that regional valve-mediated hemodynamics may provide prognostic information for aortic wall disease (100).

On the evidence of our current study, the magnitude of the mean WSS in the thoracic aorta decreased significantly in OP after surgery. In NOP, however, no significant change in the mean WSS magnitude was observed over time. In particular, in OP, the mean WSS demonstrated a statistically significant reduction in the ascending (p value: 0.03) and descending aortas (p value: 0.03), as well as a borderline decrease in the aortic arch (p value: 0.05). On the other hand, in NOP, there was no significant change in mean WSS magnitude in either ascending aorta, aortic arch, or descending aorta over time. Komoriyama et al. reported similar results in a study published in 2021, in which they examined WSS magnitude and distribution as well as blood flow patterns in the ascending aorta before and after transcatheter aortic valve replacement (TAVR). After TAVR, there was a significant decrease in WSS along the ascending aortic circumference (101).

Additionally, in our current study, a re-analysis of the WSS in the thoracic aorta based on dividing it into outer and inner curvature revealed that:
With aortic valve disease progression (as in the OP group in the primary study), there was a trend toward a higher WSS along the outer curvature of the ascending aorta than the inner curvature (p value: 0.09); otherwise, there was no significant difference between the outer and inner curvature of the aortic arch or the descending aorta. Our findings agree with several previous studies, which also noted the highest WSS along the outer curvature of the ascending aorta (102,103,104, and more recently 105). The curvature of the aortic arch affects the WSS distribution in the ascending aorta as it changes the direction of blood exiting the heart. The fluid at the vessel's center travels at a faster velocity than

the fluid closer to the wall and is more difficult to displace. The blood is thus skewed towards the outer curvature of the bend (106).

We also observed a significant decline in the mean WSS along the inner curvature of the ascending aorta in NOP over time. In contrast, the mean WSS along the outer curvature of the ascending aorta and aortic arch, as well as the inner curvature of the descending aorta, decreased significantly in OP.

Furthermore, a re-analysis was done based on dividing the aorta into segments, which showed that:

In NOP, the WSS in the ascending aorta was higher than the aortic arch and descending aorta in both P and FU: ascending aorta (P: 1.33±0.39 N/m^2, FU: 1.28±0.33 N/m^2), aortic arch (P: 0.82±0.13 N/m^2, FU: 0.87±0.15 N/m^2), and descending aorta (P: 0.85±0.14 N/m^2, FU: 0.79±0.14 N/m^2). The descending aorta had higher WSS than the aortic arch in P but it was lower in FU.

In OP, the WSS in the ascending aorta was higher than the aortic arch and descending aorta: ascending aorta (P: 1.61±0.57 N/m^2, FU: 1.33±0.32 N/m^2), aortic arch (P: 0.93±0.15 N/m^2, FU: 0.71±0.09 N/m^2), and descending aorta (P: 0.67±0.13 N/m^2, FU: 0.6±0.11 N/m^2). The aortic arch had higher WSS than the descending aorta in both P and FU.

Furthermore, WSS magnitudes and distributions also changed at the segmental level. In NOP, 2 of the 18 segments showed a significant change over time. While segment 7 showed a significant increase in mean WSS, segment 14 showed a significant decrease. Meanwhile, 5 out of 18 segments along the outer aortic curvature showed a significant decline in OP. The mean WSS decreased significantly in segments 3, 7, 9, 11, and 15.

Along with changes in WSS magnitude, the distribution of WSS has also changed. Several observations were made regarding the change in WSS distribution. First, the top 6 segments with the highest WSS in the entire thoracic aorta were located in the ascending aorta in OP (P and FU) and NOP (P). In NOP (FU), the top 5 segments were located in the ascending aorta, while the segment in sixth place was the outer proximal aortic arch.

In NOP, the distribution of the top 3 WSS segments in the ascending aorta was identical in both P and FU. The top 3 segments were confined to the proximal and mid ascending aorta. In contrast, the distribution of the bottom three segments in the ascending aorta changed in FU. This led to a slightly higher WSS in the distal outer ascending aorta in comparison to P. In the aortic arch, the only change between P and FU was that segments 7 and 12 had exchanged

places (the segment with the highest WSS in the aortic arch changed from being the inner distal to being the outer proximal aortic arch). In the descending aorta, the distribution of both the top and bottom three segments was the same in both P and FU. Note that the top 2 segments in the descending aorta were 14 and 13. The top 2 segments in the descending aorta were the same in all four groups.

In the OP group in P, the distribution of the top 3 WSS segments in the ascending aorta was markedly changed compared to the NOP group in P. The top 3 segments in OP (P) were distributed along the entire ascending aorta, whereas in NOP (P), they were confined to only the proximal and mid ascending aorta. We could refer to the change in the distribution of WSS in the top 3 segments in the ascending aorta from being confined to the proximal and mid ascending aorta in NOP (P) to extending to the distal ascending aorta in OP (P) as a distal displacement of the WSS distribution, which might be a sign of aortic valvular disease progression. The WSS distribution changed once again in OP in FU (i.e., after aortic valve replacement). A regression of the previously described distal displacement of the WSS distribution was clearly evident. After surgery, the top 3 segments were again confined to the proximal and mid ascending aorta rather than reaching the distal ascending aorta. Interestingly, the top 2 segments retained their positions even after surgery, although with lower WSS values. The regression of the WSS distribution distal displacement may signify hemodynamic improvement after surgery.

In the aortic arch in the OP in P, the top 3 segments were confined to the proximal and mid arch. Segment 8, representing the inner proximal aortic arch, ranked 2nd in all four groups. The change in the top 3 segments of the aortic arch was limited to segments 1 and 3. In NOP (P), the top 3 segments in the aortic arch were 12, 8 and 10, respectively. All top 3 WSS segments in NOP (P) were confined to the inner aortic arch curvature. In NOP (FU), we observed that segment 7 (outer proximal arch) took the lead from segment 12 (inner distal arch), while segments 10 and 8 (inner mid and proximal arch) kept their places. In OP (P), both the first and second segments kept their places, while segment 9 (mid outer arch) took third place. That means that two of the top 3 segments are located in the outer aortic arch (outer proximal and mid arch). Comparing WSS distribution between NOP and OP, we observed a tendency for an outer displacement of WSS distribution (outer aortic arch) over time (i.e., with disease progression). WSS distribution outer displacement might also signify aortic valve disease progression. Another interesting finding in the WSS distribution of the aorta arch was WSS in segment 7 (the outer proximal aortic arch). In NOP (P), it ranked fourth. In NOP (FU), even though the patients in this group showed no obvious overall aortic valve disease progression, segment 7 showed a marked

increase in the WSS, taking the lead in the aortic arch from segment 12, and it kept that lead in OP (P) and (FU). An increase in WSS in segment 7 might be an early sign of aortic valve disease progression. Interestingly, in the descending aorta in both NOP and OP at both P and FU, segments 14 and 13, respectively, (representing the proximal descending aorta distal to the origin of the left subclavian artery) kept their places as the top 2 segments in the descending aorta. The proximal descending aorta was exposed to the highest WSS magnitudes in the descending aorta in both groups and over time.

To summarize, certain areas of the thoracic aorta are exposed to high WSS in all groups and over time: the proximal and mid ascending aorta, the proximal aortic arch, and the descending aorta proximally just distal to the origin of the left subclavian artery. The ascending aorta is exposed to the highest WSS magnitudes, while the descending aorta ranks in second place, and the aortic arch comes third. Conversely, the aortic arch takes second place with aortic valve disease progression, and the descending aorta comes third. It is interesting to note that approximately 65% of aortic dissection intimal tears occur in the ascending aorta, 30% in the descending aorta, less than 10% in the aortic arch, and that most ascending aortic dissections begin within a few centimeters of the aortic valve (approximately 2-2.5 cm above the aortic root), and most descending aortic dissections begin just distal to the left subclavian artery (107). Interestingly, aortic dissections occur most frequently in the thoracic aorta segments exposed to the highest WSS magnitudes, and there seems to be an apparent correlation between WSS magnitude and the occurrence of aortic dissection. Chi et al. published a small study in 2017. They included five patients with Stanford type A aortic dissection and two normal aortas. Using the original imaging data, the structure of the aortas before the type A dissection was reconstructed. According to the flow analysis of the reconstructed premorbid structures, in three out of five cases, the rupture positions corresponded to areas of maximum elevated WSS.

In addition, the WSS at the junction of the descending aorta and the aortic arch was elevated. Furthermore, the WSS in the patients with aortic dissection was almost double what it was in the control group. Moreover, they also found that the ascending aorta's dilated areas were exposed to higher WSS than the areas with a normal diameter (108).

Osswald et al. published a pilot study in 2017. The purpose of this study was to retrospectively compare CT angiography images from 10 patients with type B dissections who later experienced a retrograde type A aortic dissection (RTAD) with CT images from 10 control subjects. On the basis of CT angiography datasets, computational flow dynamics simulations were performed to assess pressures, velocity magnitudes, and wall shear stress (WSS) at the future RTAD

entry tear site. At the site of the future entry tear, the WSS was notably higher than in the surrounding wall, and in the RTAD group, it was higher than in the control group. However, there were no significant differences in pressure or velocity magnitudes between the entry tear, the surrounding aortic wall, or the control group (109).

Furthermore, we saw a statistically significant increase in the diameter of the ascending aorta in NOP over time, but without a significant increase in the mean WSS magnitude. In contrast, we observed a significant decrease in WSS magnitude in the inner proximal ascending aorta with a slight increase along the outer distal ascending aorta in response to change in WSS distribution over time. Overall, the WSS along the outer curvature of ascending aorta was slightly higher than the inner curvature (p-value 0.4). The dilatation of ascending aorta may be a compensatory mechanism to reduce elevated WSS forces by aortic remodeling. Statistically, we observed no significant correlation between WSS and aortic diameter. In contrast, in 2022, Soulat et al. published a study. They aimed to determine whether wall shear stress (WSS) predicts the growth of the ascending aorta (AAo). Seventy-two patients with BAV, aged 45±12 years, underwent CMR for aortic dilation surveillance both at baseline and after five years of follow-up. In 4D flow MRI analysis, WSS heat maps were calculated for individual patients and compared with the averages of 136 healthy age- and sex-matched controls. They measured the portion of the AAo that was exposed to high WSS. The average yearly growth rate of the AAo was 0.24±0.20 mm. Patients whose growth rates were higher than 0.24 mm/y had a larger proportion of the AAo exposed to high WSS than those below 0.24 mm/y. Elevated WSS in the AAo was linked to higher rates of AAo dilation, exceeding 0.24 mm/y. By analyzing the area of elevated AAo WSS, 4D flow MRI can identify patients with bicuspid aortic valve (BAV) who are at higher risk of aortic dilation. This information can be helpful in determining which patients require closer monitoring (110).

In the same context, Guala et al. observed in their study (n = 47) published in 2021 that circumferential WSS, but not WSS magnitude, showed statistically significant positive associations with the ascending aortic growth rate in patients with BAV (111). In the same context, Salmasi et al. showed, in a study published in 2021 using CMR on 10 patients with ascending aortic aneurysms who had no BAV or connective tissue disease, that areas in the aortic wall exposed to elevated WSS exhibit medial degeneration more than areas with lower WSS. Medial degeneration is a sort of maladaptive remodeling which could lead to aortic wall thinning, dilatation, and aneurysmal formation (105). Additionally, a study published by Pasta et al. in 2020 aimed to determine the relationship

between wall shear stress and aortic strain biomarkers, particularly matrix metalloproteinases, tissue inhibitors of metalloproteinase and microRNA, by looking at patients with ascending aortic aneurysms with either bicuspid or tricuspid aortic valve. Aortic strain biomarker activity correlated positively with the systolic wall shear stress observed in the proximal ascending aorta. Aortic aneurysms are associated with increased circulating biomarkers related to flow-based and structural descriptors, suggesting mechanotransduction-induced vascular remodeling in the dilated aorta. Combining shear stress and circulating biomarkers could enhance patient-specific decision-making for ascending aortic aneurysms (112).

While WSS is difficult to calculate, its relationship to endothelial function and vascular remodeling as well as its possible role in initiating aortic dilatation and dissection is apparent. However, large longitudinal studies are still lacking to determine if altered hemodynamic metrics (such as increased WSS) contribute to aortic disease progression (113).

12.4. Peak systolic velocity

The accuracy and reliability of measuring blood flow and velocity through 2D velocity-encoded flow MRI (2D flow MRI) have improved over time. In the case of examining the aorta, 2D flow MRI has been found to be dependable and comparable to TTE (114). However, it necessitates an experienced operator to identify the vessel of interest and can only measure flow velocity perpendicular to the imaging slice direction (115). Furthermore, it is difficult to visualize the exact position of the acquisition plane before planning the acquisition, which can result in reduced measurement accuracy. As a result, 2D flow MRI may underestimate flow rate and velocity (116). On the other hand, 4D flow MRI enables the visualization and quantification of flow patterns in the heart and blood vessels. Unlike 2D flow MRI, 4D flow MRI allows for velocity encoding (VENC) in three main spatial directions, providing a practical tool to evaluate blood flow. In 2021, Hälvä et al. conducted a study to evaluate the accuracy of 2D and 4D flow MRI techniques in measuring aortic transvalvular peak systolic flow in patients with severe AS. The study included 90 patients with severe AS and 10 control subjects. The patients received echocardiography and 2D and 4D flow MRI. The results showed that 4D flow MRI underestimated peak flow velocity in the AS group compared to TTE and 2D flow MRI. However, there was no significant difference between TTE and 2D flow MRI. Interestingly, the control group showed a higher peak flow velocity by 4D flow MRI than in 2D flow MRI (117).

In 4D flow MRI, volume acquisition encompasses the entire heart and does not require specific imaging planes or knowledge of cardiac anatomy (118). As part

of the 4D Flow MRI, the analysis plane may be positioned offline anywhere within the acquisition area (82). The 4D Flow MRI parameters have been replicated accurately in research conducted on healthy volunteers (119). 4D Flow MRI can, therefore, provide a comprehensive assessment of blood flow and energy distribution in both healthy and diseased individuals (120). However, 4D flow MRI has its limitations. First, the post-processing and analysis of 4D flow MRI require a great deal of time and effort, thus limiting its clinical application. The post-processing time for measuring 4D flow MRI data in our study was approximately 40 to 60 minutes per patient, and the segmentation time for the thoracic aorta (region of interest) was another 30 to 60 minutes. Due to manual intervention in 3D segmentation, the operator's experience also influences blood flow estimation accuracy (121). Therefore, it is essential to automate and improve the analysis workflow to ensure an acceptable level of clinical interaction. Based on the results of our current study, we observed no significant changes in peak systolic velocity in NOP over time.

In contrast, we observed a significant decrease in the peak systolic velocity in both ascending aorta and aortic arch in OP. At the level of planes, there was a significant decrease in peak systolic velocity in planes 1, 2, and 6 in OP. Furthermore, as expected, there was a very strong correlation between peak velocity and WSS in the ascending aorta, aortic arch, and descending aorta in both NOP and OP. The reduction in peak systolic velocity after aortic valve replacement in OP indicates improved aortic hemodynamics after surgery.

12.5. Helical and vortical flow

Neither helical nor vortical flow showed statistically significant changes over time in NOP or OP, although there were changes in some individuals. A decrease in semi-quantified helical flow intensity was found in OP after surgery, but the difference was not statistically significant (P: 2.3 ±0.95, FU: 1.8 ±0.90, p value 0.14). Helical flow intensity tends to be related to the severity of aortic valve stenosis (helical flow in P (NOP): 1.6±0.87, helical flow in P (OP): 2.3±0.95, p value 0.06). The aortic valve morphology was significantly correlated with the helical flow intensity. Statistically, BAV patients showed more intense helical flow than TAV patients during primary study (p value = 0.002) and subsequent follow-up study (p value = 0.009). Those findings were noted in our primary studies (1,3) and substantiated in our follow-up study. Clearly, the intensity of helical flow formation did not correlate with the presence of vortical flow formation. Although all patients had some degree of helical flow, not all of them had vortical flow. In a study published in 2021, Komoriyama et al. investigated blood flow patterns (along with other parameters) in the ascending aorta using 4D flow CMR for 17 patients before and after TAVR. After TAVR, helical flow in the ascending aorta

decreased significantly (1.4 ± 0.6 vs. 1.9 ± 0.8, p value = 0.002), whereas vortical flow did not change (101). Moreover, based on our current results, helical flow formation intensity was positively correlated with WSS in both P and FU. The presence of vortical flow did not correlate with the magnitude of the WSS. The helical flow regression observed in individual cases after aortic valve replacement in OP indicates improved aortic hemodynamics after surgery.

13. Conclusion

Aortic valve pathologies impact the left ventricle and aortic hemodynamics resulting in LV remodeling, altered blood flow patterns, and elevated WSS. The aortic hemodynamic changes, including helical flow formation and elevated WSS, are associated with the severity of aortic valve pathology and valve morphology. There is a strong correlation between altered aortic hemodynamics and LV remodeling. In addition, WSS is strongly correlated with LV mass. WSS regression can therefore be applied together with LV mass regression as indicators of reverse cardiac remodeling following surgery. Furthermore, the change in WSS distribution might be an early sign of aortic valve disease progression, and its regression after surgery indicates improvement of hemodynamics. Altered hemodynamics may contribute to aortic wall remodeling, leading to aortic dilatation and eventually dissection. The WSS is highest in segments where aortic dissections most frequently occur.

Aortic valve replacement affects both cardiac remodeling and aortic hemodynamics. The parameters improve during follow-up. However, some areas of the thoracic aorta continue to display high WSS values even after surgery. This may account for further aortic dilation and dissection postoperatively in some patients. Currently, aortic aneurysm management guidelines only consider aortic size in the making of decisions. The size of the aorta at which surgery should be performed varies according to the guidelines. Aortic aneurysms crave new parameters that can improve surgery decision-making and predict dissection. We propose developing non-size criteria such as WSS as a possible parameter for individualized decision-making in aortic disease management. It would still be necessary to conduct longitudinal studies with large sample sizes to apply these non-size criteria to clinical practice.

14. Limitations

Several factors limited the study. Firstly, one of the major limitations was the small number of patients recruited. Our study, at most, can provide hypotheses for future more extensive studies that will be necessary to further validate our conclusions. Secondly, the two groups which comprised our follow-up study differed significantly in age and BMI, and it has already been shown that WSS varies with age. In healthy aging, WSS of the aorta undergoes significant changes, which emphasizes the necessity of age-matched control cohorts in clinical studies for identifying patients with altered WSS.

Additionally, the acquisition and processing of 4D flow data require a lot of time and expertise, so its use in clinical practice is still very challenging, especially with current post-processing and analysis software. Based on the semiautomatic workflow we employed in our study, the post-processing time for measuring 4D flow MRI data was approximately 40 to 60 minutes, and the segmentation time for the thoracic aorta (region of interest) was another 30 to 60 minutes per patient. Therefore, it would be helpful to have software that automates the acquisition and post-processing and minimizes the operator's involvement. In addition, the hemodynamic values measured by 4D flow MRI are generally underestimated. The operator's experience further compromises the accuracy of blood flow estimation due to manual intervention during 3D segmentation. Therefore, the analysis workflow needs to be improved and automated to ensure that clinical interaction is at an acceptable level. Nevertheless, the relative pattern of expression and magnitude of WSS can be reliably assessed when the procedure for estimating WSS is consistent across samples.

15. References

1. von Knobelsdorff-Brenkenhoff F, Karunaharamoorthy A, Trauzeddel RF, Barker AJ, Blaszczyk E, Markl M, Schulz-Menger J. Evaluation of Aortic Blood Flow and Wall Shear Stress in Aortic Stenosis and Its Association With Left Ventricular Remodeling. Circ Cardiovasc Imaging. 2016 Mar;9(3):e004038.

2. van Ooij P, Markl M, Collins JD, Carr JC, Rigsby C, Bonow RO, Malaisrie SC, McCarthy PM, Fedak PWM, Barker AJ. Aortic Valve Stenosis Alters Expression of Regional Aortic Wall Shear Stress: New Insights From a 4-Dimensional Flow Magnetic Resonance Imaging Study of 571 Subjects. J Am Heart Assoc. 2017 Sep 13;6(9):e005959.

3. Lorenz R, Bock J, Barker AJ, von Knobelsdorff-Brenkenhoff F, Wallis W, Korvink JG, Bissell MM, Schulz-Menger J, Markl M. 4D flow magnetic resonance imaging in bicuspid aortic valve disease demonstrates altered distribution of aortic blood flow helicity. Magn Reson Med. 2014 Apr;71(4):1542-53.

4. Barker AJ, Markl M, Bürk J, Lorenz R, Bock J, Bauer S, Schulz-Menger J, von Knobelsdorff-Brenkenhoff F. Bicuspid aortic valve is associated with altered wall shear stress in the ascending aorta. Circ Cardiovasc Imaging. 2012 Jul;5(4):457-66.

5. Vahanian A, Beyersdorf F, Praz F, Milojevic M, Baldus S, Bauersachs J, Capodanno D, Conradi L, De Bonis M, De Paulis R, Delgado V, Freemantle N, Gilard M, Haugaa KH, Jeppsson A, Jüni P, Pierard L, Prendergast BD, Sádaba JR, Tribouilloy C, Wojakowski W; ESC/EACTS Scientific Document Group. 2021 ESC/EACTS Guidelines for the management of valvular heart disease. Eur Heart J. 2022 Feb 12;43(7):561-632.

6. Demer LL. Cholesterol in vascular and valvular calcification. Circulation. 2001;104:1881–1883.

7. O'Brien KD, Shavelle DM, Caulfield MT, McDonald TO, Olin-Lewis K, Otto CM, Probstfield JL. Association of angiotensin-converting enzyme with low-density lipoprotein in aortic valvular lesions and in human plasma. Circulation. 2002;106:2224–2230.

8. Miller JD, Chu Y, Brooks RM, Richenbacher WE, Pena-Silva R, Heistad DD. Dysregulation of antioxidant mechanisms contributes to increased oxidative stress in calcific aortic valvular stenosis in humans. Journal of the American College of Cardiology. 2008;52:843–850.

9. Hoffman JI, Kaplan S. The incidence of congenital heart disease. J Am Coll Cardiol. 2002 Jun 19;39(12):1890-900.

10. Borger MA, Fedak PWM, Stephens EH, Gleason TG, Girdauskas E, Ikonomidis JS, Khoynezhad A, Siu SC, Verma S, Hope MD, Cameron DE, Hammer DF, Coselli JS,

Moon MR, Sundt TM, Barker AJ, Markl M, Della Corte A, Michelena HI, Elefteriades JA. The American Association for Thoracic Surgery consensus guidelines on bicuspid aortic valve-related aortopathy: Full online-only version. J Thorac Cardiovasc Surg. 2018 Aug;156(2):e41-e74.

11. Rassi AN, Pibarot P, Elmariah S. Left ventricular remodelling in aortic stenosis. Can J Cardiol. 2014 Sep;30(9):1004-11.

12. Elmariah S. Patterns of left ventricular remodeling in aortic stenosis: therapeutic implications. Curr Treat Options Cardiovasc Med. 2015 Jul;17(7):391.

13. Yarbrough WM, Mukherjee R, Ikonomidis JS, Zile MR, Spinale FG. Myocardial remodeling with aortic stenosis and after aortic valve replacement: mechanisms and future prognostic implications. J Thorac Cardiovasc Surg. 2012 Mar;143(3):656-64.

14. Bing R, Cavalcante JL, Everett RJ, Clavel MA, Newby DE, Dweck MR. Imaging and Impact of Myocardial Fibrosis in Aortic Stenosis. JACC Cardiovasc Imaging. 2019 Feb;12(2):283-296.

15. Coady MA, Rizzo JA, Goldstein LJ, Elefteriades JA. Natural history, pathogenesis, and etiology of thoracic aortic aneurysms and dissections. Cardiol Clin. 1999 Nov;17(4):615-35; vii.

16. Elefteriades JA, Farkas EA. Thoracic aortic aneurysm clinically pertinent controversies and uncertainties. J Am Coll Cardiol. 2010 Mar 2;55(9):841-57.

17. Kallenbach K, Karck M, Pak D, Salcher R, Khaladj N, Leyh R, Hagl C, Haverich A. Decade of aortic valve sparing reimplantation: are we pushing the limits too far? Circulation. 2005 Aug 30;112(9 Suppl):I253-9.

18. Saliba E, Sia Y; In collaboration with. The ascending aortic aneurysm: When to intervene?. *Int J Cardiol Heart Vasc*. 2015;6:91-100. Published 2015 Jan 20.

19. Davies RR, Gallo A, Coady MA, Tellides G, Botta DM, Burke B, Coe MP, Kopf GS, Elefteriades JA. Novel measurement of relative aortic size predicts rupture of thoracic aortic aneurysms. Ann Thorac Surg. 2006 Jan;81(1):169-77.

20. Hagan PG, Nienaber CA, Isselbacher EM, Bruckman D, Karavite DJ, Russman PL, Evangelista A, Fattori R, Suzuki T, Oh JK, Moore AG, Malouf JF, Pape LA, Gaca C, Sechtem U, Lenferink S, Deutsch HJ, Diedrichs H, Marcos y Robles J, Llovet A, Gilon D, Das SK, Armstrong WF, Deeb GM, Eagle KA. The International Registry of Acute Aortic Dissection (IRAD):new insights into an old disease. JAMA. 2000 Feb 16;283(7):897-903.

21. El-Hamamsy I, Yacoub MH. Cellular and molecular mechanisms of thoracic aortic aneurysms. Nat Rev Cardiol. 2009 Dec;6(12):771-86.

22. Coady MA, Rizzo JA, Goldstein LJ, Elefteriades JA. Natural history, pathogenesis, and etiology of thoracic aortic aneurysms and dissections. Cardiol Clin 1999;17:615–35.

23. Tan JL, Gatzoulis MA, Ho SY. Aortic root disease in tetralogy of Fallot. Curr Opin Cardiol. 2006 Nov;21(6):569-72.

24. Lang RM, Bierig M, Devereux RB, Flachskampf FA, Foster E, Pellikka PA, Picard MH, Roman MJ, Seward J, Shanewise JS, Solomon SD, Spencer KT, Sutton MS, Stewart WJ; Chamber Quantification Writing Group; American Society of Echocardiography's Guidelines and Standards Committee; European Association of Echocardiography. Recommendations for chamber quantification: a report from the American Society of Echocardiography's Guidelines and Standards Committee and the Chamber Quantification Writing Group, developed in conjunction with the European Association of Echocardiography, a branch of the European Society of Cardiology. J Am Soc Echocardiogr. 2005 Dec;18(12):1440-63.

25. Hartnell GG. Imaging of aortic aneurysms and dissection: CT and MRI. J Thorac Imaging. 2001 Jan;16(1):35-46.

26. von Knobelsdorff-Brenkenhoff F, Gruettner H, Trauzeddel RF, Greiser A, Schulz-Menger J. Comparison of native high-resolution 3D and contrast-enhanced MR angiography for assessing the thoracic aorta. Eur Heart J Cardiovasc Imaging. 2014 Jun;15(6):651-8.

27. Vasan RS, Larson MG, Benjamin EJ, Levy D. Echocardiographic reference values for aortic root size: the Framingham Heart Study. J Am Soc Echocardiogr. 1995 Nov-Dec;8(6):793-800.

28. Davies RR, Goldstein LJ, Coady MA, Tittle SL, Rizzo JA, Kopf GS, Elefteriades JA. Yearly rupture or dissection rates for thoracic aortic aneurysms: simple prediction based on size. Ann Thorac Surg. 2002 Jan;73(1):17-27; discussion 27-8.

29. Fedak PW, Verma S, David TE, Leask RL, Weisel RD, Butany J. Clinical and pathophysiological implications of a bicuspid aortic valve. Circulation. 2002 Aug 20;106(8):900-4.

30. Della Corte A, Bancone C, Quarto C, Dialetto G, Covino FE, Scardone M, Caianiello G, Cotrufo M. Predictors of ascending aortic dilatation with bicuspid aortic valve: a wide spectrum of disease expression. Eur J Cardiothorac Surg. 2007 Mar;31(3):397-404; discussion 404-5.

31. Nistri S, Sorbo MD, Marin M, Palisi M, Scognamiglio R, Thiene G. Aortic root dilatation in young men with normally functioning bicuspid aortic valves. Heart. 1999 Jul;82(1):19-22.

32. Ferencik M, Pape LA. Changes in size of ascending aorta and aortic valve function with time in patients with congenitally bicuspid aortic valves. Am J Cardiol. 2003 Jul 1;92(1):43-6.

33. Keane MG, Wiegers SE, Plappert T, Pochettino A, Bavaria JE, Sutton MG. Bicuspid aortic valves are associated with aortic dilatation out of proportion to coexistent valvular lesions. Circulation. 2000 Nov 7;102(19 Suppl 3):III35-9.

34. Roman MJ, Rosen SE, Kramer-Fox R, Devereux RB. Prognostic significance of the pattern of aortic root dilation in the Marfan syndrome. J Am Coll Cardiol. 1993 Nov 1;22(5):1470-6.

35. Meijboom LJ, Timmermans J, Zwinderman AH, Engelfriet PM, Mulder BJ. Aortic root growth in men and women with the Marfan's syndrome. Am J Cardiol. 2005 Nov 15;96(10):1441-4.

36. Lazarevic AM, Nakatani S, Okita Y, Marinkovic J, Takeda Y, Hirooka K, Matsuo H, Kitamura S, Yamagishi M, Miyatake K. Determinants of rapid progression of aortic root dilatation and complications in Marfan syndrome. Int J Cardiol. 2006 Jan 13;106(2):177-82.

37. Biddinger A, Rocklin M, Coselli J, Milewicz DM. Familial thoracic aortic dilatations and dissections: a case control study. J Vasc Surg. 1997 Mar;25(3):506-11.

38. Milewicz DM, Regalado E. Thoracic Aortic Aneurysms and Aortic Dissections. In: Pagon RA, Adam MP, Bird TD, Dolan CR, Fong CT, Stephens K, editors. GeneReviews Seattle (WA); 1993.

39. Coucke PJ, Willaert A, Wessels MW, Callewaert B, Zoppi N, De Backer J, Fox JE, Mancini GM, Kambouris M, Gardella R, Facchetti F, Willems PJ, Forsyth R, Dietz HC, Barlati S, Colombi M, Loeys B, De Paepe A. Mutations in the facilitative glucose transporter GLUT10 alter angiogenesis and cause arterial tortuosity syndrome. Nat Genet. 2006 Apr;38(4):452-7.

40. Wenstrup RJ, Meyer RA, Lyle JS, Hoechstetter L, Rose PS, Levy HP, Francomano CA. Prevalence of aortic root dilation in the Ehlers-Danlos syndrome. Genet Med. 2002 May-Jun;4(3):112-7.

41. Coady MA, Rizzo JA, Hammond GL, Mandapati D, Darr U, Kopf GS, Elefteriades JA. What is the appropriate size criterion for resection of thoracic aortic aneurysms? J Thorac Cardiovasc Surg. 1997 Mar;113(3):476-91; discussion 489-91.

42. Hiratzka LF, Bakris GL, Beckman JA, Bersin RM, Carr VF, Casey Jr DE, et al. ACCF/AHA/ AATS/ACR/ASA/SCA/SCAI/SIR/STS/SVM guidelines for the diagnosis and management of patients with thoracic aortic disease: executive summary: a report of the American College of Cardiology Foundation/American Heart Association Task Force on Practice Guidelines, American Association for Thoracic Surgery, American College of

Radiology, American Stroke Association, Society of Cardiovascular Anesthesiologists, Society for Cardiovascular Angiography and Interventions, Society of Interventional Radiology, Society of Thoracic Surgeons, and Society for Vascular Medicine. Anesth Analg 2010;111:279–315.

43. Otto CM, Nishimura RA, Bonow RO, Carabello BA, Erwin JP 3rd, Gentile F, Jneid H, Krieger EV, Mack M, McLeod C, O'Gara PT, Rigolin VH, Sundt TM 3rd, Thompson A, Toly C. 2020 ACC/AHA Guideline for the Management of Patients With Valvular Heart Disease: A Report of the American College of Cardiology/American Heart Association Joint Committee on Clinical Practice Guidelines. Circulation. 2021 Feb 2;143(5):e72-e227.

44. Izumi C, Eishi K, Ashihara K, Arita T, Otsuji Y, Kunihara T, Komiya T, Shibata T, Seo Y, Daimon M, Takanashi S, Tanaka H, Nakatani S, Ninami H, Nishi H, Hayashida K, Yaku H, Yamaguchi J, Yamamoto K, Watanabe H, Abe Y, Amaki M, Amano M, Obase K, Tabata M, Miura T, Miyake M, Murata M, Watanabe N, Akasaka T, Okita Y, Kimura T, Sawa Y, Yoshida K; Japanese Circulation Society Joint Working Group. JCS/JSCS/JATS/JSVS 2020 Guidelines on the Management of Valvular Heart Disease. Circ J. 2020 Oct 23;84(11):2037-2119.

45. Fry DL. Acute vascular endothelial changes associated with increased blood velocity gradients. Circ Res 1968, 22, 165-197.

46. Vascular Imaging for Biologists. Module 7. Vascular hemodynamics

47. C.G. Caro, J.M. Fitz-Gerald, R.C. Schroter. Arterial wall shear and distribution of early atheroma in man. Nature, 223 (1969), pp. 1159-1160

48. Friedman MH, O'Brien V, Ehrlich LW. Calculations of pulsatile flow through a branch: implications for the hemodynamics of atherogenesis. Circ Res. 1975 Feb;36(2):277-85.

49. Sirs JA. The flow of human blood through capillary tubes. J Physiol. 1991 Oct;442:569-83. doi: 10.1113/jphysiol.1991.sp018809.

50. Mezger, T. (2011). The Rheology Handbook. 3rd revised ed. Hanover: Vincentz Network.

51. Kalsi, A., & Balani, N. (2016). Fluid dynamics: Laminar and turbulent flow. In *Physics for the Anaesthetic Viva* (pp. 27-28). Cambridge: Cambridge University Press.

52. Stepanchuk AP. Blood motion: turbulent or laminar? Wiad Lek. 2017;70(2 pt 2):331-334.

53. Moffatt HK. The degree of knottedness of tangled vortex lines. J Fluid Mech. 1969;35(1):117–129.

54. Moffatt HK, Tsinober A. Helicity in laminar and turbulent flow. Annu Rev Fluid Mech.1992; 24:281–312.

55. Lehoux S, Tedgui A. Cellular mechanics and gene expression in blood vessels. J Biomech. 2003 May;36(5):631-43.

56. Lehoux S, Castier Y, Tedgui A. Molecular mechanisms of the vascular responses to haemodynamic forces. J Intern Med. 2006 Apr;259(4):381-92.

57. Shi ZD, Tarbell JM. Fluid flow mechanotransduction in vascular smooth muscle cells and fibroblasts. Ann Biomed Eng. 2011 Jun;39(6):1608-19.

58. El-Hamamsy I, Yacoub MH. Cellular and molecular mechanisms of thoracic aortic aneurysms. Nat Rev Cardiol. 2009 Dec;6(12):771-86.

59. Tseng WY, Su MY, Tseng YH. Introduction to Cardiovascular Magnetic Resonance: Technical Principles and Clinical Applications. Acta Cardiol Sin. 2016 Mar;32(2):129-44.

60. Markl M, Frydrychowicz A, Kozerke S, Hope M, Wieben O. 4D flow MRI. J Magn Reson Imaging. 2012 Nov;36(5):1015-36.

61. McConnell MV, Khasgiwala VC, Savord BJ, Chen MH, Chuang ML, Edelman RR, Manning WJ. Comparison of respiratory suppression methods and navigator locations for MR coronary angiography. AJR Am J Roentgenol. 1997 May;168(5):1369-75. doi: 10.2214/ajr.168.5.9129447. PMID: 9129447.

62. Wang Y, Rossman PJ, Grimm RC, Riederer SJ, Ehman RL. Navigator-echo-based real-time respiratory gating and triggering for reduction of respiration effects in three-dimensional coronary MR angiography. *Radiology* 1996; 198: 55– 60.

63. Bailes DR, Gilderdale DJ, Bydder GM, Collins AG, Firmin DN. Respiratory ordered phase encoding (ROPE): a method for reducing respiratory motion artefacts in MR imaging. *J Comput Assist Tomogr* 1985; 9: 835– 838.

64. Felmlee JP, Ehman RL, Riederer SJ, Korin HW. Adaptive motion compensation in MRI: accuracy of motion measurement. *Magn Reson Med* 1991; 18: 207– 213.

65. C TefÃ-Silva, K M Mata, C R Fernandes, P S Prudente, C M Prado, M A Rossi, S G Ramos University of Sao Paulo. Pathogenesis of abdominal aortic aneurysms: the role of metalloproteinases and their inhibitors. doi:10.1136/heartjnl-2013-304019.175.

66. von Knobelsdorff-Brenkenhoff F, Rudolph A, Wassmuth R, Bohl S, Buschmann EE, Abdel-Aty H, Dietz R, Schulz-Menger J. Feasibility of cardiovascular magnetic resonance to assess the orifice area of aortic bioprostheses. Circ Cardiovasc Imaging. 2009 Sep;2(5):397-404, 2 p following 404.

67. von Knobelsdorff-Brenkenhoff F, Rudolph A, Wassmuth R, Abdel-Aty H, Schulz-Menger J. Aortic dilatation in patients with prosthetic aortic valve: comparison of MRI and echocardiography. J Heart Valve Dis. 2010 May;19(3):349-56.

68. Markl M, Harloff A, Bley TA, Zaitsev M, Jung B, Weigang E, Langer M, Hennig J, Frydrychowicz A. Time-resolved 3D MR velocity mapping at 3T: improved navigator-gated assessment of vascular anatomy and blood flow. J Magn Reson Imaging. 2007 Apr;25(4):824-31.

69. Markl M, Kilner PJ, Ebbers T. Comprehensive 4D velocity mapping of the heart and great vessels by cardiovascular magnetic resonance. J Cardiovasc Magn Reson. 2011 Jan 14;13(1):7.

70. Walker PG, Cranney GB, Scheidegger MB, Waseleski G, Pohost GM, Yoganathan AP. Semiautomated method for noise reduction and background phase error correction in MR phase velocity data. J Magn Reson Imaging. 1993 May-Jun;3(3):521-30.

71. Berhane H, Scott M, Elbaz M, Jarvis K, McCarthy P, Carr J, Malaisrie C, Avery R, Barker AJ, Robinson JD, Rigsby CK, Markl M. Fully automated 3D aortic segmentation of 4D flow MRI for hemodynamic analysis using deep learning. Magn Reson Med. 2020 Oct;84(4):2204-2218.

72. Dyverfeldt P, Bissell M, Barker AJ, Bolger AF, Carlhäll CJ, Ebbers T, Francios CJ, Frydrychowicz A, Geiger J, Giese D, Hope MD, Kilner PJ, Kozerke S, Myerson S, Neubauer S, Wieben O, Markl M. 4D flow cardiovascular magnetic resonance consensus statement. J Cardiovasc Magn Reson. 2015 Aug 10;17(1):72.

73. Napel S, Lee DH, Frayne R, Rutt BK. Visualizing three-dimensional flow with simulated streamlines and three-dimensional phase-contrast MR imaging. J Magn Reson Imaging. 1992 Mar-Apr;2(2):143-53.

74. Buonocore MH. Visualizing blood flow patterns using streamlines, arrows, and particle paths. Magn Reson Med. 1998 Aug;40(2):210-26.

75. Nordmeyer S, Riesenkampff E, Messroghli D, Kropf S, Nordmeyer J, Berger F, Kuehne T. Four-dimensional velocity-encoded magnetic resonance imaging improves blood flow quantification in patients with complex accelerated flow. J Magn Reson Imaging. 2013 Jan;37(1):208-16.

76. Markl M, Draney MT, Miller DC, Levin JM, Williamson EE, Pelc NJ, Liang DH, Herfkens RJ. Time-resolved three-dimensional magnetic resonance velocity mapping of aortic flow in healthy volunteers and patients after valve-sparing aortic root replacement. J Thorac Cardiovasc Surg. 2005 Aug;130(2):456-63.

77. Lantz J, Renner J, Länne T, Karlsson M. Is aortic wall shear stress affected by aging? An image-based numerical study with two age groups. Med Eng Phys. 2015 Mar;37(3):265-71.

78. Callaghan FM, Grieve SM. Normal patterns of thoracic aortic wall shear stress measured using four-dimensional flow MRI in a large population. Am J Physiol Heart Circ Physiol. 2018 Nov 1;315(5):H1174-H1181.

79. Rank N, Stoiber L, Nasser M, Tanacli R, Stehning C, Knierim J, Schoenrath F, Pieske B, Falk V, Kuehne T, Meyer A, Kelle S. Assessment of 10-Year Left-Ventricular-Remodeling by CMR in Patients Following Aortic Valve Replacement. Front Cardiovasc Med. 2021 Mar 22;8:645693.

80. Treibel TA, Kozor R, Schofield R, Benedetti G, Fontana M, Bhuva AN, Sheikh A, López B, González A, Manisty C, Lloyd G, Kellman P, Díez J, Moon JC. Reverse Myocardial Remodeling Following Valve Replacement in Patients With Aortic Stenosis. J Am Coll Cardiol. 2018 Feb 27;71(8):860-871.

81. Une D, Mesana L, Chan V, Maklin M, Chan R, Masters RG, Mesana TG, Ruel M. Clinical Impact of Changes in Left Ventricular Function After Aortic Valve Replacement: Analysis From 3112 Patients. Circulation. 2015 Aug 25;132(8):741-7.

82. Dyvorne H, Knight-Greenfield A, Jajamovich G, Besa C, Cui Y, Stalder A, Markl M, Taouli B. Abdominal 4D flow MR imaging in a breath hold: combination of spiral sampling and dynamic compressed sensing for highly accelerated acquisition. Radiology. 2015 Apr;275(1):245-54.

83. Katritsis D, Kaiktsis L, Chaniotis A, Pantos J, Efstathopoulos EP, Marmarelis V. Wall shear stress: theoretical considerations and methods of measurement. Prog Cardiovasc Dis. 2007 Mar-Apr;49(5):307-29.

84. Farag ES, van Ooij P, Planken RN, Dukker KCP, de Heer F, Bouma BJ, Robbers-Visser D, Groenink M, Nederveen AJ, de Mol BAJM, Kluin J, Boekholdt SM. Aortic valve stenosis and aortic diameters determine the extent of increased wall shear stress in bicuspid aortic valve disease. J Magn Reson Imaging. 2018 Aug;48(2):522-530.

85. Potters WV, van Ooij P, Marquering H, vanBavel E, Nederveen AJ. Volumetric arterial wall shear stress calculation based on cine phase contrast MRI. J Magn Reson Imaging. 2015 Feb;41(2):505-16.

86. Sotelo J, Dux-Santoy L, Guala A, Rodríguez-Palomares J, Evangelista A, Sing-Long C, Urbina J, Mura J, Hurtado DE, Uribe S. 3D axial and circumferential wall shear stress from 4D flow MRI data using a finite element method and a laplacian approach. Magn Reson Med. 2018 May;79(5):2816-2823.

87. van Ooij P, Garcia J, Potters WV, Malaisrie SC, Collins JD, Carr JC, Markl M, Barker AJ. Age-related changes in aortic 3D blood flow velocities and wall shear stress:

Implications for the identification of altered hemodynamics in patients with aortic valve disease. J Magn Reson Imaging. 2016 May;43(5):1239-49.

88. van Ooij P, Potters WV, Collins J, Carr M, Carr J, Malaisrie SC, Fedak PW, McCarthy PM, Markl M, Barker AJ. Characterization of abnormal wall shear stress using 4D flow MRI in human bicuspid aortopathy. Ann Biomed Eng. 2015 Jun;43(6):1385-97.

89. Mynard JP, Wasserman BA, Steinman DA. Errors in the estimation of wall shear stress by maximum Doppler velocity. Atherosclerosis. 2013 Apr;227(2):259-66.

90. Markl M, Wallis W, Harloff A. Reproducibility of flow and wall shear stress analysis using flow-sensitive four-dimensional MRI. J Magn Reson Imaging. 2011 Apr;33(4):988-94.

91. van Ooij P, Powell AL, Potters WV, Carr JC, Markl M, Barker AJ. Reproducibility and interobserver variability of systolic blood flow velocity and 3D wall shear stress derived from 4D flow MRI in the healthy aorta. J Magn Reson Imaging. 2016 Jan;43(1):236-48.

92. Malek AM, Jackman R, Rosenberg RD, Izumo S. Endothelial expression of thrombomodulin is reversibly regulated by fluid shear stress. Circ Res. 1994 May;74(5):852-60.

93. Hope MD, Sigovan M, Wrenn SJ, Saloner D, Dyverfeldt P. MRI hemodynamic markers of progressive bicuspid aortic valve-related aortic disease. J Magn Reson Imaging. 2014 Jul;40(1):140-5.

94. Barker AJ, Lanning C, Shandas R. Quantification of hemodynamic wall shear stress in patients with bicuspid aortic valve using phase-contrast MRI. Ann Biomed Eng. 2010 Mar;38(3):788-800.

95. Bissell MM, Hess AT, Biasiolli L, Glaze SJ, Loudon M, Pitcher A, Davis A, Prendergast B, Markl M, Barker AJ, Neubauer S, Myerson SG. Aortic dilation in bicuspid aortic valve disease: flow pattern is a major contributor and differs with valve fusion type. Circ Cardiovasc Imaging. 2013 Jul;6(4):499-507.

96. Mahadevia R, Barker AJ, Schnell S, Entezari P, Kansal P, Fedak PW, Malaisrie SC, McCarthy P, Collins J, Carr J, Markl M. Bicuspid aortic cusp fusion morphology alters aortic three-dimensional outflow patterns, wall shear stress, and expression of aortopathy. Circulation. 2014 Feb 11;129(6):673-82.

97. Shan Y, Li J, Wang Y, Wu B, Barker AJ, Markl M, Wang C, Wang X, Shu X. Aortic shear stress in patients with bicuspid aortic valve with stenosis and insufficiency. J Thorac Cardiovasc Surg. 2017 Jun;153(6):1263-1272.e1.

98. Rodríguez-Palomares JF, Dux-Santoy L, Guala A, Kale R, Maldonado G, Teixidó-Turà G, Galian L, Huguet M, Valente F, Gutiérrez L, González-Alujas T, Johnson KM, Wieben O, García-Dorado D, Evangelista A. Aortic flow patterns and wall shear

stress maps by 4D-flow cardiovascular magnetic resonance in the assessment of aortic dilatation in bicuspid aortic valve disease. J Cardiovasc Magn Reson. 2018 Apr 26;20(1):28.

99. van Ooij P, Markl M, Collins JD, Carr JC, Rigsby C, Bonow RO, Malaisrie SC, McCarthy PM, Fedak PWM, Barker AJ. Aortic Valve Stenosis Alters Expression of Regional Aortic Wall Shear Stress: New Insights From a 4-Dimensional Flow Magnetic Resonance Imaging Study of 571 Subjects. J Am Heart Assoc. 2017 Sep 13;6(9):e005959.

100. Guzzardi DG, Barker AJ, van Ooij P, Malaisrie SC, Puthumana JJ, Belke DD, Mewhort HE, Svystonyuk DA, Kang S, Verma S, Collins J, Carr J, Bonow RO, Markl M, Thomas JD, McCarthy PM, Fedak PW. Valve-Related Hemodynamics Mediate Human Bicuspid Aortopathy: Insights From Wall Shear Stress Mapping. J Am Coll Cardiol. 2015 Aug 25;66(8):892-900.

101. Komoriyama H, Kamiya K, Nagai T, Oyama-Manabe N, Tsuneta S, Kobayashi Y, Kato Y, Sarashina M, Omote K, Konishi T, Sato T, Tsujinaga S, Iwano H, Shingu Y, Wakasa S, Anzai T. Blood flow dynamics with four-dimensional flow cardiovascular magnetic resonance in patients with aortic stenosis before and after transcatheter aortic valve replacement. J Cardiovasc Magn Reson. 2021 Jun 28;23(1):81.

102. Bieging ET, Frydrychowicz A, Wentland A, et al. In vivo three-dimensional MR wall shear stress estimation in ascending aortic dilatation. *J Magn Reson Imaging*. 2011;33(3):589-597.

103. Bürk J, Blanke P, Stankovic Z, Barker A, Russe M, Geiger J, Frydrychowicz A, Langer M, Markl M. Evaluation of 3D blood flow patterns and wall shear stress in the normal and dilated thoracic aorta using flow-sensitive 4D CMR. J Cardiovasc Magn Reson. 2012 Dec 13;14(1):84. doi: 10.1186/1532-429X-14-84.

104. van Ooij P, Potters WV, Collins J, Carr M, Carr J, Malaisrie SC, Fedak PW, McCarthy PM, Markl M, Barker AJ. Characterization of abnormal wall shear stress using 4D flow MRI in human bicuspid aortopathy. Ann Biomed Eng. 2015 Jun;43(6):1385-97. doi: 10.1007/s10439-014-1092-7.

105. Salmasi MY, Pirola S, Sasidharan S, Fisichella SM, Redaelli A, Jarral OA, O'Regan DP, Oo AY, Moore JE Jr, Xu XY, Athanasiou T. High Wall Shear Stress can Predict Wall Degradation in Ascending Aortic Aneurysms: An Integrated Biomechanics Study. Front Bioeng Biotechnol. 2021 Oct 18;9:750656.

106. Caballero, A. D., and Laín, S. (2013). A Review on Computational Fluid Dynamics Modelling in Human Thoracic Aorta. *Cardiovasc. Eng. Tech.* 4 (2), 103–130.

107. Braunwald's heart disease. A textbook of cardiovascular medicine. The 10th edition. Diseases of the aorta. Page 1487.

108. Chi Q, He Y, Luan Y, Qin K, Mu L. Numerical analysis of wall shear stress in ascending aorta before tearing in type A aortic dissection. Comput Biol Med. 2017 Oct 1;89:236-247.

109. Osswald A, Karmonik C, Anderson JR, Rengier F, Karck M, Engelke J, Kallenbach K, Kotelis D, Partovi S, Böckler D, Ruhparwar A. Elevated Wall Shear Stress in Aortic Type B Dissection May Relate to Retrograde Aortic Type A Dissection: A Computational Fluid Dynamics Pilot Study. Eur J Vasc Endovasc Surg. 2017 Sep;54(3):324-330.

110. Soulat G, Scott MB, Allen BD, Avery R, Bonow RO, Malaisrie SC, McCarthy P, Fedak PWM, Barker AJ, Markl M. Association of Regional Wall Shear Stress and Progressive Ascending Aorta Dilation in Bicuspid Aortic Valve. JACC Cardiovasc Imaging. 2022 Jan;15(1):33-42.

111. Guala A, Dux-Santoy L, Teixido-Tura G, Ruiz-Muñoz A, Galian-Gay L, Servato ML, Valente F, Gutiérrez L, González-Alujas T, Johnson KM, Wieben O, Casas-Masnou G, Sao Avilés A, Fernandez-Galera R, Ferreira-Gonzalez I, Evangelista A, Rodríguez-Palomares JF. Wall Shear Stress Predicts Aortic Dilation in Patients With Bicuspid Aortic Valve. JACC Cardiovasc Imaging. 2022 Jan;15(1):46-56.

112. Pasta S, Agnese V, Gallo A, Cosentino F, Di Giuseppe M, Gentile G, Raffa GM, Maalouf JF, Michelena HI, Bellavia D, Conaldi PG, Pilato M. Shear Stress and Aortic Strain Associations With Biomarkers of Ascending Thoracic Aortic Aneurysm. Ann Thorac Surg. 2020 Nov;110(5):1595-1604.

113. Garcia J, Barker AJ, Markl M. The Role of Imaging of Flow Patterns by 4D Flow MRI in Aortic Stenosis. JACC Cardiovasc Imaging. 2019 Feb;12(2):252-266.

114. Wentland AL, Grist TM, Wieben O. Repeatability and internal consistency of abdominal 2D and 4D phase contrast MR flow measurements. Acad Radiol. 2013 Jun;20(6):699-704.

115. Dyvorne H, Knight-Greenfield A, Jajamovich G, Besa C, Cui Y, Stalder A, Markl M, Taouli B. Abdominal 4D flow MR imaging in a breath hold: combination of spiral sampling and dynamic compressed sensing for highly accelerated acquisition. Radiology. 2015 Apr;275(1):245-54.

116. da Silveira JS, Smyke M, Rich AV, Liu Y, Jin N, Scandling D, Dickerson JA, Rochitte CE, Raman SV, Potter LC, Ahmad R, Simonetti OP. Quantification of aortic stenosis diagnostic parameters: comparison of fast 3 direction and 1 direction phase contrast CMR and transthoracic echocardiography. J Cardiovasc Magn Reson. 2017 Mar 7;19(1):35.

117. Hälvä R, Vaara SM, Peltonen JI, Kaasalainen TT, Holmström M, Lommi J, Suihko S, Rajala H, Kylmälä M, Kivistö S, Syväranta S. Peak flow measurements in patients with severe aortic stenosis: a prospective comparative study between

cardiovascular magnetic resonance 2D and 4D flow and transthoracic echocardiography. J Cardiovasc Magn Reson. 2021 Nov 15;23(1):132.

118. Feneis JF, Kyubwa E, Atianzar K, Cheng JY, Alley MT, Vasanawala SS, Demaria AN, Hsiao A. 4D flow MRI quantification of mitral and tricuspid regurgitation: Reproducibility and consistency relative to conventional MRI. J Magn Reson Imaging. 2018 Oct;48(4):1147-1158.

119. Markl M, Wallis W, Harloff A. Reproducibility of flow and wall shear stress analysis using flow-sensitive four-dimensional MRI. J Magn Reson Imaging. 2011 Apr;33(4):988-94.

120. Kamphuis VP, Westenberg JJM, van der Palen RLF, Blom NA, de Roos A, van der Geest R, Elbaz MSM, Roest AAW. Unravelling cardiovascular disease using four dimensional flow cardiovascular magnetic resonance. Int J Cardiovasc Imaging. 2017 Jul;33(7):1069-1081.

121. Schnell S, Entezari P, Mahadewia RJ, Malaisrie SC, McCarthy PM, Collins JD, Carr J, Markl M. Improved Semiautomated 4D Flow MRI Analysis in the Aorta in Patients With Congenital Aortic Valve Anomalies Versus Tricuspid Aortic Valves. J Comput Assist Tomogr. 2016 Jan-Feb;40(1):102-8.

122. Analyse der Blutflussmuster in der Aorta ascendens nach verschiedenen Formen des chirurgischen Aortenklappenersatzes mittels kardiovaskulärer Magnetresonanztomographie. Dissertation zur Erlangung des akademischen Grades Doctor medicinae (Dr. med.) von Ralf Felix Trauzeddel.

16. Declaration of academic honesty (eidesstattliche Versicherung)

„Ich, Ahmed Elagamy Musa, versichere an Eides statt durch meine eigenhändige Unterschrift, dass ich die vorgelegte Dissertation mit dem Thema: [*Longitudinal evaluation of aortic hemodynamics in patients with aortic valve pathology using four-dimensional flow cardiovascular magnetic resonance imaging/ Longitudinale Evaluierung der Aortenhämodynamik bei Patienten mit Aortenklappenpathologie mittels vierdimensionaler kardiovaskulärer Magnetresonanztomographie*] selbstständig und ohne nicht offengelegte Hilfe Dritter verfasst und keine anderen als die angegebenen Quellen und Hilfsmittel genutzt habe.

Alle Stellen, die wörtlich oder dem Sinne nach auf Publikationen oder Vorträgen anderer Autoren/innen beruhen, sind als solche in korrekter Zitierung kenntlich gemacht. Die Abschnitte zu Methodik (insbesondere praktische Arbeiten, Laborbestimmungen, statistische Aufarbeitung) und Resultaten (insbesondere Abbildungen, Graphiken und Tabellen) werden von mir verantwortet.

Ich versichere ferner, dass ich die in Zusammenarbeit mit anderen Personen generierten Daten, Datenauswertungen und Schlussfolgerungen korrekt gekennzeichnet und meinen eigenen Beitrag sowie die Beiträge anderer Personen korrekt kenntlich gemacht habe (siehe Anteilserklärung). Texte oder Textteile, die gemeinsam mit anderen erstellt oder verwendet wurden, habe ich korrekt kenntlich gemacht.

Meine Anteile an etwaigen Publikationen zu dieser Dissertation entsprechen denen, die in der untenstehenden gemeinsamen Erklärung mit dem/der Erstbetreuer/in, angegeben sind. Für sämtliche im Rahmen der Dissertation entstandenen Publikationen wurden die Richtlinien des ICMJE (International Committee of Medical Journal Editors; www.icmje.og) zur Autorenschaft eingehalten. Ich erkläre ferner, dass ich mich zur Einhaltung der Satzung der Charité – Universitätsmedizin Berlin zur Sicherung Guter Wissenschaftlicher Praxis verpflichte.

Weiterhin versichere ich, dass ich diese Dissertation weder in gleicher noch in ähnlicher Form bereits an einer anderen Fakultät eingereicht habe.

Die Bedeutung dieser eidesstattlichen Versicherung und die strafrechtlichen Folgen einer unwahren eidesstattlichen Versicherung (§§156, 161 des Strafgesetzbuches) sind mir bekannt und bewusst.“

Datum Unterschrift

17. Anteilserklärung an etwaigen erfolgten Publikationen

Ahmed Musa hatte folgenden Anteil an der folgenden Publikation:

Wiesemann S, Trauzeddel RF, Musa A, Hickstein R, Mayr T, von Knobelsdorff-Brenkenhoff F, Bollache E, Markl M, Schulz-Menger J. Changes of aortic hemodynamics after aortic valve replacement-A four dimensional flow cardiovascular magnetic resonance follow up study. Front Cardiovasc Med. 2023 Feb 14;10:1071643. • DOI: 10.3389/fcvm.2023.1071643

Beitrag im Einzelnen:

Mitkonzipierung des Studiendesigns, Patientenrekrutierung und Terminplanung und Anwesenheit bei der Durchführung von CMR-Studien, Datenerhebung, Nachbearbeitung, Auswertung, Interpretation und Diskussion.

_____

Unterschrift, Datum und Stempel der erstbetreuenden Hochschullehrerin

_____

Unterschrift des Doktoranden

18. Lebenslauf

Mein Lebenslauf wird aus datenschutzrechtlichen Gründen in der elektronischen Version meiner Arbeit nicht veröffentlicht.

19. Publikationsliste

1. Wiesemann S, Trauzeddel RF, **Musa A**, Hickstein R, Mayr T, von Knobelsdorff-Brenkenhoff F, Bollache E, Markl M, Schulz-Menger J. Changes of aortic hemodynamics after aortic valve replacement-A four dimensional flow cardiovascular magnetic resonance follow up study. Front Cardiovasc Med. 2023 Feb 14;10:1071643. • DOI: 10.3389/fcvm.2023.1071643

2. **Musa, A.** , Grimmig, O. and Sonke, J. (2022) Aortic Valve in Black: A Case of Aortic Valve Ochronosis. World Journal of Cardiovascular Surgery, 12, 128-134. **DOI:** 10.4236/wjcs.2022.126010

20. Danksagung

Mein herzlicher Dank gilt Frau Prof. Dr. med. Jeanette Schulz-Menger, die mir durch ihre unendliche Geduld und professionelle Betreuung die Möglichkeit gegeben hat, meine Dissertation abzuschließen. Frau Dr. med. Stephanie Wiesemann, die mir mit Rat und Tat zur Seite stand, gilt mein besonderer Dank. Den medizinisch-technischen Assistentinnen des Helios Klinikums Berlin-Buch, die die Untersuchungen durchgeführt haben, möchte ich meinen herzlichen Dank aussprechen. Ohne ihre Hilfe wäre das Projekt nicht durchführbar gewesen. Den Study Nurses Annette Köhler und Elke Nickel gebührt ein großes Lob für ihre Unterstützung bei der Organisation und Durchführung der Untersuchungen. Zudem möchte ich mich bei Dr. Ulrich Gauger für seine Hilfe bei der Erstellung der Statistik bedanken. Mein aufrichtiger Dank gilt auch meinen Eltern für ihre ständige Ermutigung und Unterstützung und meiner wunderbaren Frau für ihre unermüdliche Unterstützung über all die Jahre. Ohne sie wäre ich nicht so weit gekommen.

21. Bescheinigung des akkreditierten Statistikers

Dr. Ulrich Gauger
Pappelallee 72 • 10437 Berlin
Fon 030/4459882 • Mobil 0160/97936812
ulrich.gauger@gmail.com

Dr. Ulrich Gauger • Pappelallee 72 • 10437 Berlin

statistikhilfe.de
medizin-statistik.de

03. Mai 2023

Bestätigung für Ahmed Elagamy Musa

Hiermit bescheinige ich, dass Herr Ahmed Elagamy Musa bei mir eine statistische Beratung zu ihrem Promotionsvorhaben:

Longitudinal evaluation of aortic hemodynamics in patients with aortic valve pathology using four-dimensional flow cardiovascular magnetic resonance imaging – a follow-up study

zu folgenden Terminen wahrgenommen hat:

Termin 1: Montag, 03. April 2023

Termin 2: Mittwoch, 12. April 2023

Termin 3: Montag, 24. April 2023

Folgende Ratschläge hinsichtlich einer sinnvollen und adäquaten Auswertung und Interpretation der vorgelegten Daten wurden hierbei erteilt:

- Empfehlung zur adäquaten Darstellung der Patientengruppen mittels geeigneter statistischer Parameter und Grafiken (abhängig von Skalenniveau und Verteilungseigenschaft der Merkmale).
- Empfehlungen zur korrekten Anwendung statistischer Verfahren in Abhängigkeit der Fragestellung (t-Test, Wilcoxon-Test, lineare Regressionsanalyse).
- Empfehlungen zur Adjustierung des p-Wertes (Bonferroni-Korrektur) bei multiplem

Dr. Ulrich Gauger
Pappelallee 72 • 10437 Berlin
Fon 030/4459882 • Mobil 0160/97936812
ulrich.gauger@gmail.com

Testen.

- Hinweise zur Interpretation der Ergebnisse.

Diese Bescheinigung garantiert nicht die richtige Umsetzung der Empfehlungen. Die korrekte Umsetzung obliegt der Promovierenden.

Berlin, den 03. Mai 2023

akkreditierter Statistiker am Promotionsbüro der Charité Berlin.